Mathematical Modelling of Morphological Processes in Estuaries

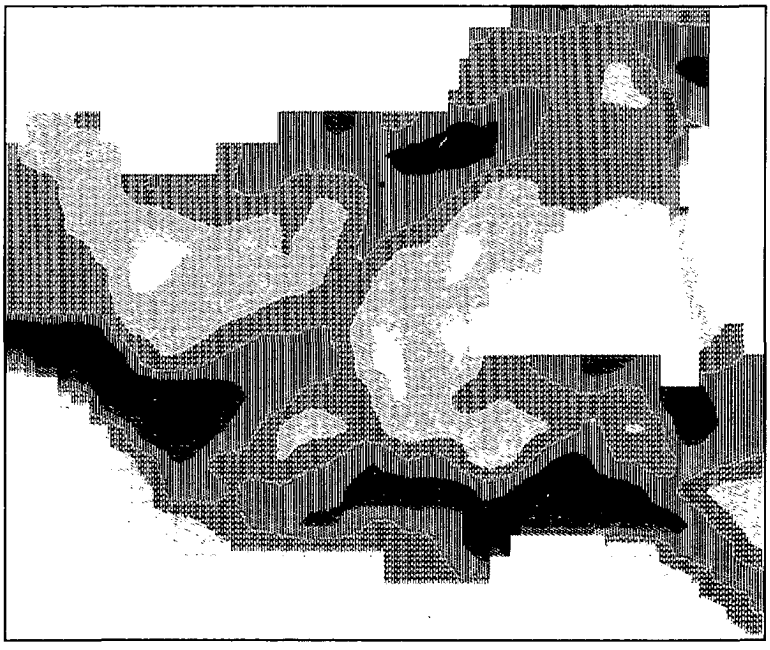

Z.B. Wang

This thesis is also published in the series 'Communications on hydraulic and geotechnical engineering' of the Faculty of Civil Engineering, Delft University of Technology, report nr. 89-1.

Mathematical Modelling of Morphological Processes in Estuaries

Proefschrift

ter verkrijging van de graad van doctor aan
de Technische Universiteit Delft, op gezag van
de Rector Magnificus, prof.drs. P.A. Schenck,
in het openbaar te verdedigen ten overstaan van een
Commissie aangewezen door het College van Dekanen
op donderdag 2 maart 1989 te 14.00 uur

door
Zheng Bing Wang
geboren te Shandong, China
civiel ingenieur

1989

Dit proefschrift is goedgekeurd door de promotoren
prof.dr.ir. M. de Vries en prof.dr.ir. C.B. Vreugdenhil

CONTENTS

SAMENVATTING

In de huidige studie is een wiskundig model (ESMOR) ontwikkeld voor de morfologische ontwikkelingen in estuaria. Het model is bedoeld voor goed gemengde estuaria aangezien het effect van dichtheidstromen niet in rekening is gebracht. Verder zijn de invloeden van de wind en van korte golven verwaarloosd.

Het model ESMOR bestaat uit drie deelmodellen, namelijk het stromingsmodel, het sedimenttransport-model en het bodemniveau-model. Het stromingsmodel is opgebouwd uit het bestaande twee-dimensionale getijstromingsmodel DUCHESS, een eenvoudig snelheidsprofiel model en een vereenvoudigd secundair-stromingsmodel. Het sedimenttransport is verdeeld in bodemtransport en zwevend transport. Het bodemtransport is berekend met een transportformule terwijl voor het zwevende transport een diepte-geintegreerd model is toegepast. Het bodemniveau is berekend uit het totale sedimenttransport-veld in een getijperiode gebaseerd op de massabalans.

Speciale aandacht is geschonken aan het diepte-geintegreerde modelleren van het zwevende sedimenttransport. Het model is afgeleid uit een asymptotische oplossing van de convectie-diffusie vergelijking zoals het model van Galappatti. De theorie van Galappatti is gegeneraliseerd en verbeterd.

Een theoretische analyse is uitgevoerd op het diepte-geintegreerde model voor het zwevende sedimenttransport. Aandacht is vooral geschonken aan de convergentie van de asymptotische oplossing van de convectie-diffusie vergelijking en het morfologische gedrag van de verschillende modellen. Voor een paar geschematiseerde gevallen zijn de verschillende diepte-geintegreerde modellen vergeleken met het exacte model. Een goed inzicht is verkregen in de geldigheid en de toepasbaarheid van het model.

Het model ESMOR is geverifieerd door het met het meer geavanceerde volledige drie-dimensionale model SUTRENCH te vergelijken. Voor het toetsgeval is goede overeenkomst tussen de twee modellen verkregen. Verder levert de vergelijking tussen de twee modellen ook een toets voor de resultaten van de theoretische analyse.

Tenslotte is het model ESMOR toegepast voor lange termijn morfologische berekeningen voor een gebied in het Yantze estuarium. Ondanks de vele grote moeilijkheden zijn bemoedigende resultaten bereikt.

ABSTRACT

In the present study a mathematical model has been developed for the morphological development in estuaries (ESMOR). The model is aimed for well mixed estuaries since the density flow effect is not taken into account. Further the influence of the wind and short waves has been neglected.

The ESMOR model consists of three submodels, viz. the flow model, the sediment transport model and the bed level model. The flow model is constructed from the existing two-dimensional tidal flow model DUCHESS, a simple velocity profile model, and a simplified secondary flow model. The sediment transport is divided into bed load and suspended load transport. The bed load transport is calculated with a transport formula while the suspended load transport is calculated from a depth-integrated model. The bed level change is calculated from the total sediment transport field in a tidal period based on the mass balance.

Special attention has been paid to the depth-integrated modelling of the suspended sediment transport. The model is derived from an asymptotic solution of the convection-diffusion equation following the theory of Galappatti. The theory of Galappatti has been generalized and improved.

A theoretical analysis has been carried out on the depth-integrated model for suspended sediment transport. Special attention has been paid to the convergence of the asymptotic solution of the convection-diffusion equation and the morphological behaviour of the different models. For some schematized cases different depth-integrated models have been compared with the exact model. Good insight has been gained into the validity and applicability of the model.

The ESMOR model has been verified by comparing it with a more sophisticated fully three-dimensional model (SUTRENCH). For the test case good agreement has been obtained between the two models. Further the comparison provides also a test for the results from the theoretical analysis.

The ESMOR model has been applied for long term morphological prediction in a part of the Yantze estuary. Despite a lot of great difficulties some encouraging results have been achieved.

ACKNOWLEDGEMENT

I am very grateful to Dr. H.J. de Vriend and Dr. J.S. Ribberink for their good advises, constructive comments on the work and many helpful discussions. I wish to thank Dr. L.C. van Rijn for providing information of the SUTRENCH computation.

The field data used to apply the model in the Yantze estuary were made available by the East China Investigation and Design Institute in Shanghai, Ministry of Water Resources and Electric Power. I wish to express my gratitude to the staff of this institute for their support and collaboration during my stay in Shanghai.

I am indebted to Dr. G.J.H. van Nes for helping me making the figures 8.11...8.16.

The present study has been carried out at the Hydraulic Engineering Department of the Faculty of Civil Engineering, Delft University of Technology. I wish to thank De Stichting 'Het Laminga Fonds' for financing the main part of the study.

Chapter 1 INTRODUCTION

Estuaries are places where rivers meet the sea. Because of their special geographical positions most estuaries are very important for mankind. They provide water and possibilities for navigation and waste discharge, all economically important. It is certainly not a coincidence that many big cities are located at large estuaries.

Estuaries are continually under morphological development, including sudden changes and gradual evolution. Sudden changes may be caused by e.g. tectonic movements or human interference such as dredging and land reclamation. Gradual evolution is the natural near-equilibrium process. In the present study only the gradual morphological development will be considered.

Morphological development in estuaries can have beneficial as well as adverse effects. Sedimentation of estuaries has provided a lot of fertile land, but, on the other hand, sedimentation of the channels in estuaries can cause serious problems to navigation. Large amounts of money are spent by harbour authorities all over the world for maintenance dredging of navigation channels. When these activities are not effective, the harbour may decline in importance or even be abandoned altogether. It is therefore very important to be able to predict the morphological development, under natural conditions as well as due to human interference. However, a satisfactory technique to do this is not yet available. In fact, morphological modelling for estuaries, especially the mathematical modelling, is still in a early stage of development and requires a lot of further research.

The morphological development of an estuary is a very complicated physical process. Morphological change is a result of the interaction between the water movement and the bed topography. Any influence on the water movement in the estuary will also induce morphological development. If the estuary is considered as a water body, then all these influences can be detected at the boundaries of this water body(see fig.1.1): at the upstream boundary the river inflow, at downstream boundary the saline water intrusion and the tidal motion, at the water surface the wind which generates waves and

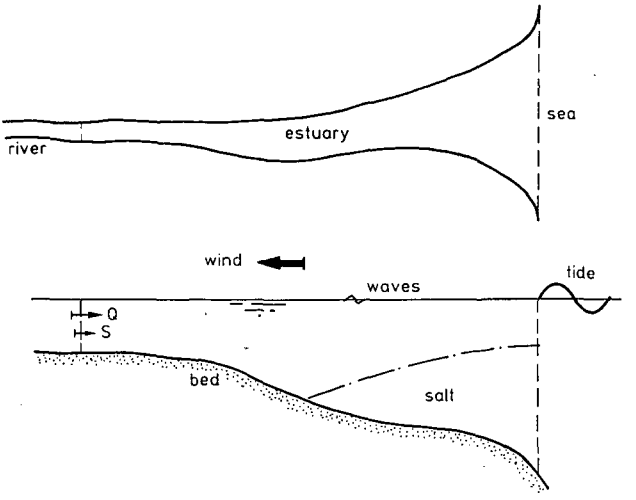

Fig.1.1 An illustration of an estuary and the influences on the morphological development in it.

exerts forces on the flow, and the bed forms which induce resistance. All these influences together determine the hydraulic conditions in the estuary and thereby the morphological process. The morphological development in an estuary is also influenced by the sediment influx from the upstream river and the sediment exchange with the "downstream" sea, and by the properties of the sediment. After all, morphological changes, erosion and sedimentation, are results of non-uniformity of the sediment transport. Processes within the estuary, which can cause changes of the sediment properties, will thus also influence the morphological development. An ideal morphological model should take all these factors into account.

Due to the insufficient understanding of the processes and the lack of sufficient facilities, developing such an ideal morphological model is still hardly possible. Simplifications are virtually inevitable, and consequently the model can only be applied to limited classes of problems. In the present study a mathematical model is developed for the morphological development in estuaries (ESMOR). In this model the density flow effect and the influence of short waves are not taken into account. Therefore the model will only be applicable to well-mixed estuaries. Furthermore the flocculation of cohesive

sediment particles is not included in the model, so the model cannot be applied for regions where flocculation is important.

In the following chapter the general aspects of the model are discussed. The structure of the model is outlined, and the state of art of the subject is described. The two most important submodels in the morphological model, viz. the flow model and the sediment transport model, are described in chapter 3 and chapter 4 respectively. In chapter 4 special attention is paid to the modelling of the suspended sediment transport. The approach is an extension of the model of Galappatti (1983) (also see Galappatti and Vreugdenhil, 1985). Not only is his two-dimensional model extended to three dimensions but also the basic theory on the model has been generalized. The theory developed in chapter 4 is studied analytically in chapter 5. From this analysis a good insight into the validity and applicability of the suspended sediment transport model has been gained. In chapter 6 the numerical aspects of the model are discussed. The ESMOR model is verified in chapter 7 by comparing it with a more sophisticated fully three-dimensional model. Besides, the comparison provides a test for the results from the theoretical analysis in chapter 5. Chapter 8 describes a practical application of the ESMOR model to the Yantze estuary, which, despite a lot of great difficulties, gives some encouraging results. Finally the conclusions from the present study are summarized in chapter 9.

Chapter 2 GENERAL ASPECTS OF THE MODEL

2.1 Structure of the Model

The morphological process is in fact a mechanical process if only non-cohesive sediment is considered. The whole process could thus be described completely by momentum and mass balances, applied to the water as well as to every sediment particle. The dependent variables would then be the flow variables and the positions of all sediment particles in motion. It is easily understood that this approach is unrealistic. In fact the investigation of the motion of a single particle only makes sense to obtain more insight into the sediment transport process(see e.g. van Rijn, 1984a). In morphological computations the dependent variables describing the process are the flow variables, the sediment transport and the bed level. In that case, the momentum balance is only applied to determine the flow field. This schematisation is applied in all mathematical models for morphology so far.

The three groups of dependent variables, related to the flow, sediment transport and the bed level also depend on each other. When the system is not in equilibrium all these variables are continually changing in time. The water motion gives rise to sediment transport and when the sediment transport is not uniform, the bed level will change. The changed bed level will modify the flow field and hence the sediment transport pattern. In this way the whole system is always in development. Therefore a complete mathematical model for morphological development should be a set of coupled equations, the solution of which yields the time dependent flow field, the sediment transport field and the bed level (see fig.2.1).

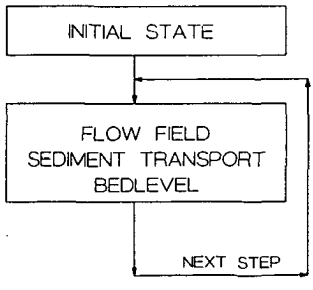

Fig.2.1 Computation procedure of a morphological model without simplifications.

Because of its complexity this approach has rarely been adopted. In most morphological models simplifications are made on the basis of two important assumptions. One is the low concentration assumption, stating that the influence of the suspended sediment on the flow can be neglected as long as the sediment concentration is not too high. The other one is the assumption of quasi-steadiness (de Vries 1959, 1965): from an analysis of the characteristics of the system it can be shown that for small Froude number the flow computation and the bed level computation can be carried out separately. This means that during the flow computation the bed level can be considered as invariant and during the bed level computation the flow is considered as invariant. With these two assumptions the morphological model can be schematized as in fig.2.2.

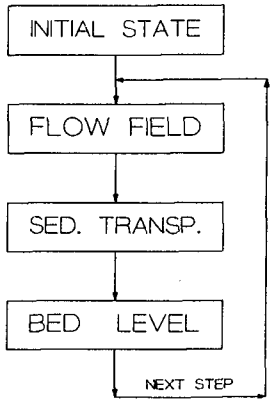

Fig.2.2 Computation procedure of a morphological model in quasi-steady flows.

In general the time step for the bed level computation can be much larger than the time step in the flow computation. In the case of quasi-steady flow this is easily realized by assuming that the flow field does not change during the time step of the bed level computation. In the case of tidal flow it is often assumed that the flow field and the sediment transport field remain periodic during several tidal periods. This means that the time step for the bed level is equal to a number of tidal periods (see de Vriend, 1985). Furthermore, the bed level change after one time step is often small so that the modification of the flow field is so small that a simple flow adjustment model can be applied. An often used method is the continuity

correction method (Hauguel, 1978, de Vriend, 1985). In this method the distribution of the water discharge and the water level is assumed to be the same as those in the previous step (or tidal period). The water depth and the velocity field change only due to the bed level change. Hauguel (1978) developed a more sophisticated method in which the difference between the new and the old flow field is assumed to be a potential flow field. This method is more laborious than the continuity correction method but still much simpler than a completely new tidal flow computation. The simplified flow adjustment can be applied a number of times, depending on the rate of bed level change. When the bed level change exceeds some limit, the complete flow computation has to be carried out again. In fig.2.3 the morphological model is outlined for tidal flow situations.

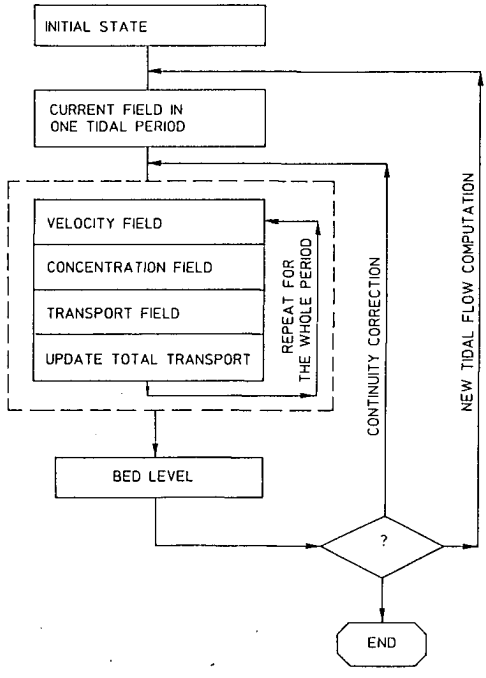

Fig.2.3 Computation procedure of a morphological model in tidal regions.

2.2 State of the Art

Mathematical modelling of morphological processes in estuaries is still in an early stage of development. Due to the amount of computational effort involved, the development of morphological computation methods has been dependent on the development of computers. It was only a few decades ago that the first one-dimensional morphological models, with quasi-steady flow and equilibrium sediment transport formulae were applied to river engineering problems (de Vries, 1959). Morphological computations for estuaries have hardly been carried out so far.

As outlined in the previous section a mathematical model for morphological processes consists of a number of submodels. Therefore, reviews of previous work are given separately for each of the submodels and for the morphological model as a whole.

Flow Model

The many flow models developed for estuaries can be divided into two large groups, viz. density flow models and models without density flow effects. Only the last group is considered here since the present study only concerns well-mixed estuaries.

Flow models can also be divided into one-dimensional, two-dimensional and three-dimensional models. The one-dimensional models such as the FLOWS model developed by Delft University of Technology (DUT, 1983) and the two-dimensional models such as WAQUA (Stelling, 1983) and DUCHESS (DUT, 1986, 1987) have already been operational for application as well as research purposes for some time. Nowadays three-dimensional flow models start also to be operational.

The one or two-dimensional models only describe the depth-averaged flow fields. Velocity profile models are needed to calculate the vertical distribution of the flow velocity. The simplest profile model is assuming the logarithmic velocity profile. This model has been widely applied (Galappatti and Vreugdenhil, 1985, van Rijn, 1987). A more sophisticated

model for deriving velocity profiles from the depth averaged flow field is given by Davies (1986).

The three-dimensional character of the flow field can be improved by adding the secondary flow to a depth averaged two-dimensional model. This has been particularly successful for describing flows in river bends (de Vriend, 1976, 1977, 1981; Kalkwijk and de Vriend, 1980, Olesen, 1987). For the secondary flow in estuaries a model has been developed by Kalkwijk and Booij (1986, also see Booij and Kalkwijk, 1982).

Sediment Transport Model

The sediment transport problem has been studied for a long time. As early as 1879, Duboys published a sediment transport formula. Many transport formulae can now be found in the literature. These transport formulae were derived for the equilibrium transport rate in a uniform flow. However, when suspended load transport is important the sediment transport rate is in general not equal to the equilibrium value. Therefore non-equilibrium transport models are needed for suspended load transport.

The suspended sediment concentration in a flow is described by a convection-diffusion equation. Based on direct numerical solution of this equation two-dimensional vertical (2DV) models (e.g. Kerssens, 1974) and fully three-dimensional (3D) models (van Rijn, 1987) are developed. Another approach is depth-integrated modelling. This kind of models is based on the solution of depth-integrated convection-diffusion equation (Lin et al, 1983, Lin and Shen, 1984). In these models empirical relations are needed, especially for the sediment exchange rate between the bed and the flow.

Galappatti(1983, also see Galappatti and Vreugdenhil, 1985) presented another approach for depth-integrated modelling of suspended transport. An equation for the depth-averaged concentration is derived from an asymptotic solution of the convection-diffusion equation. This approach has the advantage of being flexible with respect to the bed boundary condition and of containing no extra empirical parameters in the depth-averaged concentration equation.

Bed Level Model

When the sediment transport field is known the bed level can be calculated from the mass-balance equation for sediment. The major problem in this submodel is the numerical solution technique. For the one-dimensional case the problem has been thoroughly analysed by Vreugdenhil (1982). A numerical diffusion term appears to be necessary to maintain stability of the computation when the equation is solved explicitly and the equilibrium transport model is applied (Vreugdenhil and de Vries, 1967). Physically it means that a bed gradient dependent transport has to be included. The same applies to two-dimensional problems (de Vriend, 1986, Olesen, 1987).

Morphological Model as a Whole

Depending on how the bed topography is schematized, a morphological model can either be one-dimensional or two-dimensional. Nowadays in river engineering one-dimensional models are commonly used whereas two-dimensional models are still in a developing stage.

Distinction should also be made between models for non-tidal rivers and models for tidal regions. A recently developed two-dimensional model for non-tidal river bends is due to Olesen (1987, also see Struiksma et al, 1985). For tidal regions only "initial models", predicting the initial bed level change rate, are widely applied in practice (Holz and Crotogino, 1984, McAnaly, 1986, van Rijn, 1987). One of the rare examples of long term morphological predictions in tidal regions is reported by Hauguel (1978).

Concerning the theoretical aspects the behaviour of the one-dimensional morphological models, at least those models with quasi-steady flow and equilibrium transport model, have been well understood (de Vries, 1981). However, the behaviour of the two-dimensional models is still far from understood. The theoretical analysis by de Vriend (1984, 1986) is the pioneering work in this area. Much remains to be done in order to gain a thorough understanding of the problem.

Chapter 3 THE FLOW MODEL

3.1 Introduction

The flow in an estuary is a very complicated physical phenomenon. It is unsteady since it is influenced by the upstream river flow and the tidal motion in the surrounding sea or ocean. The geometry of an estuary is often such that the geostrophic forces and wind can have a significant influence on the flow, and the flow must be considered as three-dimensional. Further the density flow effect caused by the density difference between the saline sea water and the fresh river water is often important. It is unrealistic at present to include all these aspects in the morphological model to be developed. Only the most important aspects can be taken into account.

In the preparatory study (Wang, 1985) the question which aspects should be taken into account in the present study was investigated. It was decided to neglect the influence of density flow and short waves. This means that the model will only be applicable to well-mixed estuaries.

It is not the intention of this study to carry out fundamental investigations on the flow or to develop new flow models. Therefore the flow model is constructed from existing models.

The flow model has to satisfy the following requirements.

* It has to be able to predict the flow field accurately enough for further use in morphological computations. The unsteady and three-dimensional character should thus be taken into account.

* It has to be a two-dimensional model based on some similarity assumptions. This is needed because a depth-integrated model will be applied to describe the suspended sediment transport. A depth-integrated model should only be applied if the velocity profiles can be described by a small number of parameters.

* It has to be available and not too expensive to use.

Based on these considerations the flow model has been constructed from two components, a main flow model and a secondary flow model. The main flow model consist of a tidal flow model and a simple profile model for the velocity distribution. For the tidal flow model the model DUCHESS developed at the Delft University of Technology is chosen. For the secondary flow model the approach of Kalkwijk and Booij (1986) is applied. It is assumed that the secondary flow has no influence on the main flow. The main and the secondary flow models are briefly described in the next two sections.

3.2 Main flow model

The depth-averaged flow field is calculated with the DUCHESS model. This model is based on the two-dimensional shallow water equations.

$$\frac{\partial H}{\partial t} + \frac{\partial q_x}{\partial x} + \frac{\partial q_y}{\partial y} = 0 \qquad (3\text{-}1)$$

$$\frac{\partial q_x}{\partial t} + \frac{\partial}{\partial x}\left(q_x \frac{q_x}{D}\right) + \frac{\partial}{\partial y}\left(\frac{q_y}{D} q_x\right) - \frac{\partial}{\partial x}\left(DE \frac{\partial}{\partial x}\left\{\frac{q_x}{D}\right\}\right) +$$

$$- \frac{\partial}{\partial y}\left(DE \frac{\partial}{\partial y}\left\{\frac{q_x}{D}\right\}\right) + gD \frac{\partial H}{\partial x} + \frac{g Q q_x}{C^2 D^2} - f q_y = 0 \qquad (3\text{-}2)$$

$$\frac{\partial q_y}{\partial t} + \frac{\partial}{\partial x}\left(q_y \frac{q_x}{D}\right) + \frac{\partial}{\partial y}\left(\frac{q_y}{D} q_y\right) - \frac{\partial}{\partial x}\left(DE \frac{\partial}{\partial x}\left\{\frac{q_y}{D}\right\}\right) +$$

$$- \frac{\partial}{\partial y}\left(DE \frac{\partial}{\partial y}\left\{\frac{q_y}{D}\right\}\right) + gD \frac{\partial H}{\partial y} + \frac{g Q q_y}{C^2 D^2} + f q_x = 0 \qquad (3\text{-}2)$$

Therein
- H = water level,
- q_x = discharge per unit width in x-direction,
- q_y = discharge per unit width in y-direction,
- $Q = \sqrt{q_x^2 + q_y^2}$
- t = time,
- x,y = horizontal coordinates,
- g = gravity acceleration,
- C = Chezy coefficient,
- f = coefficient for geostrophic acceleration,

D = water depth,

E = horizontal diffusion coefficient.

Equation (3-1) is the continuity equation and equations (3-2) and (3-3) are the momentum equations in x- and y- directions respectively.

The Alternating Direction Implicit (ADI) method with a staggered grid (see fig.3.1) is applied for the numerical solution of equations (3-1) through (3-3). More information on the DUCHESS model is given in DUT(1986, 1987).

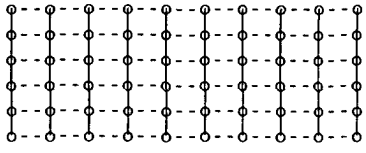

Fig.3.1 The staggered grid

The DUCHESS model calculates only the water level and the current field (averaged velocity * water depth). For the vertical velocity distribution a simple profile model is applied, i.e. the velocity in the direction of the current is assumed to be distributed in the vertical according to the logarithmic law. Based on the logarithmic velocity distribution the normalized velocity profile above a distance z_a from the bed (fig.3.2) is derived by Galappatti(1983).

$$p(\zeta) = \frac{u_s}{\bar{u}_s} = 1 + \frac{u_*}{\bar{u}_s \kappa}\left(\ln\frac{\beta+\zeta}{\beta+1} - \ln\frac{\beta+1}{\beta} + 1\right) \qquad (3\text{-}4)$$

where $\beta = z_a/h$,

$h = D - z_a$,

u_s = velocity in the main flow direction,

$\bar{u}_s$ = mean flow velocity above the bed boundary,

$\zeta = (z-z_b-z_a)/h$,

z_b = bed level.

It should be noted that by definition

$$\int_0^1 p(\zeta)\, d\zeta = 1 \qquad (3\text{-}5)$$

This simple profile model is only applicable for gradually varying flow.

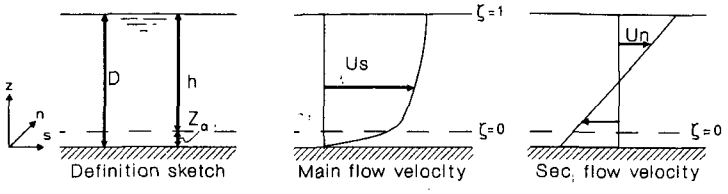

Fig.3.2 Definition sketch and velocity profiles

3.3 The Secondary Flow Model

The secondary flow is the difference between the actual flow and the main flow. It is assumed that the secondary flow component in the direction of the depth averaged flow can be neglected. Thus the horizontal velocity component perpendicular to the direction of the depth averaged flow(the main flow) is the horizontal component of the secondary flow; the vertical flow is such that the secondary flow satisfies the equation of continuity, irrespective of the main flow. Only the horizontal component of the secondary flow will be considered here.

There are many sources of secondary flow. The two most important sources are the main flow curvature and the geostrophic acceleration. The secondary flow velocity caused by the main flow curvature is directed towards the outer bend at the water surface and towards the inner bend at the bottom. The geostrophic acceleration causes a secondary flow directed towards the right (on the Northern Hemisphere and looking in the main flow direction) at the water surface and towards the left near the bottom. Both kinds of secondary flow are considered hereafter.

Secondary flow has been studied for a long time. Well known works on this subject are van Bendegom (1947), Rozovskii (1961) and de Vriend (1981). The secondary flow model described in the following is due to Kalkwijk and

Booij(1985) (see also Booij and Kalkwijk, 1984). It is based on the following main assumptions.

* The flows considered are slowly varying and nearly horizontal.
* The secondary flow field is quasi-steady.
* The eddy viscosity is completely determined by the main flow.
* The logarithmic velocity distribution applies to the main flow.
* The friction in the vertical planes can be neglected.
* All inertia terms except the centrifugal one can be neglected.

Based on these assumptions the equation governing the secondary flow velocity turns out to be linear, so the two kinds of secondary flows can be considered separately.

$$u_n = u_{nc} + u_{nb} \tag{3-6}$$

where u_n = secondary flow velocity,
u_{nb} = secondary flow due to curvature,
u_{nc} = secondary flow due to geostrophic acceleration.

For both u_{nb} and u_{nc} a local equilibrium or fully developed value can be defined. It is determined by the local flow parameters only.

$$u_{ce} = \frac{fD}{\kappa^2} f_c\left(\frac{z-z_b}{D}, \frac{\sqrt{g}}{\kappa C}\right) \tag{3-7a}$$

$$u_{be} = \frac{2\bar{u}_s D}{\kappa^2 R_s} f_b\left(\frac{z-z_b}{D}, \frac{\sqrt{g}}{\kappa C}\right) \tag{3-7b}$$

where R_s = the radius of curvature of the streamline of the main flow
κ = von Karman constant

For the profile functions f_b and f_c linear approximations are applied.

$$f_b = f_c = 3\left(\frac{1}{2} - \frac{g}{\kappa C}\right)\left(2\,\frac{z-z_b}{D} - 1\right) \tag{3-8}$$

With this approximation equation (3-7a) and (3-7b) can be normalized as

$$u_{nce} = I_{ce} q(\zeta) \tag{3-9a}$$

$$u_{nbe} = I_{be} q(\zeta) \tag{3-9b}$$

where I_{be} and I_{ce} are intensities of the fully developed secondary flow and q is the normalized profile function(see fig.3.2).

$$q(\zeta) = 4 \frac{\beta+\zeta}{1+\beta} - 2 \tag{3-10}$$

Due to the variation of the main flow in the main flow direction s, the actual secondary flow velocity will in general not be equal to the fully developed value. This effect is taken into account as follows.

$$u_{nc} = K_c u_{nce} \tag{3-11a}$$

$$u_{nb} = K_b u_{nbe} \tag{3-11b}$$

These equations imply the assumption that the secondary flow velocity has the same vertical distribution everywhere. K_c and K_b are functions of s and can be solved from the following differential equations respectively.

$$\frac{1-2\alpha}{2\alpha^2\kappa^2} \frac{d}{ds}(K_c h) + K_c = 1 \tag{3-12a}$$

$$\frac{1-2\alpha}{2\alpha^2\kappa^2} \frac{d}{ds}\left(\frac{\bar{u}_s h K_b}{R_s}\right) + K_b = 1 \tag{3-12b}$$

$$\alpha = \frac{\sqrt{g}}{\kappa C} \tag{3-12c}$$

Up to now only of the secondary flow velocity has been considered. However, secondary flow can also have influence on the bed shear stress. The bed shear stress due to the secondary flow is treated in a way similar to that for the velocity, only the relaxation length is smaller than for the velocity.

$$\tau_n = \tau_{nc} + \tau_{nb} \tag{3-13}$$

$$\tau_{nc} = K'_c \tau_{nce} \tag{3-14a}$$

$$\tau_{nb} = K'_b \tau_{nbe} \tag{3-14b}$$

$$\tau_{nce} = -\rho\alpha^2 f \bar{u}_s h \tag{3-15a}$$

$$\tau_{nbe} = 2\rho\alpha^2 (1-\alpha)\frac{h}{R_s} \bar{u}_s^2 \tag{3-15b}$$

$$\frac{1-2\alpha}{8\alpha^2\kappa^2}\frac{d}{ds}(K'_c h) + K'_c = 1 \tag{3-16a}$$

$$\frac{1-2\alpha}{8\alpha^2\kappa^2}\frac{d}{ds}\left(\frac{\bar{u}_s h K'_b}{R_s}\right) + K'_b = 1 \tag{3-16b}$$

In these equations

τ_n = bed shear stress due to the secondary flow (in the normal direction),

τ_{nb} = secondary bed shear stress due to curvature,

τ_{nc} = secondary bed shear stress due to geostrophic acceleration,

τ_{nbe} = equilibrium value of τ_{nb},

τ_{nce} = equilibrium value of τ_{nc},

ρ = density of the fluid,

Chapter 4 THE SEDIMENT TRANSPORT MODEL

4.1 Introduction

The sediment transport model is the heart of the whole morphological model. The accuracy of the prediction of morphological development is mainly determined by the accuracy of the sediment transport model.

Sediment transport is usually divided into bed load and suspended load transport. The bed load transport is defined as the transport of particles by rolling, sliding and saltating (Bagnold, 1956). The suspended load transport is defined as that in which the excess weight of particles is supported wholly by a random succession of upward impulses imparted by turbulent eddies (van Rijn, 1987). It should be noted that in natural conditions there will be no sharp division between bed load transport and suspended load transport. This division is introduced only because it is necessary for the mathematical representation. Therefore other definitions are possible(see e.g. Einstein, 1950).

It is a widely accepted assumption that the bed load transport adjusts instantaneously to the local flow conditions. Under this assumption the bed load transport will only depend on the local conditions. This means that the transport rate can be written as

$$S = f(\text{flow param.}, \text{sediment param.}, \text{geometric param.}) \qquad (4\text{-}1)$$

The most important flow parameter is the bed shear stress, often expressed by the bed shear velocity u_* defined as

$$u_* = \sqrt{\frac{\tau}{\rho}} \qquad (4\text{-}2)$$

where ρ = density of water,

τ = bed shear stress.

For non-cohesive sediment the grain size d and the density ρ_s are the most important sediment parameters. The geometric parameters are the parameters such as the bedlevel gradient.

Many transport formulae have been developed by various researchers. Well known examples are the formulae of Einstein (1950), Bagnold (1956), Meyer-Peter and Muller (1948), and Engelund and Hansen (1967). A recently developed transport formula is the one proposed by van Rijn (1984). Here no specific choice is made. The model is built in such a way that different options can be chosen when it is applied. A special option is S=0, which means that bed load transport is neglected.

For the suspended transport a local equilibrium transport rate can be defined in the same way as for the bed load transport. However, the actual transport rate is in general not equal to the equilibrium value, since the adjustment of the transport rate to the flow condition needs more time than in case of bed load transport. Various approaches are possible for modelling the suspended sediment transport. The simplest approach is assuming the transport rate to be in local equilibrium. The suspended transport rate is then calculated from the local conditions with a transport formula similar to that for the bed load transport. This approach can be applied only when the adaptation time and the adaptation length of the sediment transport rate are relatively small compared with the length and time scales of the phenomenon to be modelled.

The most sophisticated approach is the fully three-dimensional model. In this model the convection-diffusion equation describing the suspended sediment concentration is solved to determine the sediment concentration field. The transport rate is then determined by integration. The basic theory for this approach will be outlined in the next section.

In the ESMOR model an approach in between these two extreme cases is chosen. This is the depth-integrated model, which is often derived by integrating the convection-diffusion equation over the depth. However, as the convection-diffusion equation is in fact a mass balance equation, the integrated form of this equation remains a mass balance equation. This

integrated mass balance equation, and hence the morphological model are mainly based on an empirical relation for the exchange rate of sediment between the flow and the bed. This will be shown in subsection 4.2.6. A new approach for developing a depth-integrated model has been introduced by Galappatti(1983, also see Galappatti and Vreugdenhil, 1985). Based on an asymptotic solution of the convection-diffusion equation a linear differential equation is derived for the depth-averaged concentration. This equation can be solved instead of the convection-diffusion equation. In section 4.3 a generalized theory of this approach will be presented and section 4.4 gives some examples of models derived from this general theory. The model which will be used in the present study is described in section 4.5. In section 4.6 the significance of the influences of secondary flow and horizontal diffusion is investigated.

4.2 Basic Theory

4.2.1 Convection-diffusion equation

The sediment concentration in the flow is governed by the mass balance equation

$$\frac{\partial}{\partial t}(\rho_s c) + \mathrm{div}(\rho_s c \vec{u}_{sed}) = 0 \qquad (4\text{-}3)$$

In this equation c and $\vec{u}_{sed}$ are instantaneous variables.

ρ_s = sediment density,
c = sediment concentration,
$\vec{u}_{sed}$ = local sediment velocity,
t = time.

It is further assumed that the sediment density is constant and that the velocity of the sediment particles is equal to the local flow velocity except in the vertical direction, thus

$$\vec{u}_{sed} = \vec{u} - w_s \vec{e}_z \qquad (4\text{-}4)$$

in which $\vec{u}$ = local flow velocity,

w_s = fall velocity of sediment particles,

$\vec{e}_z$ = the unit vector in the vertical direction.

By applying the Reynolds procedure and introducing the eddy-viscosity concept equation (4-3) becomes

$$\frac{\partial c}{\partial t} + \text{div}(c\vec{u}) - \frac{\partial}{\partial s}\left(\epsilon_s \frac{\partial c}{\partial s}\right) - \frac{\partial}{\partial n}\left(\epsilon_n \frac{\partial c}{\partial n}\right) = w_s \frac{\partial c}{\partial z} + \frac{\partial}{\partial z}\left(\epsilon_z \frac{\partial c}{\partial z}\right) \qquad (4\text{-}5)$$

In this equation c and $\vec{u}$ are averaged variables and

ϵ_s, ϵ_n, ϵ_z = turbulent diffusion coefficients,

s, n = horizontal coordinates in the main flow direction and the normal direction respectively,

z = vertical coordinate.

In many applications this equation is further simplified by assuming that

* the convection term in the vertical direction can be neglected compared with the convection term in the main flow direction;

* the horizontal diffusion term in the main flow direction s can be neglected compared with the convection term.

Here the first assumption will be used while neglecting of the horizontal diffusion term will be reconsidered, (see section 4.6).

4.2.2 Boundary conditions

For solving the convection-diffusion equation the following boundary conditions are needed.

* Initial condition.

At t=0 the sediment concentration field c(t=0,s,n,z) has to be specified. Usually this condition is not very important, since its influence will disappear after some time.

* Inflow boundary condition.

At the inflow boundary the concentration c(t,z) has to be given. This is an essential condition, although the necessary information is seldom available in practice.

* Outflow boundary condition.

At the outflow boundary a condition is also needed due to the diffusion term. Often a weak condition of the form

$$\frac{\partial^2 c}{\partial N^2} = 0 \qquad \text{or} \qquad \frac{\partial c}{\partial N} = 0 \tag{4-6}$$

is applied. Herein N is the coordinate normal to the boundary. This condition, if formulated properly, has little influence on the solution in the computational domain.

* Closed boundary.

Closed boundaries such as a river bank are assumed to be solid so there will be no sediment flux across the boundary. The condition can thus be written as

$$\frac{\partial c}{\partial N} = 0 \tag{4-7}$$

* Water surface boundary condition.

At this boundary it is assumed that there is no sediment flux across the water surface, or in equation form

$$\left[w_s c + \epsilon_z \frac{\partial c}{\partial z}\right]_{z=z_b+D} = 0 \tag{4-8}$$

* Bed boundary condition.

The bed boundary is located at a small height z_a above the bed level. The sediment transport below this boundary is assumed to be bed load transport. According to van Rijn(1987) z_a should be about half the bed form height. In this study z_a is chosen as a certain fraction of the water depth D. Thus

$$\beta = \frac{z_a}{D-z_a} = \frac{z_a}{h} = \text{constant} \qquad (4\text{-}9)$$

Based on an accuracy consideration van Rijn(1985) stated that β should not be too small(>0.01). On the other hand it should not be too large either because otherwise the adjustment at the boundary cannot be assumed instantaneous. In this study the β value ranges from 0.01 to 0.05.

Mathematically the required condition can be satisfied by specifying either the sediment concentration, or the vertical concentration gradient or a combination of them at the bed. Practically this condition causes one of the biggest problems in the model. It is the most important boundary condition since it determines the magnitude of the sediment transport while the convection-diffusion equation determines the relative distribution of the sediment concentration in the flow. Nevertheless an exact condition at the bed can seldom be given because the mechanism of the sediment exchange between the bed and the flow is not well understood up to now. This problem is solved by assuming that the equilibrium state at the boundary is adjusted instantaneously.

Two kinds of conditions are often applied at the bed boundary viz. the concentration type and the gradient type. The concentration type condition assumes that the sediment concentration at the bed boundary adjusts instantaneously to the equilibrium value.

$$c(z=z_b+z_a) = C_a \qquad (4\text{-}10)$$

The gradient type condition assumes that the upward sediment flux is only determined by the local conditions.

$$\left[\epsilon_z \frac{\partial c}{\partial z}\right]_{z=z_b+z_a} = -w_s C_a \qquad (4\text{-}11)$$

In both equations C_a is the equilibrium bed concentration. This equilibrium bed concentration can be derived from the equilibrium suspended transport rate if the concentration distribution over the depth is known. It depends thus on the local flow parameters and sediment parameters. Many formulae for the equilibrium transport rate can be found in literature. At present no specific formula is chosen, different options can be used in the model.

4.2.3 Turbulent diffusion coefficients

Without any reasoning the convection-diffusion equation has been written as equation(4-5) in subsection 4.2.1. It should be noted that this equation implies the assumption that s, n, and z are the three principal directions of the diffusion tensor. In fact very little is known about the diffusion tensor in a three-dimensional flow. The assumption is based on the following two considerations.

* For shallow water flow it is logical to assume that the vertical direction z is one of the principal directions.

* Since little is known about the horizontal mixing it is convenient to assume that the mixing in the horizontal plane is isotropic ($\epsilon_s=\epsilon_n$), so any direction in the horizontal plane can be considered as a principal direction.

A distinction should be made between vertical and horizontal mixing. For the vertical mixing the information gained from the studies in the two-dimensional flows can be used. Since Schmidt (1925) introduced a general equation for the equilibrium suspended sediment concentration profile, one

of the most used expression for the vertical diffusion coefficient for sediment is the parabolic function

$$\epsilon_z = \Gamma \frac{z-z_b}{D}\left(1 - \frac{z-z_b}{D}\right) \kappa u_* D \qquad (4\text{-}12)$$

where Γ is a constant. For Γ=1 this agrees with the eddy viscosity coefficient for fluid momentum, leading to a logarithmic velocity distribution in uniform shear flow. In other words, Γ is the ratio between the diffusion coefficient of sediment and that of the fluid (turbulent Schmidt number).

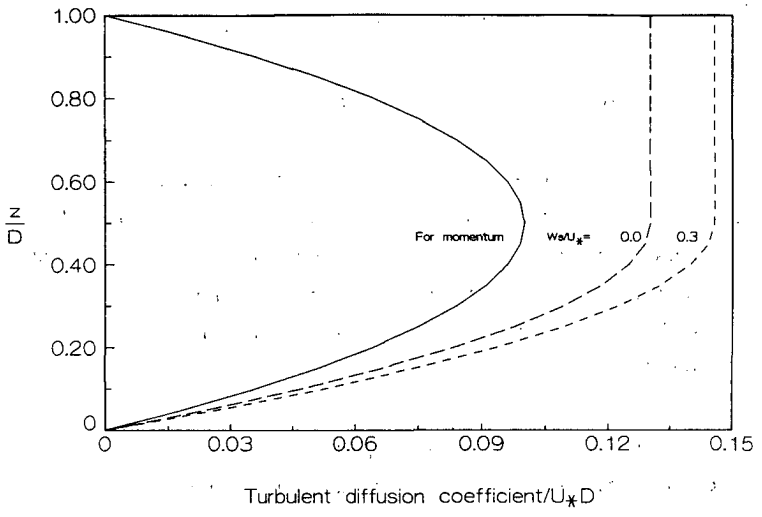

Fig.4.1 Vertical diffusion coefficient for momentum and sediment

Here the parabolic-constant sediment diffusion coefficient introduced by Kerssens (1974, 1977, also see van Rijn, 1987) is applied. This diffusion coefficient distribution is based on the experimental data of Coleman(1970). In equation form this distribution reads

$$\epsilon_z = \epsilon_{max} = \left\{0.13+0.2\left(\frac{w_s}{u_*}\right)^{2.12}\right\} u_* D \qquad \text{for } \frac{z-z_b}{D} \geq 0.5 \qquad (4\text{-}13a)$$

$$\epsilon_z = 4\epsilon_{max} \frac{z-z_b}{D}\left(1 - \frac{z-z_b}{D}\right) \qquad \text{for } \frac{z-z_b}{D} \leq 0.5 \qquad (4\text{-}13b)$$

This distribution is depicted in fig.4.1, together with the parabolic distribution.

Relatively little is known about the horizontal diffusion coefficient. In studies on two-dimensional problems the horizontal diffusion is often neglected. Most information about horizontal mixing in the literature is related to dispersion rather than to diffusion. Dispersion includes not only horizontal diffusion, but also convective effects introduced by the depth averaging process. The dispersion concept was first introduced by Taylor(1954) for non-buoyant matter and later it was applied by Elder(1959) for sediment particles. Since then the gradient type model has been widely applied to describe dispersion of matter in flows. The dispersion coefficient is often used as calibration parameter.

Based on the examination of data from the literature (mostly on dispersion) van Rijn (1987) states that the horizontal diffusion coefficient is in the range 0.1 to 1 m^2/s. Compared with the vertical mixing coefficient this is relatively large. According to equation (4-12) for u_*=0.05 m/s and D=20 m, the maximum value of the vertical diffusion coefficient is 0.1 m /s. Further van Rijn assumes that the horizontal diffusion coefficient is constant in the whole flow field. Here it is assumed that the horizontal diffusion coefficient is related to the vertical diffusion coefficient according to :

$$\epsilon_s = \epsilon_n = A\epsilon_z + B \qquad (4\text{-}14)$$

where A and B are constant coefficients. This rather complicated formulation is chosen in order to keep the model as flexible as possible, especially for being able to make ideal comparisons with other models. This is thus only done for research purposes. For practical application it may be sufficient to assume that the horizontal diffusion coefficient is constant.

4.2.4 Suspended sediment transport

The suspended sediment transport consists of a convective part and a diffusive part. In formula, the transport vector can be written as

$$\vec{S} = \int_{z_b+z_a}^{z_b+D} c\vec{u}\, dz - \int_{z_b+z_a}^{z_b+D} \epsilon_s \text{grad}(c)\, dz \qquad (4\text{-}15)$$

where $\vec{S}$ = the suspended sediment transport vector,

$\vec{u}$ = the horizontal velocity vector,

grad(c) = the horizontal gradient of c.

4.2.5 The Equilibrium Concentration Profile

When the left hand side of the convection-diffusion equation (4-5) vanishes the equilibrium concentration profile results. This approach of determining the equilibrium sediment concentration profile was first applied by Schmidt (1925). For this special case the two types of the bed boundary conditions give the same result. Integrating the equation with respect to z once and applying the water surface boundary condition (4-8) yields

$$w_s c + \epsilon_z \frac{dc}{dz} = 0 \qquad (4\text{-}16)$$

The general solution of equation (4-16) with boundary condition (4-10) is

$$c_e = C_a \exp\left(\int_0^{\zeta} \frac{1}{\epsilon'}\, d\zeta \right) \qquad (4\text{-}17)$$

in which the subscript e is for equilibrium and

$$\zeta = \frac{z - z_b - z_a}{h} \qquad (4\text{-}18)$$

$$\epsilon' = \frac{\epsilon_z}{w_s h} \qquad (4\text{-}19)$$

This is the general equilibrium concentration profile. It can be normalized as

$$c_e = \bar{c}_e a_0(\zeta) \tag{4-20}$$

where $\bar{c}_e$ = the depth averaged equilibrium concentration,
a_0 = the normalized equilibrium concentration profile.

It should be noted that according to the definition

$$\int_0^1 a_0(\zeta)\, d\zeta = 1 \tag{4-21}$$

4.2.6 Integrated Form of the Convection-Diffusion Equation

Integrating the convection-diffusion equation (4-5) over the depth gives

$$\frac{\partial}{\partial t}(h\bar{c}) + \mathrm{div}(\vec{S}) = E \tag{4-22}$$

where E is the sediment exchange rate at the bed boundary.

$$E = -\left[w_s c + \epsilon_z \frac{\partial c}{\partial z}\right]_{z=z_a}$$

It should be noted that this equation is nothing else than the mass balance equation for the suspended sediment. The exchange rate E is also present in the mass balance equation for the layer under the bed boundary, which is applied for determining the bed level change rate.

$$\frac{\partial z_b}{\partial t} = -\frac{1}{1-P}\left(E - \mathrm{div}(\vec{S}_b)\right) \tag{4-23}$$

where $\vec{S}_b$ is the bed load transport vector and P is the porosity of the bed. Equation (4-22) has been used by many researchers (see e.g. Lin et al, 1983, Lin and Shen 1984) to construct a depth-integrated model for suspended sediment transport. To do this the sediment transport rate $\vec{S}$ and the sediment exchange rate at the bottom E have to be formulated in terms of the

mean concentration $\bar{c}$. The exact expressions are unknown until the original convection-diffusion equation is solved. Therefore empirical expressions have to be applied for $\vec{S}$ and E in this kind of depth-integrated models. Obviously integration of the convection-diffusion equation itself does not provide any more information. The depth-integrated models derived in this way are in fact only based on the empirical expressions used for $\vec{S}$ and E. Most of the expressions used have the following form

$$\vec{S} = \alpha \vec{uh}\, \bar{c} \tag{4-24}$$

$$E = \psi\, w_s(\bar{c}_e - \bar{c}) \tag{4-25}$$

Herein α = shape factor ,

ψ = constant coefficient.

Two examples of this kind of models are given in the following. Lin et al (1983) derived a one-dimensional depth-integrated model for the suspended sediment transport in the Qiantang estuary and later Lin and Shen (1984) extended the model to two dimensions using the following expressions.

$$\alpha = 1 \tag{4-26}$$

$$\psi = \frac{\bar{c}_a}{\bar{c}_e} = \gamma_{11} = T \left(\frac{h}{2d}\right)^{w_s/\kappa u_*} \tag{4-27}$$

where T = constant coefficient used as a calibration factor,

d = sediment grain size.

This results in the following equation for the mean concentration.

$$\frac{\partial}{\partial t}\left(h\bar{c}\right) + \frac{\partial}{\partial x}\left(\bar{u}_x h\bar{c}\right) + \frac{\partial}{\partial y}\left(\bar{u}_y h\bar{c}\right) + \gamma_{11} w_s\left(\bar{c}-\bar{c}_e\right) = 0 \tag{4-28}$$

This model has been successfully applied to calculate the sediment concentration in the Qiantang estuary. It should be noted that (4-26) can only be used for very fine sediment as present in the Qiantang estuary.

Vermaas (1984) derived the following more complicated expressions for S and E with the help of a series of two-dimensional computations (in the vertical plane) for steady unidirectional flow.

$$S = \alpha_0 \bar{u}\bar{h}\bar{c} - 4.3\bar{u}\bar{h}^2 \frac{\partial \bar{c}}{\partial x} \tag{4-29}$$

$$E = \Gamma \frac{S_e}{\bar{h}} \frac{\bar{c}-\bar{c}_e}{\bar{c}} \tag{4-30}$$

This results in the following equation for the mean concentration $\bar{c}$.

$$\alpha_0 \bar{u}\bar{h} \frac{\partial \bar{c}}{\partial x} - 4.3\bar{u}\bar{h}^2 \frac{\partial^2 \bar{c}}{\partial x^2} = \Gamma \frac{S_e}{\bar{h}} \left(\frac{\bar{c}_e - \bar{c}}{\bar{c}} \right) \tag{4-31}$$

where α_0 is the value of α when the equilibrium concentration profile is present, and Γ is a coefficient which is a function of the parameters w_s/u_* and $\bar{u}/u_*$.

It should be noted that the mean concentration equation derived with the model of Galappatti (1983, also see Galappatti and Vreugdenhil 1985) is similar to the equations (4-28) and (4-31). The only difference is that in this model no empirical expression has been used: the coefficients in the equation are determined with an asymptotic solution of the original convection-diffusion equation. A comparison between these models has been carried out by Wang(1984).

4.3 A General Asymptotic Solution of the Convection-Diffusion Equation

4.3.1 Normalization of the Equation

Written in s-n-z system of coordinates the convection-diffusion equation (4-5) combined with the continuity equation for water yields

$$\frac{\partial c}{\partial t} + u_s \frac{\partial c}{\partial s} + u_n \frac{\partial c}{\partial n} + w \frac{\partial c}{\partial z} - \frac{\partial}{\partial s}\left(\epsilon_s \frac{\partial c}{\partial s} \right) +$$

$$- \frac{\partial}{\partial n}\left(\epsilon_n \frac{\partial c}{\partial n}\right) = w_s \frac{\partial c}{\partial z} + \frac{\partial}{\partial z}\left(\epsilon_z \frac{\partial c}{\partial z}\right) \tag{4-32}$$

For convenience the following normalized system of coordinates is introduced.

$$\frac{\partial}{\partial \tau} = \frac{h}{w_s} \frac{\partial}{\partial t} \tag{4-33a}$$

$$\frac{\partial}{\partial \xi} = \frac{\bar{u}_s h}{w_s} \frac{\partial}{\partial s} \tag{4-33b}$$

$$\frac{\partial}{\partial \eta} = \frac{Ih}{w_s} \frac{\partial}{\partial n} \tag{4-33c}$$

$$\frac{\partial}{\partial \zeta} = h \frac{\partial}{\partial z} \tag{4-33d}$$

Substituting these equations into equation (4-32) yields

$$\frac{\partial c}{\partial \tau} + p(\zeta) \frac{\partial c}{\partial \xi} + q(\zeta) \frac{\partial c}{\partial \eta} + \frac{w}{w_s} \frac{\partial c}{\partial \zeta} - \frac{w_s}{\bar{u}_s} \frac{\partial}{\partial \xi}\left(\frac{u_*}{\bar{u}_s} \epsilon_s' \frac{\partial c}{\partial \xi}\right) +$$

$$- \frac{w_s}{I} \frac{\partial}{\partial \eta}\left(\frac{u_*}{I} \epsilon_n' \frac{\partial c}{\partial \eta}\right) = \frac{\partial c}{\partial \zeta} + \frac{\partial}{\partial \zeta}\left(\epsilon_z' \frac{\partial c}{\partial \zeta}\right) \tag{4-34}$$

where $p = \frac{u_s}{\bar{u}_s}$ = the normalized main flow velocity profile,

$q = \frac{u_n}{I}$ = the normalized secondary flow velocity profile,

I = the intensity of the secondary flow,

$\epsilon_s' = \frac{\epsilon_s}{u_* h}$ = normalized diffusion coefficient,

$\epsilon_n' = \frac{\epsilon_n}{u_* h}$ = normalized diffusion coefficient,

$\epsilon_z' = \frac{\epsilon_z}{w_s h}$ = normalized diffusion coefficient.

The expression for $p(\zeta)$ and $q(\zeta)$ have already been given in the previous chapter.

In this study only gradually varying flow will be considered, therefore the following assumptions are used.

* The vertical component of the flow velocity is neglected. Thus $w = 0$.

* The variation of the normalized equilibrium concentration profile ϕ_0 with time and with the horizontal coordinates can be neglected. i.e.

$$\frac{\partial \phi_0}{\partial \tau} = \frac{\partial \phi_0}{\partial \xi} = \frac{\partial \phi_0}{\partial \eta} = 0 \tag{4-35}$$

For reasons of brevity, equation(4-34) will further be written as

$$L[c] = D[c] \tag{4-36}$$

Thus

$$L[\ ] = \frac{\partial}{\partial \tau} + p(\zeta)\ \frac{\partial}{\partial \xi} + q(\zeta)\ \frac{\partial}{\partial \eta} + \frac{w}{w_s}\ \frac{\partial}{\partial \zeta} - \frac{w_s}{\bar{u}_s}\ \frac{\partial}{\partial \xi}\left(\frac{u_*}{\bar{u}_s}\ \epsilon_s'\ \frac{\partial}{\partial \xi}\right) +$$

$$- \frac{w_s}{\bar{I}}\ \frac{\partial}{\partial \eta}\left(\frac{u_*}{\bar{I}}\ \epsilon_n'\ \frac{\partial}{\partial \eta}\right) \tag{4-37a}$$

$$D[\ ] = \frac{\partial}{\partial \zeta} + \frac{\partial}{\partial \zeta}\left(\epsilon_z'\ \frac{\partial}{\partial \zeta}\right) \tag{4-37b}$$

Written in the normalized coordinate-system the water surface boundary condition becomes

$$\left[c + \epsilon_z'\ \frac{\partial c}{\partial \zeta}\right]_{\zeta=1} = 0 \tag{4-38}$$

4.3.2 Asymptotic Solution

The asymptotic solution developed here is a generalization of the asymptotic solution presented by Galappatti (1983, also see Galappatti and Vreugdenhil, 1985). Firstly, the three-dimensional problem is considered instead of the two-dimensional one. Secondly, for the two-dimensional problem the

asymptotic solution given by Galappatti is a special case of the asymptotic solution presented here.

The asymptotic solution presented here is based on the same principal assumption as the one by Galappatti (1983): the terms in the left hand side of the convection-diffusion equation (4-34) are an order of magnitude smaller than the terms in the right hand side. Obviously, this assumption can only be true if the two terms on the right hand side of the equation have the same order of magnitude and opposite signs. Such a condition can only be satisfied when the variation of the flow condition is not too rapid, or in other words the time scale and the horizontal length scale of the variation are relatively large, as stated by Galappatti (1983) after an analysis of the order of magnitude of the terms in the two-dimensional convection-diffusion equation. Under this assumption equation (4-34) can be solved asymptotically as follows

$$c = \sum_{j=0}^{n} c_j \tag{4-39}$$

where c_j is the jth order term which is an order of magnitude smaller than the term c_{j-1}.

The equation governing the term c_j can be derived by substituting equation (4-39) into equation (4-34) or (4-36) and collecting the terms of the same order of magnitude.

$$D[c_j] = \begin{cases} 0 & \text{for } j=0 \\ L[c_{j-1}] & \text{for } j>0 \end{cases} \tag{4-40}$$

The additional conditions to be satisfied by the solution (4-39) are the boundary condition at the water surface

$$\left[\sum_{j=0}^{n} c_j + \epsilon'_z \sum_{j=0}^{n} \frac{\partial}{\partial \zeta} c_j \right]_{\zeta=1} = 0 \tag{4-41}$$

and the bed boundary condition

$$\sum_{j=0}^{n} c_j(\zeta=0) = C_a \qquad (4\text{-}42)$$

It should be noted that for the time being only the concentration type bed boundary condition is considered. The type of the bed boundary condition has no influence on the structure of the asymptotic solution. It will only have influence on the equation for the depth integrated variables as will be shown in section 4.4

For n>0 equations (4-40), (4-41) and (4-42) together form an under-determined system. This means that they do not provide sufficient information for determining all the terms c_j. More assumptions are thus needed in order to have a well posed system.

In literature (see e.g. Nayfeh, 1973) on asymptotic solutions of differential equations this problem is in general solved by treating the boundary conditions in the same way as treating the differential equation. Collecting the terms of the same order of magnitude in equations (4-41) and (4-42) yields

$$\left[c_j + \epsilon'_z \frac{\partial}{\partial \zeta} c_j \right]_{\zeta=1} = 0 \qquad \text{for all } j \qquad (4\text{-}43)$$

$$c_j(0) = \begin{cases} C_a & \text{for } j=0 \\ 0 & \text{for } j>0 \end{cases} \qquad (4\text{-}44)$$

The terms in equation (4-39) can now be solved. The asymptotic solution derived in this way will be called the conventional asymptotic solution. It will be shown later that this solution does not allow for any initial condition or for any boundary condition in the horizontal plane.

Galappatti (1983) also applies assumption (4-43), but instead of (4-44) he assumes that only the zero order term contributes to the depth averaged concentration $\bar{c}$. Thus

$$\int_0^1 \tilde{c}_j \, d\zeta = \begin{cases} \bar{c} & \text{for } j=0 \\ 0 & \text{for } j>0 \end{cases} \qquad (4\text{-}45)$$

This assumption introduces a new unknown variable $\bar{c}$, the mean concentration, but the bed boundary condition is not used yet. Equations (4-39), (4-40), (4-43) and (4-45) together give an asymptotic solution with the unknown $\bar{c}$ in it as a parameter. By applying the bed boundary condition, an equation for $\bar{c}$ is obtained. For solving this equation certain boundary conditions corresponding to the operator L[ ] are required. It will be shown later that this solution is more sophisticated than the conventional asymptotic solution, but it still does not always converge to the complete solution of the original problem (Wang and Ribberink, 1986).

The general solution for the terms in (4-39) satisfying (4-40) and (4-43)) can be derived as follows.

The zero order term:

For j=0 equation (4-40) and (4-43) become

$$D[c_0] = 0 \tag{4-46}$$

$$\left[c_0 + \epsilon'_z \frac{\partial c_0}{\partial \zeta}\right]_{\zeta=1} = 0 \tag{4-47}$$

Integrating equation (4-46) twice and applying the boundary condition (4-47) give

$$c_0 = \bar{c}_0 \, a_0 \tag{4-48}$$

where a_0 is the normalized equilibrium concentration profile and $\bar{c}_0$ is the so far unknown depth-averaged value of c_0.

The first order term:

For j=1 equation (4-40) and equation (4-43) become

$$D[c_1] = L[c_0] \tag{4-49}$$

$$\left[c_1 + \epsilon'_z \frac{\partial c_1}{\partial \zeta}\right]_{\zeta=1} = 0 \tag{4-50}$$

With equation (4-37a) in mind substituting equation (4-48) into equation (4-49) yields

$$\frac{\partial c_1}{\partial \zeta} + \frac{\partial}{\partial \zeta}\left(\epsilon'_z \frac{\partial c_1}{\partial \zeta}\right) = a_0 \frac{\partial \bar{c}_0}{\partial \tau} + pa_0 \frac{\partial \bar{c}_0}{\partial \xi} + qa_0 \frac{\partial \bar{c}_0}{\partial \eta} +$$

$$- \frac{w_s}{\bar{u}_s} \frac{\partial}{\partial \xi}\left(\frac{u_*}{\bar{u}_s} a_0 \epsilon'_s \frac{\partial \bar{c}_0}{\partial \xi}\right) - \frac{w_s}{I} \frac{\partial}{\partial \eta}\left(\frac{u_*}{I} a_0 \epsilon'_n \frac{\partial \bar{c}_0}{\partial \eta}\right) \tag{4-51}$$

The solution of this equation can formally be written as

$$c_1 = a_1 \frac{\partial \bar{c}_0}{\partial \tau} + a_2 \frac{\partial \bar{c}_0}{\partial \xi} + a_3 \frac{\partial \bar{c}_0}{\partial \eta} - \frac{w_s}{\bar{u}_s} \frac{\partial}{\partial \xi}\left(\frac{u_*}{\bar{u}_s} a_4 \frac{\partial \bar{c}_0}{\partial \xi}\right) +$$

$$- \frac{w_s}{I} \frac{\partial}{\partial \eta}\left(\frac{u_*}{I} a_5 \frac{\partial \bar{c}_0}{\partial \eta}\right) + \bar{c}_1 a_0 \tag{4-52}$$

where $a_1 = D^{-1}[a_0]$ (4-53a)

$a_2 = D^{-1}[pa_0]$ (4-53b)

$a_3 = D^{-1}[qa_0]$ (4-53c)

$a_4 = D^{-1}[\epsilon'_s a_0]$ (4-53d)

$a_5 = D^{-1}[\epsilon'_n a_0]$ (4-53e)

and $\bar{c}_1$ is the unknown depth-averaged value of c_1. For convenience the same profile functions as in the model of Galappatti (1983) are used as far as possible.

The operator $D^{-1}[\ ]$ is defined by Galappatti(1983) as follows.

$$f(\zeta) = D^{-1}[g(\zeta)] \tag{4-54}$$

if and only if

$$D[f] = g \tag{4-55a}$$

$$\left[f + \epsilon_z' \frac{\partial f}{\partial \zeta}\right]_{\zeta=1} = 0 \tag{4-55b}$$

$$\int_0^1 f \, d\zeta = 0 \tag{4-55c}$$

Galappatti(1983) shows that

$$D^{-1}[g] = \int_\zeta^1 g \, d\zeta + a_0 \int_\zeta^1 \frac{g}{a_0} \, d\zeta + Ba_0 \tag{4-56}$$

where B is a constant defined by condition (4-55c).

It should be noted that the assumption (4-35) implies in general also that

$$\frac{\partial a_4}{\partial \xi} = \frac{\partial a_5}{\partial \eta} = 0 \tag{4-57}$$

so that a_4 and a_5 in the last two terms in equation (4-52) can be placed outside the derivative sign.

Higher order terms:

In the same way as above the second order term in the asymptotic solution can be determined from the first order term, and so on.

The generalized assumption

In the nth order asymptotic solution n+1 unknown variables $\bar{c}_j$ $(0 \le j \le n)$ are present. n+1 equations are thus required to determine these variables. However, there is only one equation available, i.e. the bed boundary

condition (4-42). For n>0 there are thus not enough equations to determine all unknown variables in the asymptotic solution. In the conventional asymptotic solution and the solution of Galappatti (1983) this problem is solved by making the assumptions (4-44) and (4-45) respectively. Here a more general assumption is made. Choose a set of test functions

$$\Phi = (\phi_1, \phi_2, \ldots, \phi_n) \tag{4-58}$$

For each ϕ_k it is assumed that

$$\sum_{j=k}^{n} \int_0^1 c_j \phi_k \, d\zeta = 0 \qquad \text{for } k=1,\ldots,n \tag{4-59}$$

This assumption means that only the first k terms in the asymptotic solution contribute to the internal product of the concentration vertical and the kth component of Φ.

Together with the bed boundary condition (4-42) n+1 equations are now available for the n+1 variables $\bar{c}_j$, so the asymptotic solution is determined. For each chosen set of functions Φ a particular asymptotic solution can be constructed. In the following section various examples are presented. It will be shown that the conventional solution as well as the solution of Galappatti (1983) can be derived by choosing a specific set of Φ-functions.

It should be noted that for each ϕ_k a weighted average concentration can be defined:

$$\int_0^1 \phi_k c \, d\zeta = \int_0^1 \phi_k \sum_{j=1}^{n} c_j \, d\zeta \tag{4-60}$$

which can be calculated when the asymptotic solution is determined. However, it is also possible to eliminate the n+1 variables $\bar{c}_j$ from (4-60) with the help of equations (4-42) and (4-59), resulting in a system of n equations for the n weighted average concentrations. Solving this system instead of

the n+1 equations for $\bar{c}_j$ has two advantages. Firstly the weighted average concentrations have often important physical meanings. Secondly the initial and upstream boundary conditions can easier be expressed in terms of the weighted average concentrations than in terms of $\bar{c}_j$.

4.4 Examples of Various Models

For reasons of simplicity and to facilitate a comparison with the model of Galappatti (1983) the operator L[ ] will be restricted to its two-dimensional form

$$L[\ ] = \frac{\partial}{\partial \tau} + p \frac{\partial}{\partial \xi} \tag{4-61}$$

in this section. This is exactly the case considered by Galappatti. It is easily extended to the general case.

4.4.1 The Conventional Solution

Define a delta function $\delta(\zeta)$ such that

$$\delta(\zeta) = \begin{cases} \infty & \text{for } \zeta=0 \\ 0 & \text{for } \zeta>0 \end{cases} \tag{4-62}$$

and

$$\int_0^1 \delta(\zeta)\, d\zeta = 1 \tag{4-63}$$

With the choice $\Phi = (\delta(\zeta), \delta(\zeta), \ldots, \delta(\zeta))$ or

$$\phi_k = \delta(\zeta) \qquad \text{for } 1 \le k \le n \tag{4-64}$$

the assumption (4-59) and the bed boundary condition (4-42) together give

$$c_j(0) = \begin{cases} C_a & \text{for } j=0 \\ 0 & \text{for } j>0 \end{cases} \tag{4-65}$$

which is exactly the same as equation (4-44). This means that the conventional asymptotic solution is obtained by this choice of Φ.

The zero order term is obtained by applying (4-65) for j=0 to equation (4-48).

$$c_0 = \frac{C_a}{a_0(0)}\, a_0(\zeta) = \frac{C_a}{\gamma_0}\, a_0(\zeta) = \bar{c}_e a_0(\zeta) \tag{4-66}$$

where $\bar{c}_e$ is the equilibrium mean concentration.

The first order term can be determined by applying (4-65) for j=1 to (4-52) and so on. Generally the nth order conventional asymptotic solution can be written as

$$c = \sum_{j=1}^{n+1} \sum_{k=1}^{j} b_{jk}(\zeta)\, \frac{\partial^{j-1} \bar{c}_e}{\partial \tau^{j-k} \partial \xi^{k-1}} \tag{4-67}$$

in which $b_{ij}(\zeta)$ are profile functions defined by

$$b_{11} = a_0 \tag{4-68a}$$

$$b_{j1} = D_*^{-1}[b_{j-1,1}] \tag{4-68b}$$

$$b_{jk} = D_*^{-1}[p b_{j-1,k-1} + b_{j-1,j}] \tag{4-68c}$$

$$b_{jj} = D_*^{-1}[p b_{j-1,j-1}] \tag{4-68d}$$

Herein the operator $D_*^{-1}[\ ]$ is defined similarly as the operator $D^{-1}[\ ]$, but with condition (4-55c) replaced by

$$f(0) = 0 \tag{4-69}$$

It can be shown that equation (4-56) also applies to $D_*^{-1}[\ ]$, although now B is determined by condition (4-69) instead of (4-55c). It is not difficult to show that if

$$f = D^{-1}[g]$$

and

$$f_* = D_*^{-1}[g]$$

then

$$f_* = f - \frac{f(0)}{a_0(0)}\, a_0(\zeta) \tag{4-70}$$

It should be noted that the bed boundary condition is already satisfied by the present asymptotic solution (4-67). The mean concentration as well as the sediment transport rate can be found by integrating this solution

$$\bar{c} = \int_0^1 c\, d\zeta = \sum_{j=1}^{n+1} \sum_{k=1}^{j} \delta_{jk} \frac{\partial^{j-1} \bar{c}_e}{\partial \tau^{j-k} \partial \xi^{k-1}} \tag{4-71}$$

$$S = \bar{u}h \int_0^1 pc\, d\zeta = \bar{u}h \sum_{j=1}^{n+1} \sum_{k=1}^{j} \beta_{jk} \frac{\partial^{j-1} \bar{c}_e}{\partial \tau^{j-k} \partial \xi^{k-1}} \tag{4-72}$$

Herein

$$\delta_{jk} = \int_0^1 b_{jk}\, d\zeta \tag{4-73}$$

$$\beta_{jk} = \int_0^1 p b_{jk}\, d\zeta \tag{4-74}$$

Equations (4-71) and (4-72) are not differential equations since $\bar{c}_e$ is a known function of τ and ξ via the bed boundary condition. This model is thus quite easy to apply.

For $n \to \infty$ this asymptotic solution, if convergent, satisfies the convection-diffusion equation and both boundary conditions corresponding to the operator $D[\ ]$, i.e. the water surface boundary condition and the bed

boundary condition, but in most cases it does not satisfy any boundary condition corresponding to the operator L[ ], i.e. the initial condition and the upstream boundary condition. This is because that equations (4-71) and (4-72) are not differential equations. The mean concentration and the sediment transport rate can be calculated respectively from these two equations directly since $\bar{c}_e$ follows from the bed boundary condition.

4.4.2 The Solution of Galappatti

The solution of Galappatti(1983, also see Galappatti and Vreugdenhil, 1985) is obtained by choosing $\Phi = (1, 1, 1, \ldots, 1)$, or

$$\phi_k = 1 \qquad \text{for } 1 \le k \le n \tag{4-75}$$

Substituting this equation into (4-59) and (4-60) yields

$$\int_0^1 c_j \, d\zeta = \begin{cases} \bar{c} & \text{for } j=0 \\ 0 & \text{for } j>0 \end{cases} \tag{4-76}$$

This is exactly the same as the assumption made by Galappatti.

This solution can be written as

$$c = \sum_{j=1}^{n+1} \sum_{k=1}^{j} a_{jk}(\zeta) \, \frac{\partial^{j-1} \bar{c}}{\partial \tau^{j-k} \partial \xi^{k-1}} \tag{4-77}$$

in which a_{jk} are the profile functions

$$a_{11} = a_0 \tag{4-78a}$$

$$a_{j1} = D^{-1}[a_{j-1,1}] \tag{4-78b}$$

$$a_{jk} = D^{-1}[p a_{j-1,k-1} + a_{j-1,j}] \tag{4-78c}$$

$$a_{jj} = D^{-1}[p a_{j-1,j-1}] \tag{4-78d}$$

In the solution (4-77) the unknown mean concentration $\bar{c}$ is present as a parameter. When the bed boundary condition is applied in this solution an equation is obtained for the mean concentration. Substituting (4-77) into (4-10) yields

$$\bar{c}_e(\tau,\xi) = \sum_{j=1}^{n+1} \sum_{k=1}^{j} \frac{\gamma_{jk}}{\gamma_{11}} \frac{\partial^{j-1} \bar{c}}{\partial\tau^{j-k} \partial\xi^{k-1}} \tag{4-79}$$

with

$$\gamma_{jk} = a_{jk}(0) \tag{4-80}$$

The solution for $n\to\infty$, if convergent, satisfies the convection-diffusion equation and the boundary conditions corresponding to the operator D[ ]. The boundary conditions corresponding to the operator L[ ] are only satisfied in the integrated form, i.e. only as far as the depth mean concentration is concerned (Wang and Ribberink, 1986).

For the application of this model the mean concentration equation (4-79) is solved first and the sediment transport is then calculated from

$$S = \bar{u}h \sum_{j=1}^{n+1} \sum_{k=1}^{j} \alpha_{jk} \frac{\partial^{j-1} \bar{c}}{\partial\tau^{j-k} \partial\xi^{k-1}} \tag{4-81}$$

with

$$\alpha_{jk} = \int_0^1 p a_{jk} \, d\zeta \tag{4-82}$$

This model is more complicated but also more accurate than the conventional solution.

Further information about this model is given by Galappatti (1983), Galappatti and Vreugdenhil (1985) and Ribberink (1986).

4.4.3 A General Second Order Solution

It should be noted that the nth order solution is only influenced by the first n components of Φ, so a general second order solution can be obtained by choosing $\Phi=(\phi_1, \phi_2)$. The second order solution can be written as

$$c = c_0 + c_1 + c_2 \tag{4-83}$$

with

$$c_0 = \bar{c}_0 a_{11} \tag{4-84a}$$

$$c_1 = a_{21} \frac{\partial \bar{c}_0}{\partial \tau} + a_{22} \frac{\partial \bar{c}_0}{\partial \xi} + \bar{c}_1 a_{11} \tag{4-84b}$$

$$c_2 = a_{31} \frac{\partial^2 \bar{c}_0}{\partial \tau^2} + a_{32} \frac{\partial^2 \bar{c}_0}{\partial \tau \partial \xi} + a_{33} \frac{\partial^2 \bar{c}_0}{\partial \xi^2} + \\ + a_{21} \frac{\partial \bar{c}_1}{\partial \tau} + a_{22} \frac{\partial \bar{c}_1}{\partial \xi} + \bar{c}_2 a_{11} \tag{4-84c}$$

Herein the profile functions a_{jk} are the same as in the solution of Galappatti. Thus

$$a_{11} = a_0 \tag{4-85a}$$

$$a_{21} = D^{-1}[a_{11}] \tag{4-85b}$$

$$a_{22} = D^{-1}[pa_{11}] \tag{4-85c}$$

$$a_{31} = D^{-1}[a_{21}] \tag{4-85d}$$

$$a_{32} = D^{-1}[pa_{21} + a_{22}] \tag{4-85e}$$

$$a_{33} = D^{-1}[pa_{22}] \tag{4-85f}$$

Substituting equation (4-84) into (4-59) and (4-60) yields

$$\mu_{11}^{1}\bar{c}_0 = B_1 \tag{4-86}$$

$$\mu_{11}^{2}\bar{c}_0 + \mu_{21}^{2}\frac{\partial\bar{c}_0}{\partial\tau} + \mu_{22}^{2}\frac{\partial\bar{c}_0}{\partial\xi} + \mu_{11}^{2}\bar{c}_1 = B_2 \tag{4-87}$$

$$\mu_{21}^{1}\frac{\partial\bar{c}_0}{\partial\tau} + \mu_{22}^{1}\frac{\partial\bar{c}_0}{\partial\xi} + \mu_{11}^{1}\bar{c}_1 + \mu_{11}^{1}\bar{c}_2 + \mu_{21}^{1}\frac{\partial\bar{c}_1}{\partial\tau} + \mu_{22}^{1}\frac{\partial\bar{c}_1}{\partial\xi} +$$

$$+ \mu_{31}^{1}\frac{\partial^2\bar{c}_0}{\partial\tau^2} + \mu_{32}^{1}\frac{\partial^2\bar{c}_0}{\partial\tau\partial\xi} + \mu_{33}^{1}\frac{\partial^2\bar{c}_0}{\partial\xi^2} = 0 \tag{4-88}$$

$$\mu_{11}^{2}\bar{c}_2 + \mu_{21}^{2}\frac{\partial\bar{c}_1}{\partial\tau} + \mu_{22}^{2}\frac{\partial\bar{c}_1}{\partial\xi} + \mu_{31}^{2}\frac{\partial^2\bar{c}_0}{\partial\tau^2} + \mu_{32}^{2}\frac{\partial^2\bar{c}_0}{\partial\tau\partial\xi} +$$

$$+ \mu_{33}^{2}\frac{\partial^2\bar{c}_0}{\partial\xi^2} = 0 \tag{4-89}$$

where

$$B_k = \int_0^1 \phi_k c \, d\zeta \tag{4-90}$$

$$\mu_{ij}^{k} = \int_0^1 \phi_k a_{ij} \, d\zeta \tag{4-91}$$

Four equations are now available for five variables ($\bar{c}_0$, $\bar{c}_1$, $\bar{c}_2$, B_1, and B_2). The fifth equation is obtained by applying the bed boundary condition.

$$C_a = \gamma_{11}(\bar{c}_0 + \bar{c}_1 + \bar{c}_2) + \gamma_{21}\left[\frac{\partial\bar{c}_0}{\partial\tau} + \frac{\partial\bar{c}_1}{\partial\tau}\right] + \gamma_{22}\left[\frac{\partial\bar{c}_0}{\partial\xi} + \frac{\partial\bar{c}_1}{\partial\xi}\right] +$$

$$+ \gamma_{31}\frac{\partial^2\bar{c}_0}{\partial\tau^2} + \gamma_{32}\frac{\partial^2\bar{c}_0}{\partial\tau\partial\xi} + \gamma_{33}\frac{\partial^2\bar{c}_0}{\partial\xi^2} \tag{4-92}$$

By eliminating $\bar{c}_0$, $\bar{c}_1$ and $\bar{c}_2$ two equations for B_1 and B_2 can be obtained from these five equations.

In order to obtain more insight into the behaviour of this general second order solution two specific choices for ϕ_2 are investigated in the following. For simplicity the steady ($\frac{\partial c}{\partial \tau}=0$) case is considered.

Case I

$$\phi_1 = 1 \tag{4-93a}$$

$$\phi_2 = p(\zeta) \tag{4-93b}$$

For this case the assumption (4-59) has the physical meaning that only the zero order term in the solution contributes to the depth averaged concentration and that only the zero order and first order terms contribute to the sediment transport rate. Further

$$B_1 = \int_0^1 c \, d\zeta = \bar{c} \tag{4-94a}$$

$$B_2 = \int_0^1 pc \, d\zeta = \frac{S}{\bar{u}h} = c_s \tag{4-94b}$$

$$\mu^1_{jk} = \int_0^1 a_{jk} \, d\zeta = \begin{cases} 1 & \text{for } j=1,\ k=1 \\ 0 & \text{for } j\neq 1 \text{ or } k\neq 1 \end{cases} \tag{4-95a}$$

$$\mu^2_{jk} = \int_0^1 p a_{jk} \, d\zeta = \alpha_{jk} \tag{4-95b}$$

The equations governing $\bar{c}$ and c_s can be shown to be

$$\bar{c} + \frac{\gamma_{22}}{\gamma_{11}} \frac{\partial c_s}{\partial \xi} + \left(\frac{\gamma_{33}}{\gamma_{11}} - \frac{\alpha_{22}}{\alpha_{11}} \frac{\gamma_{22}}{\gamma_{11}} \right) \frac{\partial^2 \bar{c}}{\partial \xi^2} = \bar{c}_e \tag{4-96}$$

$$\bar{c} - c_s + \frac{\alpha_{22}}{\alpha_{11}} \frac{\partial c_s}{\partial \xi} + \left(\frac{\alpha_{33}}{\alpha_{11}} - \left(\frac{\alpha_{22}}{\alpha_{11}} \right)^2 \right) \frac{\partial^2 \bar{c}}{\partial \xi^2} = 0 \qquad (4\text{-}97)$$

If $\bar{c}_e$ is constant, the solution of this system of equations can be written as

$$\begin{bmatrix} \bar{c} \\ c_s \end{bmatrix} = \begin{bmatrix} \bar{c}_e \\ 0 \end{bmatrix} + \begin{bmatrix} A_1 \\ A_2 \end{bmatrix} \exp(\lambda \xi) \qquad (4\text{-}98)$$

where λ is determined by

$$\text{Det} \begin{bmatrix} 1 + \left(\frac{\gamma_{33}}{\gamma_{11}} - \frac{\alpha_{22}}{\alpha_{11}} \frac{\gamma_{33}}{\gamma_{11}} \right) \lambda^2 & \frac{\gamma_{22}}{\gamma_{11}} \lambda \\ 1 + \left(\frac{\alpha_{33}}{\alpha_{11}} - \left(\frac{\alpha_{22}}{\alpha_{11}} \right)^2 \right) \lambda^2 & \frac{\alpha_{22}}{\alpha_{11}} \lambda - 1 \end{bmatrix} = 0 \qquad (4\text{-}99)$$

If $p(\xi)$ represents the logarithmic velocity profile, this equation appears to have three real roots, two positive and one negative, the latter about the same as the one in the model of Galappatti. The number of negative roots determines the number of the boundary conditions which have to be applied at the upstream boundary. In the original problem the upstream boundary condition is the concentration vertical at the boundary. In the depth-integrated model the upstream boundary conditions can be applied in the weighted average form of (4-59). The number of conditions available is thus equal to the number of test functions in the model. For the general second order solution two upstream boundary conditions are thus available, viz. $\bar{c}$ and c_s. However, at present it is not possible to apply both upstream boundary conditions because equation (4-99) has only one negative root.

Case II

$$\phi_1 = 1 \qquad (4\text{-}100a)$$

$$\phi_2 = 1 - p \qquad (4\text{-}100b)$$

The basic elements in Φ in this case are the same as in case I and so is the physical meaning of the assumptions (4-60a) and (4-60b). Therefore it can be expected that the infinite order solutions (with $\phi_k=\phi_2$ for k>2) in the two cases will be exactly the same. However, there is an essential difference between the two cases, viz. the linear dependence between the two components of Φ, characterized by the value of

$$\frac{\int_0^1 \phi_1\phi_2 \, d\zeta}{\left[\int_0^1 \phi_1^2 \, d\zeta \int_0^1 \phi_1^2 \, d\zeta\right]^{1/2}}$$

For case II this value is zero which means that ϕ_1 and ϕ_2 are linearly independent, or in other words that Φ is a set of orthogonal functions. In case I this value is nearly equal to unity.

In the present case the equations governing $\bar{c}$ and $\bar{c}_1$ become

$$\bar{c} + \frac{\gamma_{22}}{\gamma_{11}}\left(\frac{\partial \bar{c}}{\partial \xi} + \frac{\partial \bar{c}_1}{\partial \xi}\right) + \frac{\gamma_{33}}{\gamma_{11}} \frac{\partial^2 \bar{c}}{\partial \xi^2} = \bar{c}_e \qquad (4\text{-}101)$$

$$(1 - \alpha_{11})\bar{c}_1 + \alpha_{22} \frac{\partial \bar{c}_1}{\partial \xi} + \alpha_{33} \frac{\partial^2 \bar{c}}{\partial \xi^2} = 0 \qquad (4\text{-}102)$$

The solution of this system is still (4-98) but λ is now determined by

$$\text{Det} \begin{bmatrix} 1 + \frac{\gamma_{22}}{\gamma_{11}} \lambda + \frac{\gamma_{33}}{\gamma_{11}} \lambda^2 & \frac{\gamma_{22}}{\gamma_{11}} \lambda \\ \alpha_{33}\lambda^2 & 1 + \alpha_{22}\lambda - \alpha_{11} \end{bmatrix} = 0 \qquad (4\text{-}103)$$

This equation has three roots, one positive and two negative, one of which is nearly equal to the one in the model of Galappatti. Now the two available boundary conditions can both be applied, so that a more accurate solution can be expected.

From the comparison between case I and case II it can be concluded that the linear dependence between the components in Φ can have influence on the behaviour of the model. The best result seems to be obtained if Φ is an orthogonal set.

The influence of Φ on the asymptotic solution will further be analysed in the next chapter.

Case III

$$\phi_1 = p \tag{4-104a}$$

$$\phi_2 = 1-p \tag{4-104b}$$

This case is similar as case III. Therefore it will not be described in detail. However, it should be emphasized that $\phi_1=p$ is essentially different to $\phi_1=1$, especially for the first order solution. Physically the assumption (4-59) means then that only the zero order term contributes to the sediment transport. In the first order solution c_s is then to be determined in stead of $\bar{c}$. In the following subsection it will be shown that this choice should be preferred.

Remarks:

* The general asymptotic solution developed in this section can also be applied for ordinary differential equations. By studying the ordinary differential equations insight can be gained into the solution technique.

* Although not mathematically proved it is suggested that for $n\to\infty$ the asymptotic solution converges to the exact solution if and only if the system of functions Φ is a complete system. This suggestion is based on the observation of the behaviour of the various models described in this section.

4.4.4 Discussion on the Choice of Φ

In the previous subsection it has become clear that the test functions Φ should together form a orthogonal system. When an orthogonal system is chosen the test functions automatically form a complete system for $n \to \infty$. The question remains which functions should be chosen for the orthogonal system.

It should be noted that the internal products of the test functions and the sediment concentration are the unknown variables in the system of equations from the model. From the nth order solution a system of equations can be derived for the 'depth-integrated' variables

$$\int_0^1 \phi_j c \, d\zeta, \quad j=1,\ldots,n$$

The upstream boundary conditions for this system of equations should also be expressed in these internal products. Obviously, from a practical consideration, the test functions should be such that the internal products of them with c have significant physical meanings.

In the conventional solution the internal products between ϕ_1 $(=\phi_2=\ldots.\phi_n)$ and c is the bed concentration, which is specified as bed boundary condition. Therefore no differential equation needs to be solved in this solution, and no upstream boundary condition can be applied.

In the model of Galappatti (1983) the mean concentration $\bar{c}$ is introduced by making the assumption (4-45). This has led to an equation for $\bar{c}$, for solving which the upstream boundary condition has to be related to $\bar{c}$, which is the internal product of $\phi_1(=\phi_2=\ldots\ldots\phi_n)$ and c.

In morphological computations the purpose of the sediment transport model is to derive the sediment transport rate. Therefore it is logical to chose $\phi_1=p$, of which the internal product with c represents the sediment transport rate. This choice has clearly some advantages over the one of Galappatti (1983) as shown in the following for the case of steady one-dimensional uniform flow.

$$L[\ ] = p \frac{\partial}{\partial \xi}$$

According to the model of Galappatti the mean concentration $\bar{c}$ and the transport rate S are governed by the following equations

$$\bar{c}_e = \bar{c} + \frac{\gamma_2}{\gamma_0} \frac{\partial \bar{c}}{\partial \xi} \tag{4-105}$$

$$S = \bar{u}h \left(\alpha_0 \bar{c} + \alpha_2 \frac{\partial \bar{c}}{\partial \xi} \right) \tag{4-106}$$

According to the present approach the variables c_s and S are governed by the equations

$$c_{se} = c_s + \left(\frac{\gamma_2}{\gamma_0} - \frac{\alpha_2}{\alpha_0} \right) \frac{\partial c_s}{\partial \xi} \tag{4-107}$$

$$S = \bar{u}hc_s \tag{4-108}$$

It is clear that the procedure for calculating the transport rate is now easier than that in the model of Galappatti.

Another advantage of the present approach becomes clear when the two models are applied for the case that the water flowing in contains no sediment at the upstream boundary. From the model of Galappatti it follows

$$\bar{c} = \bar{c}_e - \bar{c}_e \exp\left(- \frac{\gamma_0}{\gamma_2} \xi \right) \tag{4-109}$$

$$S = \bar{u}h \left(\alpha_0 \bar{c} + \alpha_2 \frac{\gamma_0}{\gamma_2} (\bar{c}_e - \bar{c}) \right) \tag{4-110}$$

From the present model it follows

$$S = S_e - S_e \exp\left(\frac{\gamma_0 \alpha_0}{\gamma_0 \alpha_2 - \alpha_0 \gamma_2} \xi \right) \tag{4-111}$$

The two solutions are depicted in fig.4.2. The model of Galappatti appears to give a negative transport at the upstream boundary, while the present model gives the realistic transport rate zero. Although these are only some minor aspects of the model, it is clear that the approach given here should be preferred.

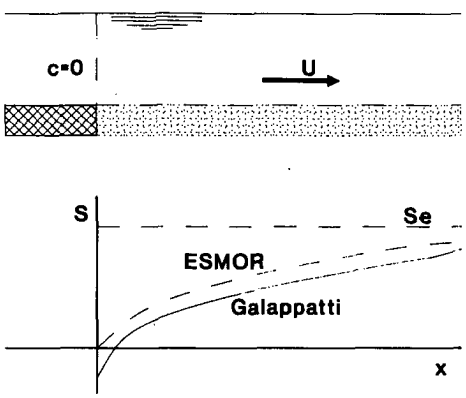

Fig.4.2 Adaptation from clear water

4.5 Model for the Three-dimensional Case

4.5.1 Equations in the Model

For the present approach the set Φ is chosen as

$$\Phi = (p,\ q-\chi p, \ldots.) \tag{4-112}$$

where

$$\chi = \frac{\int_0^1 p(\zeta)q(\zeta)\ d\zeta}{\int_0^1 p(\zeta)p(\zeta)\ d\zeta} \tag{4-113}$$

This is an orthogonal system and the first two components of the internal product between c and Φ represent the convective sediment transport in s and n directions respectively.

For unsteady three-dimensional problems no more than the first order solution can be applied in practice. Therefore only the first order solution will be outlined here. The second component of Φ will thus not influence the model in practice.

The first order solution reads

$$c = c_0 + c_1 \tag{4-114}$$

with

$$c_0 = \bar{c}_0 a_0(\zeta) \tag{4-115a}$$

$$c_1 = a_1 \frac{\partial \bar{c}_0}{\partial \tau} + a_2 \frac{\partial \bar{c}_0}{\partial \xi} + a_3 \frac{\partial \bar{c}_0}{\partial \eta} - a_4 \frac{w_s}{\bar{u}_s} \frac{\partial}{\partial \xi}\left(\frac{u_*}{\bar{u}_s} \frac{\partial \bar{c}_0}{\partial \xi}\right) +$$

$$- a_4 \frac{w_s}{\bar{I}} \frac{\partial}{\partial \eta}\left(\frac{u_*}{\bar{I}} \frac{\partial \bar{c}_0}{\partial \eta}\right) + \bar{c}_1 a_0 \tag{4-115b}$$

The conditions (4-60) and (4-59) now become

$$c_s = \int_0^1 cp \, d\zeta = \int_0^1 c_0 p \, d\zeta = \alpha_0 \bar{c}_0 \tag{4-116}$$

$$\alpha_1 \frac{\partial \bar{c}_0}{\partial \tau} + \alpha_2 \frac{\partial \bar{c}_0}{\partial \xi} + \alpha_3 \frac{\partial \bar{c}_0}{\partial \eta} - \alpha_4 \frac{w_s}{\bar{u}_s} \frac{\partial}{\partial \xi}\left(\frac{u_*}{\bar{u}_s} \frac{\partial \bar{c}_0}{\partial \xi}\right) +$$

$$- \alpha_4 \frac{w_s}{\bar{I}} \frac{\partial}{\partial \eta}\left(\frac{u_*}{\bar{I}} \frac{\partial \bar{c}_0}{\partial \eta}\right) + \bar{c}_1 \alpha_0 = 0 \tag{4-117}$$

in which

$$\alpha_j = \int_0^1 p a_j \, d\zeta \tag{4-118}$$

Applying the bed boundary condition gives

$$\bar{c}_e = \bar{c}_0 + \bar{c}_1 + \frac{\gamma_1}{\gamma_0}\frac{\partial \bar{c}_0}{\partial \tau} + \frac{\gamma_2}{\gamma_0}\frac{\partial \bar{c}_0}{\partial \xi} + \frac{\gamma_3}{\gamma_0}\frac{\partial \bar{c}_0}{\partial \eta} +$$

$$- \frac{\gamma_4}{\gamma_0}\frac{w_s}{\bar{u}_s}\frac{\partial}{\partial \xi}\left(\frac{u_*}{\bar{u}_s}\frac{\partial \bar{c}_0}{\partial \xi}\right) - \frac{\gamma_4}{\gamma_0}\frac{w_s}{\bar{I}}\frac{\partial}{\partial \eta}\left(\frac{u_*}{\bar{I}}\frac{\partial \bar{c}_0}{\partial \eta}\right) \tag{4-119}$$

Eliminating $\bar{c}_0$ and $\bar{c}_1$ with (4-116) and (4-117) gives

$$c_{se} = c_s + \left(\frac{\gamma_1}{\gamma_0} - \frac{\alpha_1}{\alpha_0}\right)\frac{\partial c_s}{\partial \tau} + \left(\frac{\gamma_2}{\gamma_0} - \frac{\alpha_2}{\alpha_0}\right)\frac{\partial c_s}{\partial \xi} + \left(\frac{\gamma_3}{\gamma_0} - \frac{\alpha_3}{\alpha_0}\right)\frac{\partial c_s}{\partial \eta} +$$

$$- \left(\frac{\gamma_4}{\gamma_0} - \frac{\alpha_4}{\alpha_0}\right)\frac{w_s}{\bar{u}_s}\frac{\partial}{\partial \xi}\left(\frac{u_*}{\bar{u}_s}\frac{\partial c_s}{\partial \xi}\right) - \left(\frac{\gamma_4}{\gamma_0} - \frac{\alpha_4}{\alpha_0}\right)\frac{u_*}{\bar{I}}\frac{\partial}{\partial \eta}\left(\frac{w_s}{\bar{I}}\frac{\partial c_s}{\partial \eta}\right) \tag{4-120}$$

This is then the equation for c_s in which

$$c_{se} = \alpha_0 \bar{c}_e \tag{4-121}$$

After this equation has been solved $\bar{c}_0$ and $\bar{c}_1$ can be calculated by substituting c_s into equations (4-116) and (4-117), so the asymptotic solution is then completely determined.

$$c = \frac{a_0}{\alpha_0} c_s + \left(\frac{a_1}{\alpha_0} - \frac{\alpha_1}{\alpha_0}\frac{a_0}{\alpha_0}\right)\frac{\partial c_s}{\partial \tau} + \left(\frac{a_2}{\alpha_0} - \frac{\alpha_2}{\alpha_0}\frac{a_0}{\alpha_0}\right)\frac{\partial c_s}{\partial \xi} +$$

$$+ \left(\frac{a_3}{\alpha_0} - \frac{\alpha_3}{\alpha_0}\frac{a_0}{\alpha_0}\right)\frac{\partial c_s}{\partial \eta} - \left(\frac{a_4}{\alpha_0} - \frac{\alpha_4}{\alpha_0}\frac{a_0}{\alpha_0}\right)\frac{w_s}{\bar{u}_s}\frac{\partial}{\partial \xi}\left(\frac{u_*}{\bar{u}_s}\frac{\partial c_s}{\partial \xi}\right) +$$

$$- \left[\frac{a_4}{\alpha_0} - \frac{\alpha_4}{\alpha_0}\frac{a_0}{\alpha_0}\right] \frac{w_s}{I} \frac{\partial}{\partial\eta}\left[\frac{u_*}{I}\frac{\partial c_s}{\partial\eta}\right] \qquad (4\text{-}122)$$

The sediment transport rates in s- and n-direction are calculated by substituting the asymptotic solution into equation (4-15).

$$S_s = \bar{u}_s h c_s - \frac{w_s}{\bar{u}_s} u_* h \frac{\partial}{\partial\xi}\left\{\frac{\mu_0}{\alpha_0} c_s + \left[\frac{\mu_1}{\alpha_0} - \frac{\alpha_1}{\alpha_0}\frac{\mu_0}{\alpha_0}\right]\frac{\partial c_s}{\partial\tau} + \right.$$

$$+ \left[\frac{\mu_2}{\alpha_0} - \frac{\alpha_2}{\alpha_0}\frac{\mu_0}{\alpha_0}\right]\frac{\partial c_s}{\partial\xi} + \left[\frac{\mu_3}{\alpha_0} - \frac{\alpha_3}{\alpha_0}\frac{\mu_0}{\alpha_0}\right]\frac{\partial c_s}{\partial\eta} +$$

$$- \left[\frac{\mu_4}{\alpha_0} - \frac{\alpha_4}{\alpha_0}\frac{\mu_0}{\alpha_0}\right]\frac{w_s}{\bar{u}_s}\frac{\partial}{\partial\xi}\left[\frac{u_*}{\bar{u}_s}\frac{\partial c_s}{\partial\xi}\right] +$$

$$\left. - \left[\frac{\mu_4}{\alpha_0} - \frac{\alpha_4}{\alpha_0}\frac{\mu_0}{\alpha_0}\right]\frac{w_s}{I}\frac{\partial}{\partial\eta}\left[\frac{u_*}{I}\frac{\partial c_s}{\partial\eta}\right]\right\} \qquad (4\text{-}123)$$

$$S_n = Ih\left\{\frac{\beta_0}{\alpha_0} c_s + \left[\frac{\beta_1}{\alpha_0} - \frac{\alpha_1}{\alpha_0}\frac{\beta_0}{\alpha_0}\right]\frac{\partial c_s}{\partial\tau} + \left[\frac{\beta_2}{\alpha_0} - \frac{\alpha_2}{\alpha_0}\frac{\beta_0}{\alpha_0}\right]\frac{\partial c_s}{\partial\xi} + \right.$$

$$+ \left[\frac{\beta_3}{\alpha_0} - \frac{\alpha_3}{\alpha_0}\frac{\beta_0}{\alpha_0}\right]\frac{\partial c_s}{\partial\eta} - \left[\frac{\beta_4}{\alpha_0} - \frac{\alpha_4}{\alpha_0}\frac{\beta_0}{\alpha_0}\right]\frac{w_s}{\bar{u}_s}\frac{\partial}{\partial\xi}\left[\frac{u_*}{\bar{u}_s}\frac{\partial c_s}{\partial\xi}\right] +$$

$$\left. - \left[\frac{\beta_4}{\alpha_0} - \frac{\alpha_4}{\alpha_0}\frac{\beta_0}{\alpha_0}\right]\frac{w_s}{I}\frac{\partial}{\partial\eta}\left[\frac{u_*}{I}\frac{\partial c_s}{\partial\eta}\right]\right\} - \frac{w_s}{I} u_* h \frac{\partial}{\partial\eta}\left\{\frac{\mu_0}{\alpha_0} c_s + \right.$$

$$+ \left[\frac{\mu_1}{\alpha_0} - \frac{\alpha_1}{\alpha_0}\frac{\mu_0}{\alpha_0}\right]\frac{\partial c_s}{\partial\tau} + \left[\frac{\mu_2}{\alpha_0} - \frac{\alpha_2}{\alpha_0}\frac{\mu_0}{\alpha_0}\right]\frac{\partial c_s}{\partial\xi} +$$

$$+ \left[\frac{\mu_3}{\alpha_0} - \frac{\alpha_3}{\alpha_0}\frac{\mu_0}{\alpha_0}\right]\frac{\partial c_s}{\partial\eta} - \left[\frac{\mu_4}{\alpha_0} - \frac{\alpha_4}{\alpha_0}\frac{a_0}{\alpha_0}\right]\frac{w_s}{\bar{u}_s}\frac{\partial}{\partial\xi}\left[\frac{u_*}{\bar{u}_s}\frac{\partial c_s}{\partial\xi}\right] +$$

$$- \left(\frac{\mu_4}{\alpha_0} - \frac{\alpha_4}{\alpha_0}\frac{\mu_0}{\alpha_0}\right) \frac{w_s}{I} \frac{\partial}{\partial \eta}\left(\frac{u_*}{I}\frac{\partial c_s}{\partial \eta}\right)\Bigg\} \tag{4-124}$$

where

$$\beta_j = \int_0^1 q a_j \, d\zeta \tag{4-125}$$

$$\mu_j = \int_0^1 \epsilon'_s a_j \, d\zeta = \int_0^1 \epsilon'_n a_j \, d\zeta \tag{4-126}$$

In the original coordinate-system these equations become

$$c_{se} = c_s + \left(\frac{\gamma_1}{\gamma_0} - \frac{\alpha_1}{\alpha_0}\right)\frac{h}{w_s}\frac{\partial c_s}{\partial t} + \left(\frac{\gamma_2}{\gamma_0} - \frac{\alpha_2}{\alpha_0}\right)\frac{\bar{u}_s h}{w_s}\frac{\partial c_s}{\partial s} +$$

$$+ \left(\frac{\gamma_3}{\gamma_0} - \frac{\alpha_3}{\alpha_0}\right)\frac{Ih}{w_s}\frac{\partial c_s}{\partial n} - \left(\frac{\gamma_4}{\gamma_0} - \frac{\alpha_4}{\alpha_0}\right) h \frac{\partial}{\partial s}\left(\frac{u_* h}{w_s}\frac{\partial c_s}{\partial s}\right) +$$

$$- \left(\frac{\gamma_4}{\gamma_0} - \frac{\alpha_4}{\alpha_0}\right) h \frac{\partial}{\partial n}\left(\frac{u_* h}{w_s}\frac{\partial c_s}{\partial n}\right) \tag{4-127}$$

$$S_s = \bar{u}_s h c_s - u_* h^2 \frac{\partial}{\partial s}\Bigg\{\frac{\mu_0}{\alpha_0} c_s + \left(\frac{\mu_1}{\alpha_0} - \frac{\alpha_1}{\alpha_0}\frac{\mu_0}{\alpha_0}\right)\frac{h}{w_s}\frac{\partial c_s}{\partial t} +$$

$$+ \left(\frac{\mu_2}{\alpha_0} - \frac{\alpha_2}{\alpha_0}\frac{\mu_0}{\alpha_0}\right)\frac{\bar{u}_s h}{w_s}\frac{\partial c_s}{\partial s} + \left(\frac{\mu_3}{\alpha_0} - \frac{\alpha_3}{\alpha_0}\frac{\mu_0}{\alpha_0}\right)\frac{Ih}{w_s}\frac{\partial c_s}{\partial n} +$$

$$- \left(\frac{\mu_4}{\alpha_0} - \frac{\alpha_4}{\alpha_0}\frac{\mu_0}{\alpha_0}\right) h \frac{\partial}{\partial s}\left(\frac{u_* h}{w_s}\frac{\partial c_s}{\partial s}\right) +$$

$$- \left(\frac{\mu_4}{\alpha_0} - \frac{\alpha_4}{\alpha_0}\frac{\mu_0}{\alpha_0}\right) h \frac{\partial}{\partial n}\left(\frac{u_* h}{w_s}\frac{\partial c_s}{\partial n}\right)\Bigg\} \tag{4-128}$$

$$S_n = Ih\left\{\frac{\beta_0}{\alpha_0} c_s + \left[\frac{\beta_1}{\alpha_0} - \frac{\alpha_1}{\alpha_0}\frac{\beta_0}{\alpha_0}\right]\frac{h}{w_s}\frac{\partial c_s}{\partial t} + \left[\frac{\beta_2}{\alpha_0} - \frac{\alpha_2}{\alpha_0}\frac{\beta_0}{\alpha_0}\right]\frac{\bar{u}_s h}{w_s}\frac{\partial c_s}{\partial s} + \right.$$

$$+ \left[\frac{\beta_3}{\alpha_0} - \frac{\alpha_3}{\alpha_0}\frac{\beta_0}{\alpha_0}\right]\frac{Ih}{w_s}\frac{\partial c_s}{\partial n} - \left[\frac{\beta_4}{\alpha_0} - \frac{\alpha_4}{\alpha_0}\frac{\beta_0}{\alpha_0}\right] h \frac{\partial}{\partial s}\left[\frac{u_* h}{w_s}\frac{\partial c_s}{\partial s}\right] +$$

$$\left. - \left[\frac{\beta_4}{\alpha_0} - \frac{\alpha_4}{\alpha_0}\frac{\beta_0}{\alpha_0}\right] h \frac{\partial}{\partial n}\left[\frac{u_* h}{w_s}\frac{\partial c_s}{\partial n}\right]\right\} - u_*h^2 \frac{\partial}{\partial n}\left\{\frac{\mu_0}{\alpha_0} c_s + \right.$$

$$+ \left[\frac{\mu_1}{\alpha_0} - \frac{\alpha_1}{\alpha_0}\frac{\mu_0}{\alpha_0}\right]\frac{h}{w_s}\frac{\partial c_s}{\partial t} + \left[\frac{\mu_2}{\alpha_0} - \frac{\alpha_2}{\alpha_0}\frac{\mu_0}{\alpha_0}\right]\frac{\bar{u}_s h}{w_s}\frac{\partial c_s}{\partial s} +$$

$$+ \left[\frac{\mu_3}{\alpha_0} - \frac{\alpha_3}{\alpha_0}\frac{\mu_0}{\alpha_0}\right]\frac{Ih}{w_s}\frac{\partial c_s}{\partial n} - \left[\frac{\mu_4}{\alpha_0} - \frac{\alpha_4}{\alpha_0}\frac{\mu_0}{\alpha_0}\right] h \frac{\partial}{\partial s}\left[\frac{u_* h}{w_s}\frac{\partial c_s}{\partial s}\right] +$$

$$\left. - \left[\frac{\mu_4}{\alpha_0} - \frac{\alpha_4}{\alpha_0}\frac{\mu_0}{\alpha_0}\right] h \frac{\partial}{\partial n}\left[\frac{u_* h}{w_s}\frac{\partial c_s}{\partial n}\right]\right\} \qquad (4\text{-}129)$$

4.5.2 Profile Functions and the Coefficients in the Model

In order to apply the depth-integrated model developed here the knowledge of the coefficients γ_j, α_j, β_j and μ_j is required. All coefficients are related to the profile functions a_j. In order to determine the coefficients in the model these profile functions have to be determined first. The analytical expressions for the profile functions as well as the coefficients are already given in the text. It should be noticed that all the profile functions are determined by four elementary profile functions, viz.

- the normalized equilibrium concentration profile a_0,
- the normalized main flow velocity profile p,
- the normalized secondary flow velocity profile q,
- the normalized horizontal diffusion coefficient ϵ'_s.

These elementary profile functions depends on the parameter $\beta=z_a/h$, in addition to which a_0 depends also on the parameter w_s/u_*, and p depends on the parameter $\bar{u}_s/u_*$. These three dimensionless parameters are the elementary parameters of the model. All profile functions in the model can be determined when these three parameters are known. Thus all coefficients in the model are functions of these three parameters. When the model is applied the parameter β is usually kept constant, so the coefficients are then only functions of the parameters w_s/u_* and $\bar{u}_s/u_*$.

The profile functions a_j are determined with the numerical procedure described by Galappatti (1983). The description of this procedure is not repeated here. Only some results are reported. In fig.4.3 the four elementary profile functions are shown, while fig.4.4 depicts the first order profile functions in the model.

When the profile functions in the model are determined the coefficients are easily obtained. Some examples of the coefficients in the model are shown in fig.4.5.

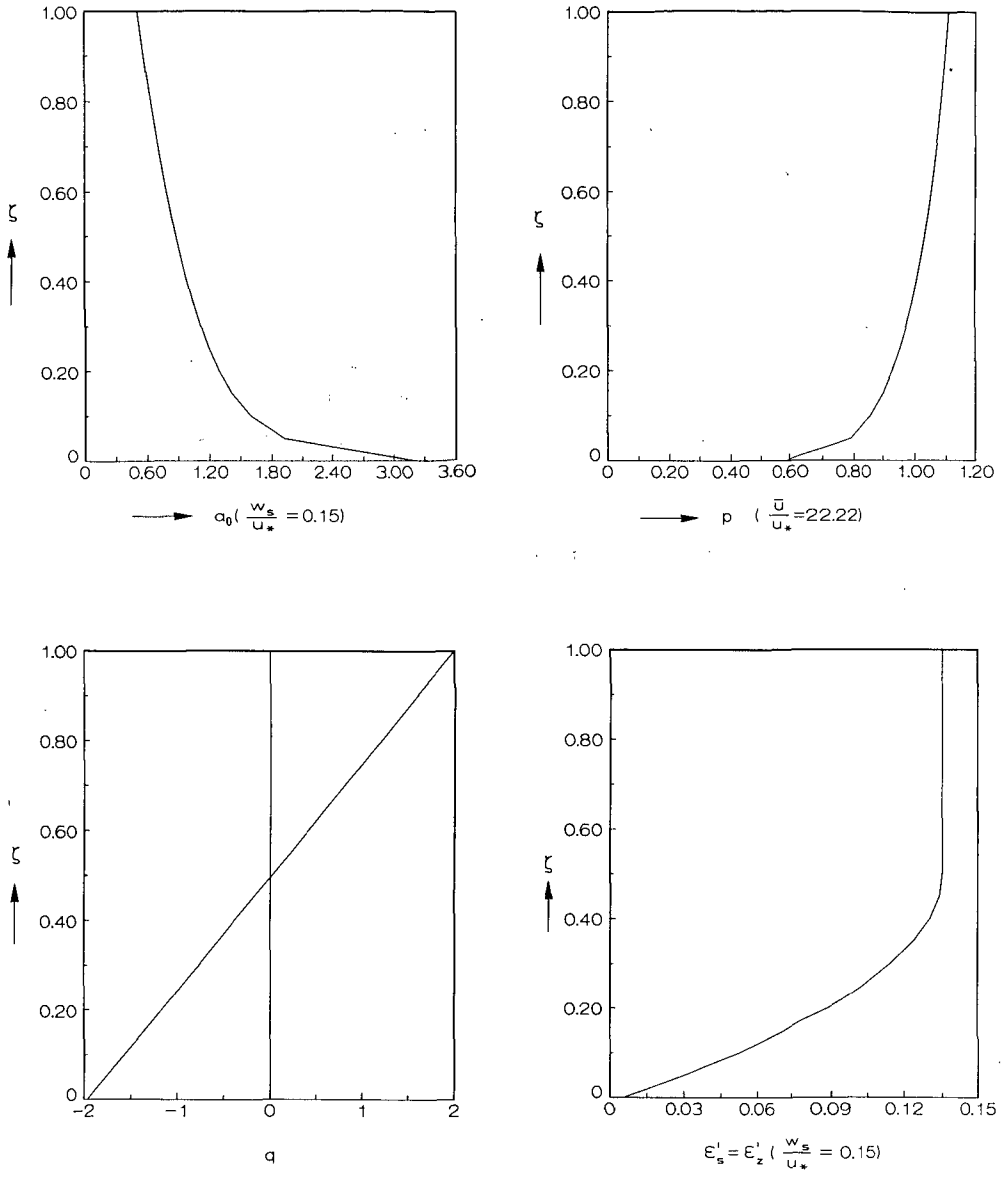

Fig.4.3 The four elementary profile functions in the model (β=0.01)

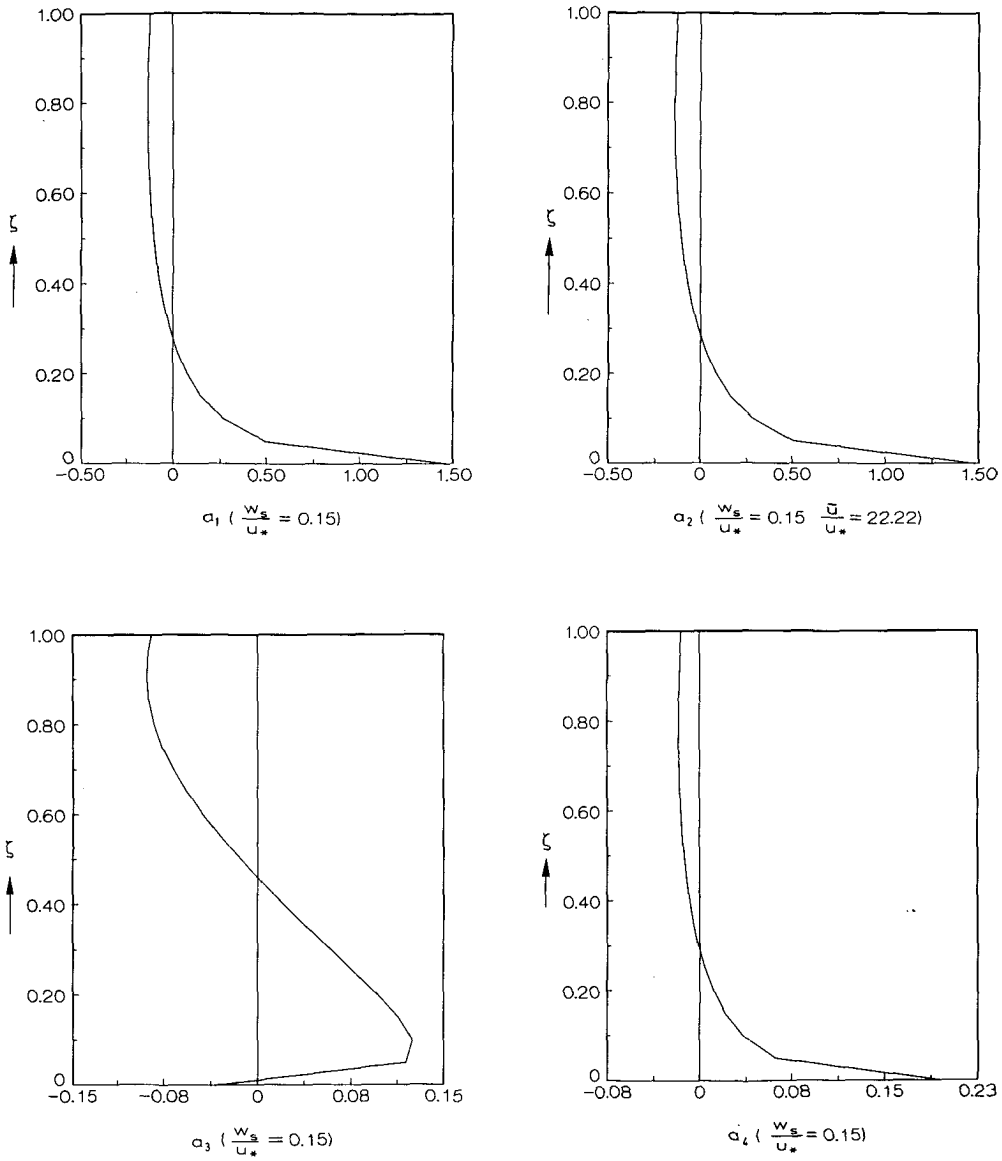

Fig.4.4 The first order profile functions with β=0.01, $\frac{w_s}{u_*} = 0.15$, and $\frac{\bar{u}}{u_*} = 22.22$

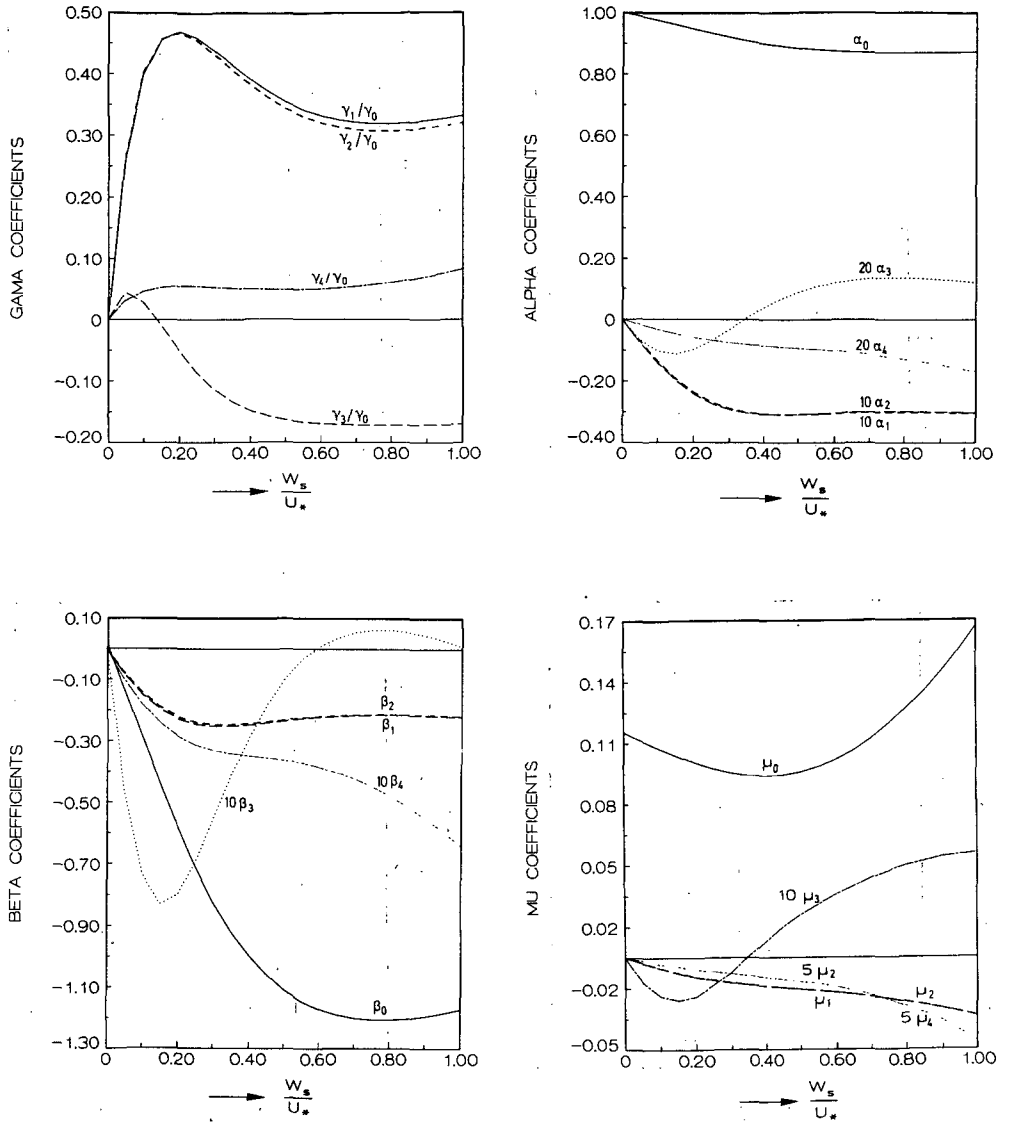

Fig.4.5 The coefficients in the model. $\frac{\bar{u}}{u_*} = 25$ $\beta = 0.01$

4.6 Influence of the Secondary Flow and Horizontal Diffusion

4.6.1 General

Compared with the two-dimensional problem there are two new components in the present three-dimensional problem, i.e. the secondary flow and the horizontal diffusion. In fact the horizontal diffusion is also present in the two-dimensional problem but it has been neglected (Galappatti, 1983).

Two influences of the secondary flow and the horizontal diffusion have to be distinguished, viz. the influence on the concentration field and the influence on the transport field. That one of the influences is negligible does not necessarily imply that the other one can also be neglected.

The influences of both the secondary flow and the horizontal diffusion are studied by analyzing the magnitude of the terms in the corresponding equations in the following subsection. In 4.6.3 the behaviour of the depth-integrated model with respect to the secondary flow and the horizontal diffusion is further analysed.

4.6.2 Analyzing the Equations

Mathematically the significance of the secondary flow and/or the horizontal diffusion for the concentration field and the transport field is represented by the importance of the corresponding terms in the following equations.

$$\frac{\partial c}{\partial t} + u_s \frac{\partial c}{\partial s} + u_n \frac{\partial c}{\partial n} - \frac{\partial}{\partial s}\left(\epsilon_s \frac{\partial c}{\partial s}\right) - \frac{\partial}{\partial n}\left(\epsilon_n \frac{\partial c}{\partial n}\right) = w_s \frac{\partial c}{\partial z} + \frac{\partial}{\partial z}\left(\epsilon_z \frac{\partial c}{\partial z}\right) \quad (4\text{-}130)$$

$$S_s = \int_{z_a+z_b}^{z_b+D} u_s c \, dz - \int_{z_a+z_b}^{z_b+D} \epsilon_s \frac{\partial c}{\partial s} \quad (4\text{-}131)$$

$$S_n = \int_{z_a+z_b}^{z_b+D} u_n c \, dz - \int_{z_a+z_b}^{z_b+D} \epsilon_n \frac{\partial c}{\partial n} \quad (4\text{-}132)$$

The importance of the different terms in these equations can be examined by comparing their order of magnitude. Suppose that the flow under consideration can be characterized by the following scales

L_s = length scale in the main flow direction,
L_n = length scale in the normal direction,
H = length scale in the vertical direction,
T = time scale,
U_s = scale for the main flow velocity,
U_n = scale for the secondary flow velocity,
E_H = scale for the horizontal diffusion coefficients,
E_v = scale for the vertical diffusion coefficient:

The convection-diffusion equation (4-130) may then be made dimensionless as follows:

$$\frac{H}{w_s T}\frac{\partial c}{\partial t'} + \frac{HU_s}{L_s w_s} u_s' \frac{\partial c}{\partial s'} + \frac{HU_n}{L_n w_s} u_n' \frac{\partial c}{\partial n'} - \frac{E_H H}{w_s L_s^2}\frac{\partial}{\partial s'}\left(\epsilon_s' \frac{\partial c}{\partial s'}\right) +$$

$$- \frac{E_H H}{w_s L_n^2}\frac{\partial}{\partial n'}\left(\epsilon_n' \frac{\partial c}{\partial n'}\right) = \frac{\partial c}{\partial z'} + \frac{E_v}{w_s H}\frac{\partial}{\partial z'}\left(\epsilon_z' \frac{\partial c}{\partial z'}\right) \qquad (4\text{-}133)$$

where all quantities marked with a prime have been made dimensionless with the corresponding scale.

The principal assumption on which the asymptotic solution is based implies that the two terms on the right hand side have the same order of magnitude and that all terms on the left hand side are an order smaller in magnitude than the two terms on the right hand side, thus

$$\frac{E_v}{w_s H} \sim 1 \quad (\sim \text{reads has the order of magnitude of}) \qquad (4\text{-}134)$$

$$\frac{H}{w_s T} \sim \frac{HU_s}{L_s w_s} \sim \frac{HU_n}{L_n w_s} \sim \frac{E_H H}{w_s L_n^2} \sim \delta \frac{E_v}{w_s H} \qquad (4\text{-}135)$$

with $\delta \ll 1$

It should be noted that the diffusion term in the main flow direction is in general much smaller than the other terms, since $L_s \gg L_n$. However, if this term is not taken into account while the diffusion term in the normal direction is taken into account the diffusion tensor in the horizontal plane is no longer isotropic. This may cause complexities in the numerical modelling. Therefore only the diffusion term in the normal direction is considered in the analysis but both horizontal diffusion terms are always taken into account or neglected together.

In order to examine the importance of the secondary flow and the horizontal diffusion the convection term in n-direction and the horizontal diffusion term are compared with the longitudinal convective term.

The ratio between the two convective terms is

$$\frac{HU_n}{L_n w_s} : \frac{HU_s}{L_s w_s} = \frac{U_n L_s}{U_s L_n} \tag{4-136}$$

From the secondary flow model described in the previous chapter it follows that

$$\frac{U_n}{U_s} \sim \frac{H}{R} \tag{4-137}$$

where R is the radius of curvature. So the ratio in (4-136) becomes

$$\frac{U_n L_s}{U_s L_n} = \frac{H}{R} \frac{L_s}{L_n} = \frac{L_s}{R} \frac{H}{L_n} \tag{4-138}$$

For the length scale in the main flow direction it is reasonable to assume that $L_s \sim R$, and for the length scale in the normal direction the river width B may be taken, so the ratio becomes H/B which is small in the cases considered in this study. According to Booij and Kalkwijk (1982) the secondary flow model described in chapter 3 may not even be used unless

H/B<1/15. The conclusion is thus that the influence of the secondary flow on the concentration field can in general be neglected.

The importance of the diffusion term is examined by comparing it with the convective term in the normal direction.

$$\frac{E_H}{w_s L_n}\frac{H}{L_n} : \frac{U_n H}{w_s L_n} = \frac{E_H}{U_n H}\frac{H}{L_n} \tag{4-139}$$

It is reasonable to assume that $E_H \sim U_* H$ and $U_n \sim U_*$ so $E_H/U_n H \sim 1$, thus the diffusion term is even unimportant compared with the convective term in the normal direction. Therefore it can be concluded that the influence of the horizontal diffusion on the concentration field is negligible.

The influence of the secondary flow and the horizontal diffusion on the sediment transport field is represented by the transport component in the normal direction S_n. Compared with the transport rate in the main flow direction S_s this is in general small since

$$\frac{S_n}{S_s} \sim \frac{U_n}{U_s} \ll 1 \tag{4-140}$$

However, the component S_n causes a deviation of the direction of the transport vector to the main flow direction. This deviation, although small, can have striking effects on the morphology for e.g. river bends. Besides it is relatively easy to take the influence of both the secondary flow and the horizontal diffusion on the transport field into account. Therefore this influence should be taken into account earlier than the influence on the concentration field.

The significance of the secondary flow and the horizontal diffusion can also be examined by comparing the order of magnitude in the depth integrated equations (4-127) through (4-129). The comparison can be carried out in the same way as above, so it is not described here in detail. Only the conclusions from this comparison are summarized in the following.

* In the concentration equation (4-127) the secondary flow term as well as the horizontal diffusion terms are not important compared with the convection term in the main flow direction. This agrees with the conclusion drawn above.

* In the equation (4-128) for the transport rate in the main flow direction the terms due to the horizontal diffusion can be neglected. So this equation can be simplified as

$$S_s = \bar{u}_s h c_s \tag{4-141}$$

* In the equation (4-129) for the transport in the normal direction the first order terms in the diffusion part can be neglected. Thus this equation can be simplified as

$$S_n = Ih\left\{\frac{\beta_0}{\alpha_0} c_s + \left[\frac{\beta_1}{\alpha_0} - \frac{\alpha_1}{\alpha_0}\frac{\beta_0}{\alpha_0}\right] \frac{h}{w_s} \frac{\partial c_s}{\partial t} + \left[\frac{\beta_2}{\alpha_0} - \frac{\alpha_2}{\alpha_0}\frac{\beta_0}{\alpha_0}\right] \frac{\bar{u}_s h}{w_s} \frac{\partial c_s}{\partial s} + \right.$$

$$+ \left[\frac{\beta_3}{\alpha_0} - \frac{\alpha_3}{\alpha_0}\frac{\beta_0}{\alpha_0}\right] \frac{Ih}{w_s} \frac{\partial c_s}{\partial n} - \left[\frac{\beta_4}{\alpha_0} - \frac{\alpha_4}{\alpha_0}\frac{\beta_0}{\alpha_0}\right] h \frac{\partial}{\partial s}\left[\frac{u_* h}{w_s} \frac{\partial c_s}{\partial s}\right] +$$

$$\left. - \left[\frac{\beta_4}{\alpha_0} - \frac{\alpha_4}{\alpha_0}\frac{\beta_0}{\alpha_0}\right] h \frac{\partial}{\partial n}\left[\frac{u_* h}{w_s} \frac{\partial c_s}{\partial n}\right]\right\} - u_*^2 h^2 \frac{\mu_0}{\alpha_0} \frac{\partial}{\partial n} c_s \tag{4-142}$$

4.6.3 The Behaviour of the Depth Integrated Model with Respect to the Secondary Flow and Horizontal Diffusion

In this subsection the behaviour of the depth integrated model with respect to the secondary flow and horizontal diffusion is analysed. The main purpose of this analysis is to gain some insight into the interaction of the influences of the secondary flow and the horizontal diffusion.

In order to simplify the problem a steady uniform main flow (e.g. a circulating flow field with closed streamlines) is considered. For this situation

$$L[\ ] = q \frac{\partial}{\partial \eta} - \frac{w_s}{I} \frac{\partial}{\partial \eta}\left(\frac{u_*}{I} \epsilon'_n \frac{\partial}{\partial \eta}\right) \qquad (4\text{-}143)$$

Further the velocity of the main flow, which is not involved in the present problem, is assumed to be uniformly distributed over the vertical (p=1). The first order solution in the present model is then the same as that in the model of Galappatti (1983).

In the previous subsection it has been shown that the diffusion term in equation (4-143) is relatively unimportant compared with the convective term. However, the two terms may interact with each other, therefore the significance of the horizontal diffusion term is reconsidered.

The equation for the mean concentration $\bar{c}$ (=c_s in this case) with and without the diffusion term are respectively

$$\bar{c}_e = \bar{c} + \frac{\gamma_3}{\gamma_0} \frac{\partial \bar{c}}{\partial \eta} \qquad \text{(without diffusion)} \qquad (4\text{-}144)$$

$$\bar{c}_e = \bar{c} + \frac{\gamma_3}{\gamma_0} \frac{\partial \bar{c}}{\partial \eta} - \frac{\gamma_4}{\gamma_0} \frac{w_s u_*}{I^2} \frac{\partial^2 \bar{c}}{\partial \eta^2} \qquad \text{(with diffusion)} \qquad (4\text{-}145)$$

If $\bar{c}_e$ and the γ coefficients are constant then the solution of the two equations are respectively.

$$\bar{c} = \bar{c}_e + A \exp(\lambda \eta) \qquad \text{(without diffusion)} \qquad (4\text{-}146)$$

$$\bar{c} = \bar{c}_e + A \exp(\lambda_1 \eta) + B \exp(\lambda_2 \eta) \qquad \text{(with diffusion)} \qquad (4\text{-}147)$$

The constants A and B have to be determined from the boundary conditions. Obviously two adaptation lengths are found when the diffusion term is taken into account while only one adaptation length is found if the diffusion term is neglected. The exponential coefficients λ, λ_1 and λ_2 are respectively shown in fig.4.6 and fig.4.7. Comparison shows that the difference between the two figures is very large. This means that taking the diffusion term into account can influence the solution in the depth-integrated model

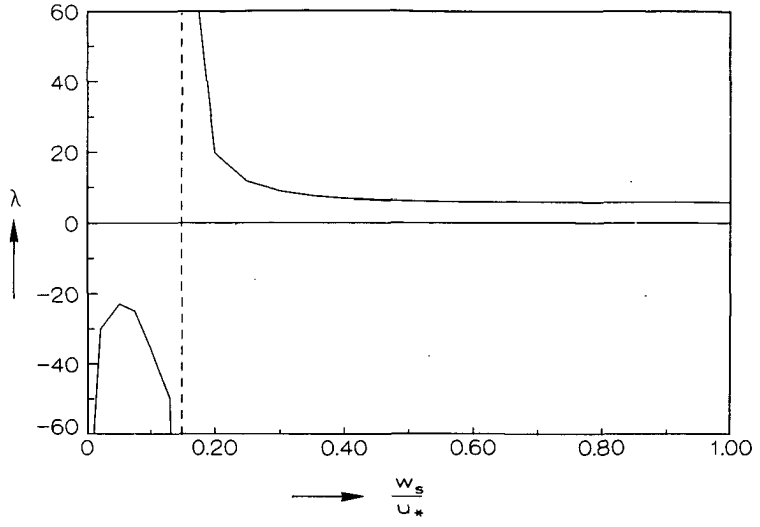

Fig.4.6 The first order solution without horizontal diffusion

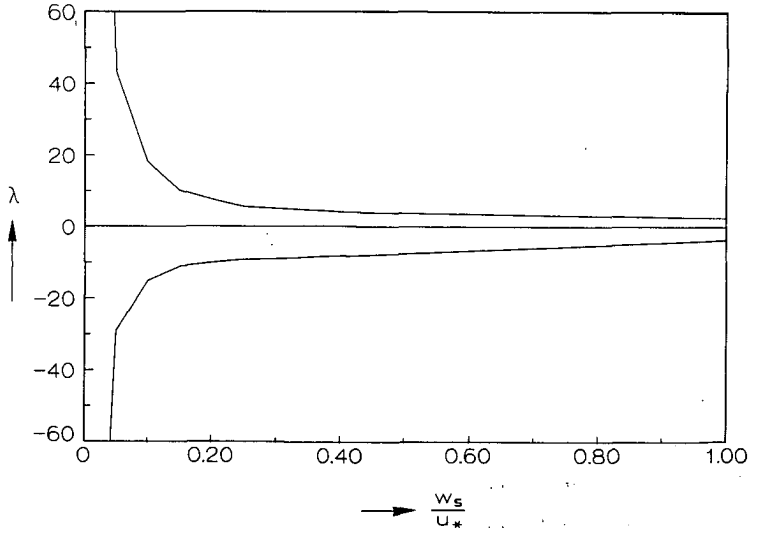

Fig.4.7 The first order solution with horizontal diffusion ($u_*/I = 1$, $\beta = 0.01$)

significantly even though the diffusion term has a relatively small magnitude.

Remark :

When the second order solution is applied two adaptation lengths are found even without the diffusion term. This is illustrated in fig.4.8 with the model of Galappatti (1983). For the second order solution the influence of the diffusion term is probably less important. However, the second order solution is further not considered since it is not applied in practice.

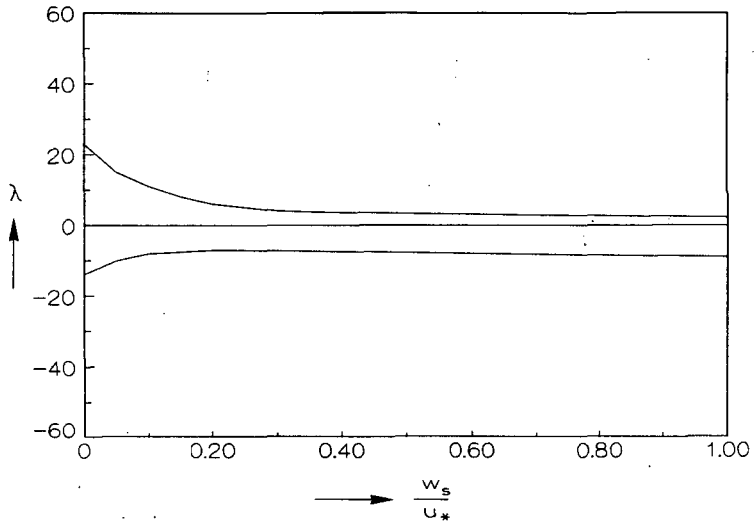

Fig.4.8 Second order solution without horizontal diffusion

It is remarkable that λ changes sign at a certain value of w_s/u_*. Obviously the sign of λ represents the direction of the convection velocity in the mean concentration equation. Direct integration of the original convection-diffusion equation over the depth (see 4.2.6) shows that the convection velocity should have the direction of the sediment transport. The secondary flow has a small mean velocity in the direction of the flow in the upper half of the depth because the bed boundary is at a small distance above the

bed. So for small w_s/u_* the transport in n-direction will be positive. For larger value of w_s/u_* the transport will change sign because of the non-uniform distribution of the concentration over the depth. The sign of λ agrees with this tendency.

Obviously the diffusion term should be taken into account in the first order solution if the secondary flow is taken into account. It is interesting to know whether this applies also to the exact model. The exact form of the original convection-diffusion equation without horizontal diffusion term is:

$$q \frac{\partial c}{\partial \eta} = D[c] \tag{4-148}$$

The solution of this equation can be written as

$$c = \sum_j A_j \phi_j(\zeta) \exp(\lambda_j \eta) \tag{4-149}$$

where A_j are constant coefficients while λ_j and ϕ_j are respectively eigenvalues and eigenfunctions of the following problem

$$D[\phi] = \lambda q\phi \tag{4-150a}$$

$$\phi(0) = 0 \tag{4-150b}$$

$$\left[\phi + \epsilon'_z \frac{\partial \phi}{\partial \zeta}\right]_{\zeta=1} = 0 \tag{4-150c}$$

It should be noted that the secondary flow velocity changes direction in the middle of the depth. This means that the "upstream" boundary of the upper half and the lower half of the flow are at the different places. When the original convection-diffusion equation is solved the boundary conditions should be applied at two different sides for the two halves of the flow. Based on such a simple physical consideration it is concluded that the eigenvalues λ_j can be divided in two groups, one group with positive real parts and the other group with negative real parts, although it is not mathematically proved. It is thus clear that the diffusion term in the original equation will not influence the solution significantly if its magnitude is not very large. The significant influence of the horizontal

diffusion term is due to the shortcoming of depth-integrated modelling that only the first order solution is applied.

To illustrate the behaviour of the different models further the following artificial case is considered (fig.4.9). The flow is uniform with a linear velocity distribution. The vertical diffusion coefficient is constant over the depth.

$$\epsilon_z = 0.1\, u_* D \qquad (4\text{-}151)$$

The bed boundary condition is applied at the bottom z=0. This is allowed for this case because the vertical diffusion coefficient does not vanish at the bottom. Also the horizontal diffusion coefficient is supposed to be constant in the whole area, having the same value as the vertical diffusion coefficient unless it is set to zero.

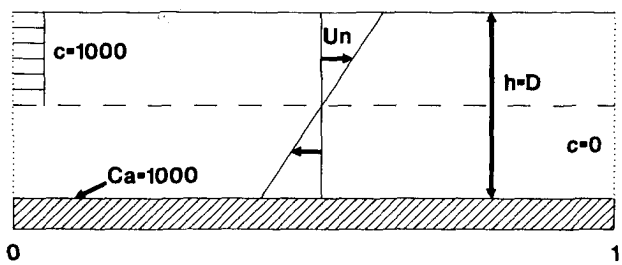

Fig.4.9 Situation sketch

It can be shown that this problem is completely characterized by two parameters, viz.

$$\frac{w_s}{u_*} \quad \text{and} \quad \frac{\epsilon_n}{Ih}$$

A simple numerical model is set up to calculate the two-dimensional solution. The upstream boundary conditions as well as the bed boundary condition for this two dimensional model are shown in fig.4.9. When ϵ_n is

not equal to zero the following condition is applied at the outflow boundaries.

$$\frac{\partial^2 c}{\partial \eta^2} = 0 \qquad (4\text{-}152)$$

The two-dimensional numerical result is compared with the depth-integrated model in fig.4.10 and fig.4.11 for two cases. It should be noted that for the depth-integrated model it is not clear what the upstream boundary conditions are. Therefore the mean concentration computed from the two-dimensional model is applied.

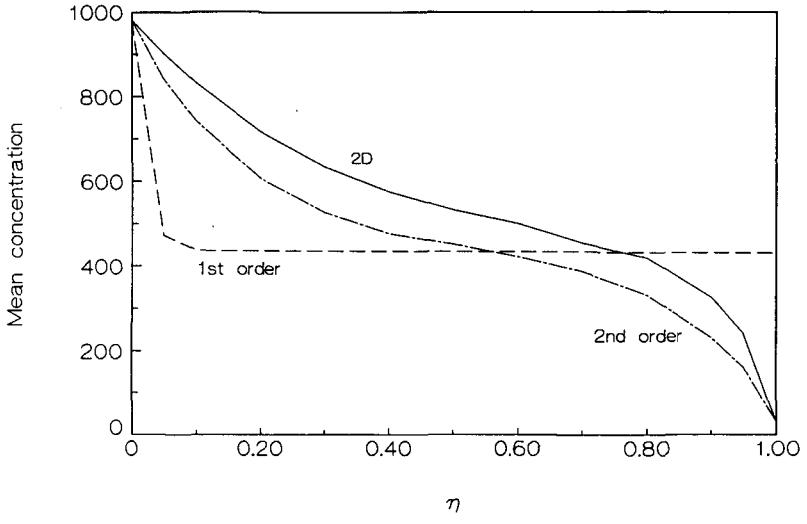

Fig.4.10 Comparison between the solutions
$\epsilon_n = 0$, $\frac{w_s}{u_*} = 0$

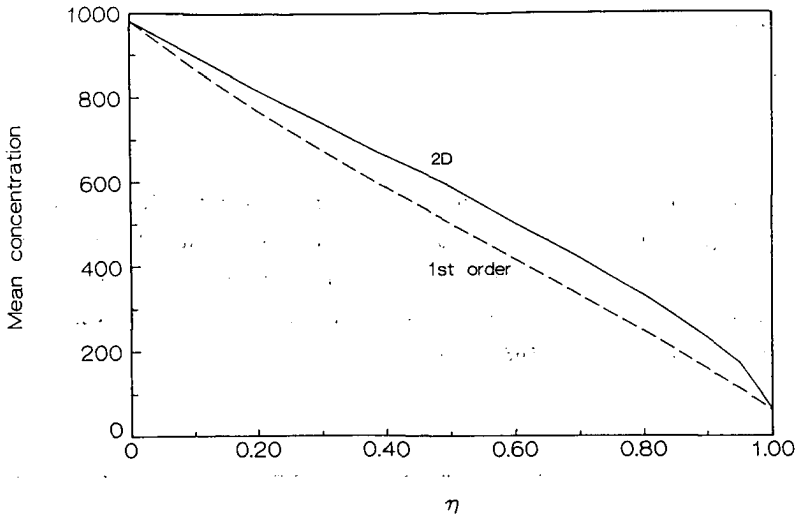

Fig.4.11 Comparison between the solutions
$\frac{\epsilon_n}{Ih} = 1.0 \quad \frac{w_s}{u_*} = 0.2$

The following conclusions are drawn from this exercise.

* The result of the depth-integrated model agrees better with the two dimensional solution when the horizontal diffusion coefficient is larger.

* The difference between the first order solution and the second order solution is large when the horizontal diffusion is not taken into account. The second order solution is acceptable.

* If the horizontal diffusion term is taken into account the first order solution is acceptable.

Chapter 5 THEORETICAL ANALYSIS

5.1 Introduction

In the previous chapter a general asymptotic solution is developed for the convection-diffusion equation. From this solution a series of depth-integrated models for the suspended sediment transport can be developed. All these models are easier to be applied and less sophisticated than the fully three-dimensional model but more complicated and sophisticated than the simple transport formula. Before a depth-integrated model can be chosen and applied the following questions should be answered first.

a) Is the depth-integrated model sufficiently accurate to replace the three-dimensional model?

b) Is it worthwhile to apply the depth-integrated model replacing the simple transport formula?

In this chapter attempts are made to answer these questions by means of a theoretical analysis. Based on the results of the analysis a choice is also made from the different models. The following section gives an analysis on the behaviour of the exact solution of the convection-diffusion equation. In section 5.3 the convergence of the asymptotic solution is studied. The morphological behaviour of the models is investigated in section 5.4 followed by a comparison of the different models in section 5.5. Finally in section 5.6 the applicability of the models is further discussed and a choice is then made.

For reasons of simplicity the flow velocity is assumed to be uniformly distributed in the vertical ($p=1$), unless otherwise specified. Under this assumption the first order solution presented in section 4.5 is the same as the first order solution of Galappatti (1983) when the two-dimensional case is considered.

5.2 Behaviour of the Exact Model

According to the three-dimensional model (the exact model) the sediment concentration field has to satisfy

* the convection-diffusion equation,

$$L[c] = D[c] \tag{5-1}$$

* the boundary conditions corresponding to the operator D[ ], i.e. the water surface boundary condition and the bed boundary condition (the concentration type is chosen as example for the analysis in this chapter),

$$\left[c + \epsilon' \frac{\partial c}{\partial \zeta}\right]_{\zeta=1} = 0 \tag{5-2}$$

$$c(\zeta=0) = \gamma_{11} \bar{c}_e \tag{5-3}$$

* the boundary conditions corresponding to the operator L[ ] i.e. the initial condition and the upstream boundary condition,

$$c(0,\xi,\eta,\zeta) = c_{\tau=0}(\xi,\eta,\zeta) \tag{5-4}$$

$$c(\tau,0,\eta,\zeta) = c_{\xi=0}(\tau,\eta,\zeta) \tag{5-5}$$

$$c(\tau,\xi,0,\zeta) = c_{\eta=0}(\tau,\xi,\zeta) \tag{5-6}$$

* Further when the horizontal diffusion is taken into account some weak conditions have to be applied at the downstream boundary. However, it is assumed that these conditions will not influence the solution significantly, therefore they are not considered in this chapter.

It should be noted that equation (5-1) and (5-2) are the same for all problems and for a particular case the concentration field is completely determined by the conditions (5-3) through (5-6). The concentration field

consists of two parts, one contributed by the initial and upstream boundary condition and the other by the bed boundary condition. For the analysis on the convergence of the asymptotic solutions it is convenient to make a distinction between these two contributions. Mathematically this distinction can be formulated as follows.

$$c(\tau,\xi,\eta,\zeta) = c_I + c_{II} \tag{5-7}$$

c_I is due to the bed boundary condition. It satisfies the convection-diffusion equation (5-1) and the boundary conditions corresponding to the operator D[ ] (5-2) and (5-3) in the whole τ-ξ-η space ($-\infty<\tau,\xi,\eta<\infty$)

$$L[c_I] = D[c_I] \tag{5-8a}$$

$$\left[c_I + \epsilon' \frac{\partial c_I}{\partial \zeta}\right]_{\zeta=1} = 0 \tag{5-8b}$$

$$c_I(\zeta=0) = \gamma_{11}\bar{c}_e \tag{5-8c}$$

Remark :

The extension of the domain to the whole τ-ξ-η space implies the assumption that the bed boundary condition ($\bar{c}_e$) is differentiable to τ, ξ and η up to infinite order at the corresponding boundaries.

c_{II} is due to the initial and upstream boundary conditions. It satisfies the convection-diffusion equation, the boundary conditions corresponding to the operator D[ ] in homogeneous form, and the adapted initial and upstream boundary conditions.

$$L[c_{II}] = D[c_{II}] \tag{5-9a}$$

$$\left[c_{II} + \epsilon' \frac{\partial c_{II}}{\partial \zeta}\right]_{\zeta=1} = 0 \tag{5-9b}$$

$$c_{II}(\zeta=0) = 0 \tag{5-9c}$$

$$c_{II}(0,\xi,\eta,\zeta) = c(0,\xi,\eta,\zeta) - c_I(0,\xi,\eta,\zeta) \tag{5-9d}$$

$$c_{II}(\tau,0,\eta,\zeta) = c(\tau,0,\eta,\zeta) - c_I(\tau,0,\eta,\zeta) \tag{5-9e}$$

$$c_{II}(\tau,\xi,0,\zeta) = c(\tau,\xi,0,\zeta) - c_I(\tau,\xi,0,\zeta) \tag{5-9f}$$

It is not difficult to verify that (5-7) is the solution of the original problem (5-1)...(5-6).

The contribution of the bed boundary condition c_I will be the complete solution if the complete τ-ξ-η space is taken into consideration. Therefore c_I will also be called the dynamic equilibrium concentration. c_{II} is in fact due to the deviation of the actual concentration field from this dynamic equilibrium concentration at the boundaries. Further c_{II} is only important near these boundaries. It is thus a kind of boundary layer.

In order to clarify the problem further the simple case

$$L[\ ] = \frac{\partial}{\partial\tau} \tag{5-10}$$

is considered as an example. For this case it can be shown that

$$c_{II} = \sum_{j=1}^{\infty} A_j \exp(\lambda_j \tau)\phi_j(\zeta) \tag{5-11}$$

or

$$\bar{c} = \bar{c}_I + \sum_{j=1}^{\infty} B_j \exp(\lambda_j \tau) \tag{5-12}$$

where A_j, B_j and λ_j are constant coefficients, $\phi_j(\zeta)$ are profile functions and $\bar{c}_I(\tau)$ is completely determined by the function $\bar{c}_e(\tau)$.

There are thus two kind of time scales in this simple problem. The first kind is the time scale characterizing the variation of $\bar{c}_e(\tau)$ and the second kind is the time scale inherent in the system itself characterized by the exponential coefficients λ_j.

For the general case

$$L[\ ] = \frac{\partial}{\partial\tau} + p(\zeta)\ \frac{\partial}{\partial\xi} + q(\zeta)\ \frac{\partial}{\partial\eta} \qquad (5\text{-}13)$$

there is another kind of time and/or length scales characterizing the variation of the initial and upstream boundary conditions.

To analyse the asymptotic solutions all three kinds of time and/or length scales have to be considered. However, as will be shown later, all can be investigated in a similar way.

5.3 Convergence of the Asymptotic Solutions

5.3.1 Convergence Radius (A Simple Case)

Consider the case

$$L[\ ] = \frac{\partial}{\partial\tau} \qquad (5\text{-}14)$$

with the following bed boundary condition

$$\gamma_{11}\bar{c}_e = \exp(\alpha\tau) \qquad (5\text{-}15)$$

where α is a complex coefficient.

The exact solution for the the dynamical equilibrium concentration in this case can be written as

$$c = f(\zeta)\exp(\alpha\tau) \qquad (5\text{-}16)$$

where $f(\zeta)$ is the solution of the following boundary value problem:

$$D[f] = \alpha f \qquad (5\text{-}17a)$$

$$\left[f + \epsilon'\frac{\partial f}{\partial\zeta}\right]_{\zeta=1} = 0 \qquad (5\text{-}17b)$$

$$f(0) = \gamma_{11} \tag{5-17c}$$

The mean concentration is obtained by integrating equation (5-16)

$$\bar{c} = \exp(\alpha\tau) \int_0^1 f(\zeta)\, d\zeta \tag{5-18}$$

According to the model of Galappatti the mean concentration is governed by

$$\gamma_{11}\bar{c} + \gamma_{21}\frac{\partial \bar{c}}{\partial \tau} + \ldots\ldots + \gamma_{n+1,1}\frac{\partial^n \bar{c}}{\partial \tau^n} = \exp(\alpha\tau) \tag{5-19}$$

The dynamical equilibrium concentration is then the particular solution of this equation.

$$\bar{c} = \frac{\exp(\alpha\tau)}{\sum_{i=1}^{n+1}\gamma_{i1}\alpha^{i-1}} \tag{5-20}$$

The conventional asymptotic solution for this case is (see eq(4-71))

$$\bar{c} = \sum_{j=1}^{n+1}\delta_{j1}\frac{\partial^{j-1}\bar{c}_e}{\partial \tau^{j-1}} = \exp(\alpha\tau)\sum_{j=1}^{n+1}\delta_{j1}\alpha^{j-1} \tag{5-21}$$

It is clear that the asymptotic solution (5-20) and (5-21) will converge if and only if the series in these two equations converge. Both series are power series, so a convergence radius R_α can be defined for each solution.

$$R_\alpha = \lim_{j\to\infty}\left|\frac{\gamma_{j-1,1}}{\gamma_{j,1}}\right| \quad \text{for the model of Galappatti} \tag{5-22}$$

$$R_\alpha = \lim_{j\to\infty}\left|\frac{\delta_{j-1,1}}{\delta_{j,1}}\right| \quad \text{for the conventional model} \tag{5-23}$$

It should be noted that α represents a time scale of the variation of the bed boundary condition which is related to the variation of the flow. That the asymptotic solution is only convergent if $|\alpha| < R_\alpha$ means in fact that

the depth-integrated models are only valid for relatively slowly varying flow or when the time scale is relatively large, as can be expected.

From a mathematical analysis (Wang, 1984) it can be shown that the limit in (5-22) is equal to the absolute value of the largest eigenvalue of the following problem.

$$D[\phi] = \lambda\phi \tag{5-24a}$$

$$\left[\phi + \epsilon'\frac{\partial\phi}{\partial\zeta}\right]_{\zeta=1} = 0 \tag{5-24b}$$

$$\int_0^1 \phi(\zeta)\, d\zeta = 0 \tag{5-24c}$$

For the case that ϵ' is constant this eigenvalue is

$$\lambda_1 = \frac{-(1+4\pi^2\epsilon'^2)}{4\epsilon'} \tag{5-25}$$

Analogously the limit in equation (5-23) is equal to the absolute value of the largest eigenvalue of the following problem.

$$D[\phi] = \lambda\phi \tag{5-26a}$$

$$\left[\phi + \epsilon'\frac{\partial\phi}{\partial\zeta}\right]_{\zeta=1} = 0 \tag{5-26b}$$

$$\phi(0) = 0 \tag{5-26c}$$

For the case that ϵ' is constant this eigenvalue is

$$\lambda_1 = \frac{-(1+4b_1^2\epsilon'^2)}{4\epsilon'} \tag{5-27}$$

where b_1 is the smallest positive root of the equation (see fig.5.1)

$$tg(b) = -2\epsilon' b \tag{5-28}$$

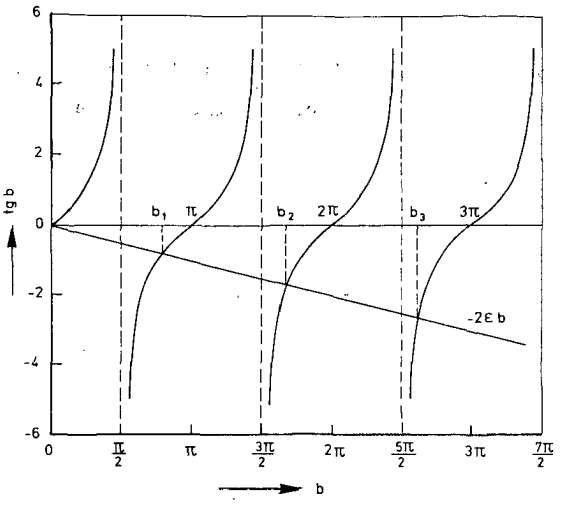

Fig.5.1

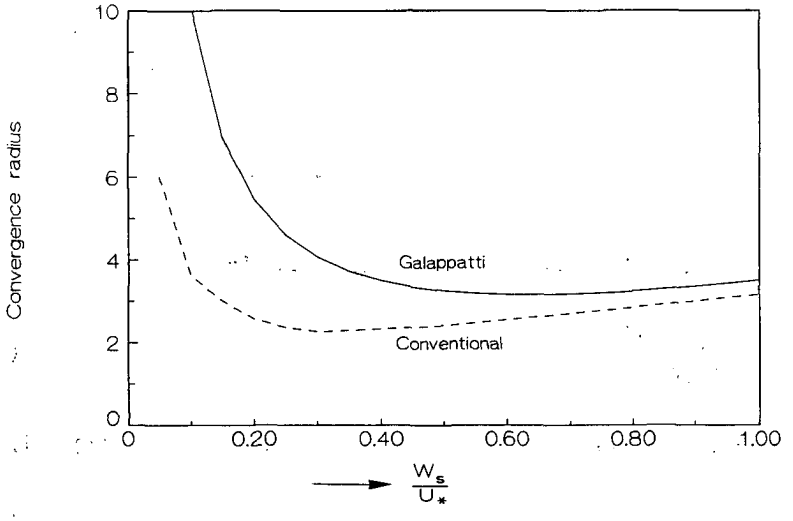

Fig.5.2 Convergence radius

It is clear that $b<\pi$. This means that the convergence radius of the model of Galappatti is larger than that of the conventional model. Figure 5.2 gives the convergence radii of the two asymptotic solutions for the case that the diffusion coefficient is constant.

$$\epsilon' = 0.1 \frac{u_*}{w_s} \tag{5-29}$$

5.3.2 Convergence Domain (A more general case)

In the previous subsection the convergence of different asymptotic solutions has been studied for a simple case. It has been shown that the convergence domain for α in equation (5-15) is a circle in the complex plane with radius R_α. In the general case more directions are involved in which the bed boundary condition can vary. Along the way outlined in the previous subsection a convergence radius can be determined for each direction separately, but the question remains whether the different directions involved will interact with each other. In this subsection it is attempted to answer this question by considering the more general case

$$L[\ ] = \frac{\partial}{\partial \tau} + p(\zeta) \frac{\partial}{\partial \xi} \tag{5-30}$$

with the bed boundary condition

$$\bar{c}_e = \gamma_{11} \exp(\alpha\tau + \beta\xi) \tag{5-31}$$

where α and β are complex numbers.

The exact solution for this case can be written as

$$c = f(\zeta) \exp(\alpha\tau+\beta\xi) \tag{5-32}$$

so

$$\bar{c} = \exp(\alpha\tau+\beta\xi) \int_0^1 f(\zeta)\, d\zeta \tag{5-33}$$

where f is determined by

$$D[f] = \alpha f + \beta pf \tag{5-34a}$$

$$\left[f + \epsilon' \frac{\partial f}{\partial \zeta}\right]_{\zeta=1} = 0 \tag{5-34b}$$

$$f(0) = \gamma_{11} \tag{5-34c}$$

The conventional model gives for this case the following solution for the mean concentration

$$\bar{c} = \exp(\alpha\tau+\beta\xi) \sum_{k=1}^{n+1} \sum_{j=1}^{k} \delta_{kj} \alpha^{k-j} \beta^{j-1} \tag{5-35}$$

and according to the model of Galappatti

$$\bar{c} = \exp(\alpha\tau+\beta\xi) \left(\sum_{k=1}^{n+1} \sum_{j=1}^{k} \gamma_{kj} \alpha^{k-j} \beta^{j-1} \right)^{-1} \tag{5-36}$$

It is clear that the conventional asymptotic solution will converge if and only if the double series in equation (5-33) converges. Similarly the asymptotic solution of Galappatti will converge if and only if the double series in equation (5-36) converges. The two asymptotic solutions can thus be studied in exactly the same way. Therefore only the conventional model will be studied in the following.

The convergence of the double series in equation (5-35) can be well studied for the simplified case p=1. For this case it is not difficult to show that (see equations 4-68 and 4-73)

$$\delta_{kj} = \delta_{k1} \begin{pmatrix} k-1 \\ j-1 \end{pmatrix} \tag{5-37}$$

where $\begin{pmatrix} k-1 \\ j-1 \end{pmatrix}$ expresses the binomial coefficients. Equation (5-35) can then be written as

$$\bar{c} = \exp(\alpha\tau + \beta\xi) \sum_{k=1}^{n+1} \delta_{k1} (\alpha+\beta)^{k-1} \tag{5-38}$$

This is again a power series and the convergence radius of $\alpha+\beta$ is thus

$$R_{\alpha+\beta} = \lim_{k\to\infty} \left| \frac{\delta_{k-1\ 1}}{\delta_{k1}} \right| \tag{5-39}$$

This is exactly the same as the convergence radius for the simple case studied in the previous subsection. This conclusion applies also for the asymptotic solution.

There are clearly interactions between the different directions. For $\alpha=-\beta$ the asymptotic solution always converges without any restriction, while the critical case is $\alpha=\beta$ for which the effective convergence radius is only one half of $R_{\alpha+\beta}$. All cases between these two extreme cases are possible. In fig.5.3 the interaction between the two directions is depicted for three cases. This figure shows that the interaction between the two directions depends on the angle between α and β in the complex plane. The larger this angle the larger the convergence limits. The two extreme cases can be represented by the two extreme values π and zero of this angle. In general it can be said that if this angle is smaller than $\pi/2$ the convergence limits of α and β are both smaller than $R_{\alpha+\beta}$. If this angle is larger then $2\pi/3$ at least one of the convergence limits can be larger than $R_{\alpha+\beta}$.

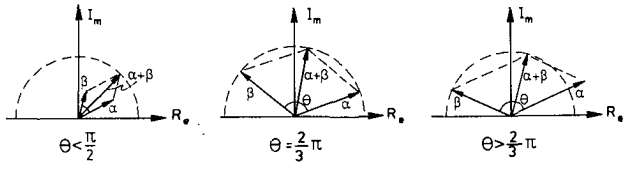

Fig.5.3 Interaction between α and β.

5.3.3 Further discussions

It should be noted that in the previous two sections only the dynamic equilibrium concentration field has been considered. The boundary layer can be studied in a similar way.

For the simple case studied in subsection 5.3.1 the boundary layer c_{II} can be written as (see Wang and Ribberink,1986)

$$c_{II} = \sum_{k=1}^{\infty} \phi_k(\zeta)\exp(\lambda_k \tau)$$

in which λ_k are the eigenvalues of problem (5-26).

$$\lambda_k = \frac{-(1+4b_k^2\epsilon'^2)}{4\epsilon'} \qquad (5\text{-}40)$$

The solution consists thus of components of exponential functions in time. It is clear that an asymptotic solution can only converge to those components in (5-40) of which the exponential coefficients are inside the convergence domain. In fig.5.1 it can be seen that inside the convergence domain of the model of Galappatti (1983) only one of the λ_k is present ($b_2 > \pi > b_1$). This means that the asymptotic solution of Galappatti can only converge to the first component in (5-40). The same conclusion has also been drawn earlier from a different analysis (Wang and Ribberink, 1986). Further none of the eigenvalues λ_k is inside the convergence domain of the conventional asymptotic solution ($|\lambda_1|$ = convergence radius). Therefore the conventional asymptotic solution does not converge to any component of c_{II}. This explains why no upstream boundary condition at all can be applied in this model.

For a more general case such as the case considered in 5.3.2 not only more boundary layers are involved but there is also another kind of variation such as the variation of the upstream boundary condition in time. Such a variation will interact with the corresponding boundary layer. This interaction can be analysed in exactly the same way as in subsection 5.3.2. This analysis is not repeated here.

Up to now only the conventional solution and the solution of Galappatti have been considered. For the general asymptotic solution the convergence domain cannot easily be determined. However, it has been shown above that the number of components of c_{II} to which a asymptotic solution converges to is equal to the number of λ coefficients inside the convergence domain of the

solution and also equal to the number of initial conditions which can be applied in the infinite order solution. This reasoning might also be used to estimate the convergence radius of a asymptotic solution. If M initial conditions can be applied in the infinite order solution in a model then the model should converge to M components in c_{II}, thus the convergence radius should can be supposed to be larger than the absolute value of λ_M according to (5-40). In the previous chapter it has been shown that if an orthogonal system is chosen for the test functions two upstream boundary conditions can be applied in the second order solution (see 4.4.3, case II). It is presumable that if the test functions form a complete system, an infinite number of upstream boundary conditions can be applied in the infinite order solution so the asymptotic solution converges to the complete solution of the original problem. Thus it is conjectured that the convergence radius of the asymptotic solution is infinitely large when the test functions form a complete system.

5.4 Morphological Behaviour of the Models (A Linear Analysis)

In order to study the morphological behaviour of the different models a linear analysis is carried out. The propagation characteristics of a small disturbance in a one-dimensional flow are derived analytically from the conventional model, the model of Galappatti and the exact model.

Consider a steady uniform flow where the suspended sediment transport is dominant and in equilibrium. Let all the quantities in this equilibrium state be denoted by the subscript $_0$ (e.g. u_0 for the mean velocity, h_0 for the water depth, etc.). Consider a disturbance in the bed level

$$z = z_0 + z' \tag{5-41}$$

where

$$z' = Z \exp(\lambda t + ikx) \tag{5-42}$$

This will cause perturbations in other quantities.

$$\bar{u} = u_0 + u' \tag{5-43a}$$

$$\bar{c} = \bar{c}_0 + c' \tag{5-43b}$$

$$s = s_0 + s' \tag{5-43c}$$

$$\bar{c}_e = \bar{c}_0 + c'_e \tag{5-43d}$$

For the analysis the following assumptions are made.

* The variation with t and x of the coefficients in the depth-integrated models can be neglected.

* The discharge remains constant, thus

$$\bar{u}h = u_0 h = q \tag{5-44}$$

* The water surface level remains unchanged, this is the rigid lid assumption. Thus

$$\frac{\partial z_b}{\partial t} = -\frac{\partial h}{\partial t}$$

The continuity equation for the sediment can then be written as

$$\frac{\partial h}{\partial t} = \frac{\partial s}{\partial x} \tag{5-45}$$

* the sediment transport capacity is governed by the power law

$$s_e = a\,\bar{u}^b \tag{5-46}$$

so the equilibrium mean concentration becomes

$$\bar{c}_e = a\,\frac{\bar{u}^b}{\alpha_{11} q} \tag{5-47}$$

With the help of equation (5-44) equation (5-47) can be linearized as

$$\bar{c}_e = c_0 \left(1 - \frac{bh'}{h_0}\right) \tag{5-48}$$

Thus

$$\bar{c}'_e = - \frac{bh'}{h_0} c_0 \tag{5-49}$$

$$s'_e = - \frac{bh'}{h_0} s_0 \tag{5-50}$$

The sediment transport s can now be determined from different models, and the propagation characteristics can be derived from equation (5-45) which can also be written as

$$\frac{\partial h'}{\partial t} = \frac{\partial s'}{\partial x} \tag{5-51}$$

The conventional model

According to the conventional model the transport rate is (see chapter 4)

$$s = q \sum_{j=1}^{n+1} \beta_{jj} \left(\frac{q}{w_s}\right)^{j-1} \frac{\partial^{j-1} \bar{c}_e}{\partial x^{j-1}} \tag{5-52}$$

The perturbation of the transport rate is then

$$s' = - \frac{bs_0}{h_0} \sum_{j=1}^{n+1} \frac{\beta_{jj}}{\alpha_{11}} \left(\frac{q}{w_s}\right)^{j-1} \frac{\partial^{j-1} h'}{\partial x^{j-1}}$$

Substituting this equation into equation (5-51) gives

$$\frac{\partial h'}{\partial t} = - \frac{bs_0}{h_0} \sum_{j=1}^{n+1} \frac{\beta_{jj}}{\alpha_{11}} \left(\frac{q}{w_s}\right)^{j-1} \frac{\partial^{j-1} h'}{\partial x^{j-1}} \tag{5-53}$$

Together with equation (5-42) this gives

$$\lambda = - ik\frac{bs_0}{h_0}\sum_{j=1}^{n+1}\frac{\beta_{jj}}{\alpha_{11}}\left(ik\,\frac{q}{w_s}\right)^{j-1} \qquad (5\text{-}54)$$

The model of Galappatti

In the model of Galappatti the mean concentration $\bar{c}$ has to be determined first before the sediment transport rate s can be determined. The equations governing c and s are (see chapter 4)

$$\bar{c}_e = \sum_{j=1}^{n+1}\frac{\gamma_{jj}}{\gamma_{11}}\left(\frac{q}{w_s}\right)^{j-1}\frac{\partial^j \bar{c}}{\partial x^j} \qquad (5\text{-}56)$$

$$s = q\sum_{j=1}^{n+1}\alpha_{jj}\left(\frac{q}{w_s}\right)^{j-1}\frac{\partial^j \bar{c}}{\partial x^j} \qquad (5\text{-}57)$$

From equation (5-56) the perturbation of the mean concentration is shown to be

$$c' = \frac{bc_0}{h_0}\,h'\left(\sum_{j=1}^{n+1}\frac{\gamma_{jj}}{\gamma_{11}}\left(ik\frac{q}{w_s}\right)^{j-1}\right)^{-1} \qquad (5\text{-}58)$$

Substituting this into equation (5-57) gives

$$s' = - \frac{bc_0}{h_0}\sum_{j=1}^{n+1}\frac{\alpha_{jj}}{\alpha_{11}}\left(ik\frac{q}{w_s}\right)^{j-1}\left(\sum_{j=1}^{n+1}\frac{\gamma_{jj}}{\gamma_{11}}\left(ik\frac{q}{w_s}\right)^{j-1}\right)^{-1} \qquad (5\text{-}59)$$

Substituting this into equation (5-51) gives

$$\frac{\partial h'}{\partial t} = - \frac{bc_0}{h_0}\sum_{j=1}^{n+1}\frac{\alpha_{jj}}{\alpha_{11}}\left(ik\frac{q}{w_s}\right)^{j-1}\left(\sum_{j=1}^{n+1}\frac{\gamma_{jj}}{\gamma_{11}}\left(ik\frac{q}{w_s}\right)^{j-1}\right)^{-1}\frac{\partial h'}{\partial x} \qquad (5\text{-}60)$$

Together with equation (5-42) this equation gives

$$\lambda = - ik \frac{bc_o}{h_o} \sum_{j=1}^{n+1} \frac{\alpha_{jj}}{\alpha_{11}} \left(ik \frac{q}{w_s} \right)^{j-1} \left[\sum_{j=1}^{n+1} \frac{\gamma_{jj}}{\gamma_{11}} \left(ik \frac{q}{w_s} \right)^{j-1} \right]^{-1} \tag{5-61}$$

The exact model

According to the exact model the concentration and the transport rate are governed by the following equations.

$$p \frac{\partial c}{\partial \xi} = D[c] \tag{5-62}$$

$$s = q \int_0^1 p(\zeta)\, c(\zeta)\, d\zeta \tag{5-63}$$

Together with the boundary conditions

$$\left[c + \epsilon' \frac{\partial c}{\partial \zeta} \right]_{\zeta=1} = 0 \tag{5-64}$$

$$c(\zeta=0) = \gamma_{11} \bar{c}_e \tag{5-65}$$

Substituting equation into the equation (5-62), (5-64) and (5-65) shows that c' is governed by

$$p \frac{\partial c'}{\partial \xi} = D[c] \tag{5-66a}$$

$$\left[c' + \epsilon' \frac{\partial c'}{\partial \zeta} \right]_{\zeta=1} = 0 \tag{5-66b}$$

$$c'(\zeta=0) = \gamma_{11} \bar{c}'_e \tag{5-66c}$$

The solution of this boundary value problem can be shown to be

$$c' = \bar{c}_e \phi(\zeta) \tag{5-67}$$

where ϕ is a complex function governed by

$$ik \frac{q}{w_s} p\phi = D[c] \tag{5-68a}$$

$$\left[\phi + \epsilon' \frac{\partial \phi}{\partial \zeta}\right]_{\zeta=1} = 0 \qquad (5\text{-}68b)$$

$$\phi(\zeta=0) = \gamma_{11} \qquad (5\text{-}68c)$$

From equation (5-63) it follows then

$$s' = q \int_0^1 p(\zeta) c'(\zeta)\, d\zeta = - \frac{bc_0}{h_0} h' \int_0^1 p(\zeta)\phi(\zeta)\, d\zeta \qquad (5\text{-}69)$$

Equation (5-51) can now be written as

$$\frac{\partial h'}{\partial t} = - \frac{bs_0}{h_0} \frac{\partial h'}{\partial x} \int_0^1 p(\zeta)\phi(\zeta)\, d\zeta \qquad (5\text{-}70)$$

Substituting equation (5-42) into this equation gives

$$\lambda = - \frac{bc_0}{h_0} ik \int_0^1 p(\zeta)\phi(\zeta)\, d\zeta \qquad (5\text{-}71)$$

It should be noted that if the sediment transport were only bed load the result would be

$$\lambda = - \frac{bc_0}{h_0} ik \qquad (5\text{-}72)$$

which is the same as the zero order solution from both depth-integrated models.

Further the convergence of the propagation factor λ from the asymptotic solutions can also be analysed as in the previous section. The same conclusions can be drawn as in the previous section. If p=1 then

$$\beta_{jj} = \delta_{jj} \qquad \text{for all } j \qquad (5\text{-}73a)$$

$$\alpha_{11} = 1 \qquad (5\text{-}73b)$$

$$\alpha_{jj} = 0 \qquad \text{for } j > 1 \qquad (5\text{-}73c)$$

For this case the results will even be exactly the same with $\alpha=ikq/w_s$. The convergence radius gives thus also a limit of wave length in the river bed for which the asymptotic solution is just convergent. The models are compared with each other in the following section.

5.5 Comparison Between the Models

In section 5.3 the convergence domains of the different asymptotic solutions are studied. Inside the convergence domain the asymptotic solution will converge to the exact solution. However, for practical applications only the first few terms in the asymptotic solution can be taken into account. Therefore not only the convergence domain but also the convergence rate of an asymptotic solution is important.

In this section comparisons are made between the low order asymptotic solutions and the exact solution, inside as well as outside the convergence domains. In order to avoid unnecessary complications only two simple cases are considered. The first case is the case considered in 5.3.2 with α is real, and the second case is the case studied in section 5.4. For further simplification of the problem the diffusion coefficient is assumed to be constant and the flow velocity is assumed to be uniformly distributed.

$$\epsilon' = 0.1 \frac{u_*}{w_s} \qquad (5\text{-}74a)$$

$$p(\zeta) = 1 \qquad (5\text{-}74b)$$

Case I α is real

For this case the exact solutions as well as all the asymptotic solutions are real. For the comparison the different solutions can better be depicted as function of b with

$$b = \frac{\sqrt{1-4\epsilon'\alpha}}{2\epsilon'} \qquad (5\text{-}75)$$

The exact solution can then be written as

$$\frac{\bar{c}}{\bar{c}_e} = \frac{2\gamma_{11}\epsilon' tg(b)}{2\epsilon' b + tg(b)} \tag{5-76}$$

The conventional solution and the solution of Galappatti (1983) are already given in 5.3.2, see equations (5-20) and (5-21). In order to examine the asymptotic solution with an orthogonal set of test functions the second and third order solution with the following test functions are considered.

$$\Phi = (1, q, r, \ldots) \tag{5-77a}$$

with

$$q = 4\zeta - 2 \tag{5-77b}$$

$$r = 6\zeta^2 - 6\zeta + 1 \tag{5-77c}$$

The second order and third order solution are then respectively

$$\frac{\bar{c}}{\bar{c}_e} = \gamma_0 \frac{(\alpha\beta_1 - \beta_0)}{\det(A_2)} \quad \text{(second order)} \tag{5-78a}$$

with

$$A_2 = \begin{bmatrix} \gamma_0 + \gamma_1\alpha + \gamma_2\alpha^2 & \gamma_1\alpha \\ \beta_2\alpha^2 & \alpha\beta_1 - \beta_0 \end{bmatrix} \tag{4-78b}$$

and

$$\frac{\bar{c}}{\bar{c}_e} = \gamma_0 \frac{(\mu_2\alpha^2 - \mu_0)\beta_1\alpha - (\beta_2\alpha^2 + \beta_1\alpha + \beta_0)(\mu_1\alpha - \mu_0)}{\det(A_3)} \quad \text{(third order)} \tag{5-79a}$$

with

$$A_3 = \begin{bmatrix} \gamma_0+\gamma_1\alpha+\gamma_2\alpha^2+\gamma_3\alpha^3 & \gamma_1\alpha+\gamma_2\alpha^2 & \gamma_1\alpha \\ \beta_3\alpha^3+\beta_2\alpha^2 & \beta_2\alpha^2+\beta_1\alpha-\beta_0 & \beta_1\alpha \\ \mu_3\alpha^3 & \mu_2\alpha^2-\mu_0 & \mu_1\alpha-\mu_0 \end{bmatrix} \qquad (5\text{-}79b)$$

In these equations

$$\gamma_j = a_{1,i+1}(0)$$

$$\beta_j = \int_0^1 q\, a_{1,j+1}\, d\zeta$$

$$\mu_j = \int_0^1 r\, a_{1,j+1}\, d\zeta$$

In fig.5.4 the conventional solution is compared with the exact solution. It can clearly be observed from this figure that for $\alpha<0$ the asymptotic

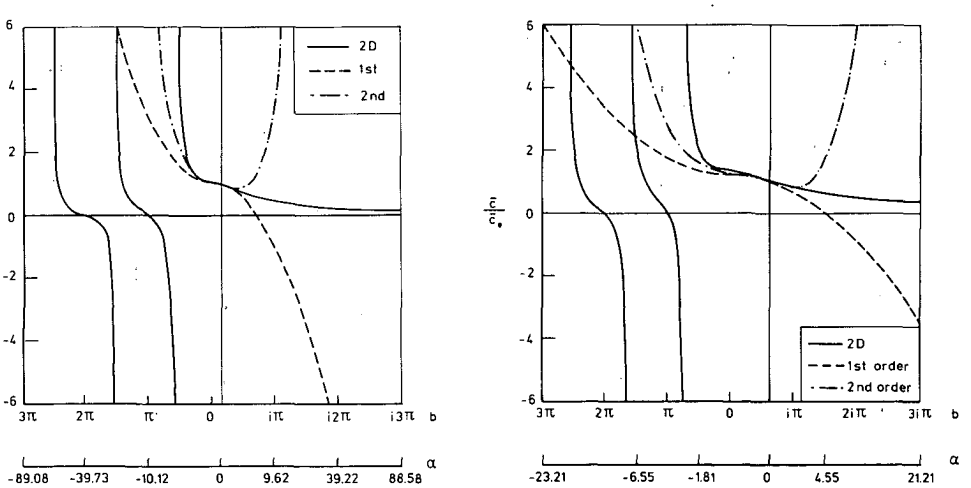

(a) $\frac{w_s}{u_*} = 0.10$ (b) $\frac{w_s}{u_*} = 0.40$

Fig.5.4 Comparison between the conventional asymptotic solution and the exact solution.

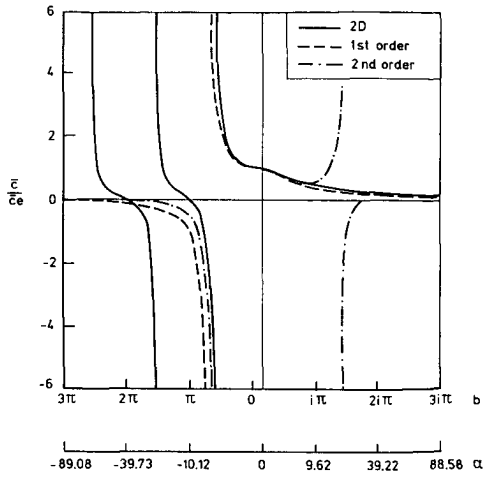

(a) $\frac{w_s}{u_*} = 0.10$

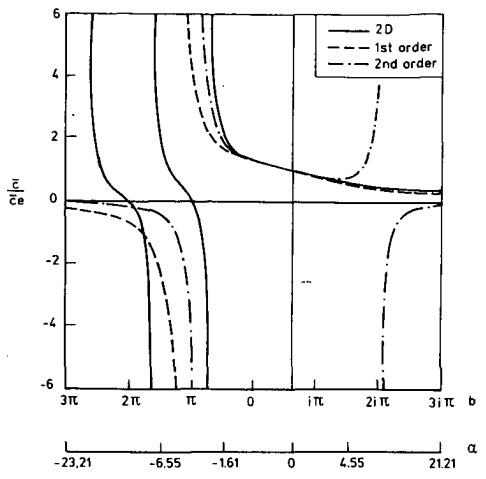

(b) $\frac{w_s}{u_*} = 0.40$

Fig.5.5 Comparison between the solution of Galappatti and the exact solution

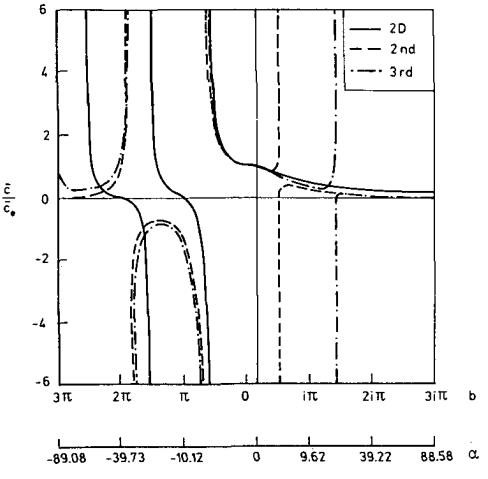

(a) $\frac{w_s}{u_*} = 0.10$

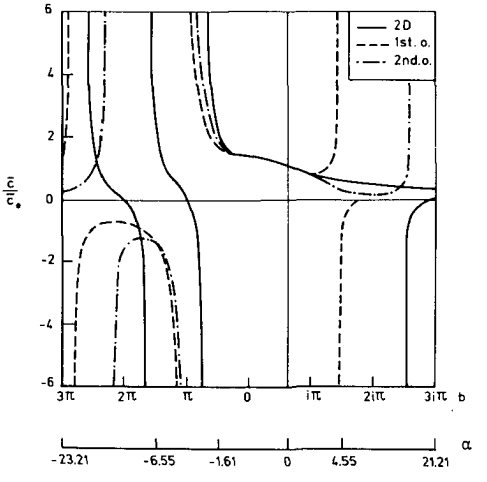

(b) $\frac{w_s}{u_*} = 0.40$

Fig.5.6 Comparison between the asymptotic solution with orthogonal test functions and the exact solution

solution does not converge outside the first singular point in the exact solution. The first singular point determines thus the convergence radius. This agrees with the analysis in 5.3.2.

The solution of Galappatti is compared with the exact solution in fig.5.5. In this asymptotic solution there is one singular point for $\alpha<0$. It can be observed that this singular point is an estimation of the singular point in the exact solution. Outside the singular point the solution does no more change sign, so the first zero point in the exact solution defines the convergence radius of this asymptotic solution. This agrees with the result in 5.3.2.

In fig.5.6 the solution with the orthogonal test functions is compared with the exact solution. In this solution there are n singular points in the nth order solution, but the way it behaves outside the first singular point does not agree with the exact solution. This fact indicates that this asymptotic solution does not have a infinite large convergence radius as suggested earlier. No definitive conclusion can be made for the convergence of this solution at this moment.

Further the following conclusions are drawn from the comparisons.

* The agreement between the model of Galappatti and the exact model is better than that between the conventional model and the exact model. The convergence radius is apparently also a measure for the accuracy of the corresponding depth-integrated model.

* In the model of Galappatti as well as in the conventional model the smaller w_s/u_* the higher the convergence rate. This may be explained by the variation of the convergence radii of the two models with w_s/u_* (see fig.5.2).

* Within the convergence domain the higher order solutions improve the accuracy while outside the convergence domain this is not necessary the case. The first order solution of Galappatti gives also a good

estimation for the exact solution outside the convergence domain when $\alpha>0$.

Remark:

The phenomenon of resonance occurs in the exact solution if α is equal to one of the eigenvalues of problem (5-26). This is then called a singular point. In such a point the boundary value problem (5-17) has no solution, which in fact means that the exact solution cannot be written in the form of equation (5-16). In asymptotic solutions a singularity occurs when the numerator is zero.

Case II β is purely imaginary

The coefficient λ derived in the previous section is a important parameter indicating the morphological behaviour of the corresponding model. It gives information on the characteristics of the development of the disturbance on the bed. Both the real and the imaginary part of λ have important physical meanings, i.e.

$-Im(\lambda)/k$ = propagation velocity
$Re(\lambda)$ = damping coefficient

The propagation velocity as well as the damping coefficient according to the different models are compared with each other in fig.5.7 and fig.5.8 for two w_s/u_* values. The following conclusions have been drawn from the comparison.

* The model of Galappatti gives a good estimation for the exact solution (both the propagation velocity and the damping coefficient) even when kq/w_s is slightly larger than the convergence radius. Within the convergence domain the agreement between this model and the exact model is better when a higher order solution is applied, when the wave number is smaller and when w_s/u_* is smaller, as can be expected.

* The conventional asymptotic solution gives also good estimation for the exact solution when kq/w_s is small(<2). However, for larger wave

numbers the deviation between the two models increases rapidly. The agreement between this model and the exact model does not depend on w_s/u_*.

* Higher order solutions can only improve the agreement with the exact solution within the convergence domain. This applies for both asymptotic solutions.

* Concerning the overall agreement with the exact solution the first order solution in the model of Galappatti which in the present case is the same as the applied solution seems to give reasonable results.

Further it has been observed that

* the propagation velocity according to the exact model decreases as the wave number increases; it is always smaller than that in the case of bed load transport which is the zero order solution;

* the damping coefficient is always negative(damping) and its absolute value increases with the increasing wave number (note that the damping coefficient in fig.5.7 has been made dimensionless with the wave number k). A consequence of this is that bed forms cannot be maintained in a uniform flow if only suspended transport is present;

* for $k\to\infty$ the damping coefficient becomes infinitely large and the propagation velocity becomes zero which agrees with the characteristic analysis.

It should be noted that for $k\to\infty$ the disturbance is infinitely small so the results from the linear analysis should provide the same information as the characteristic analysis. From fig.5.7 it can be seen that according to the exact model the propagation velocity becomes zero for $k\to\infty$. For p=1 as in fig.5.7 the first order solution in the model of Galappatti gives the same result.

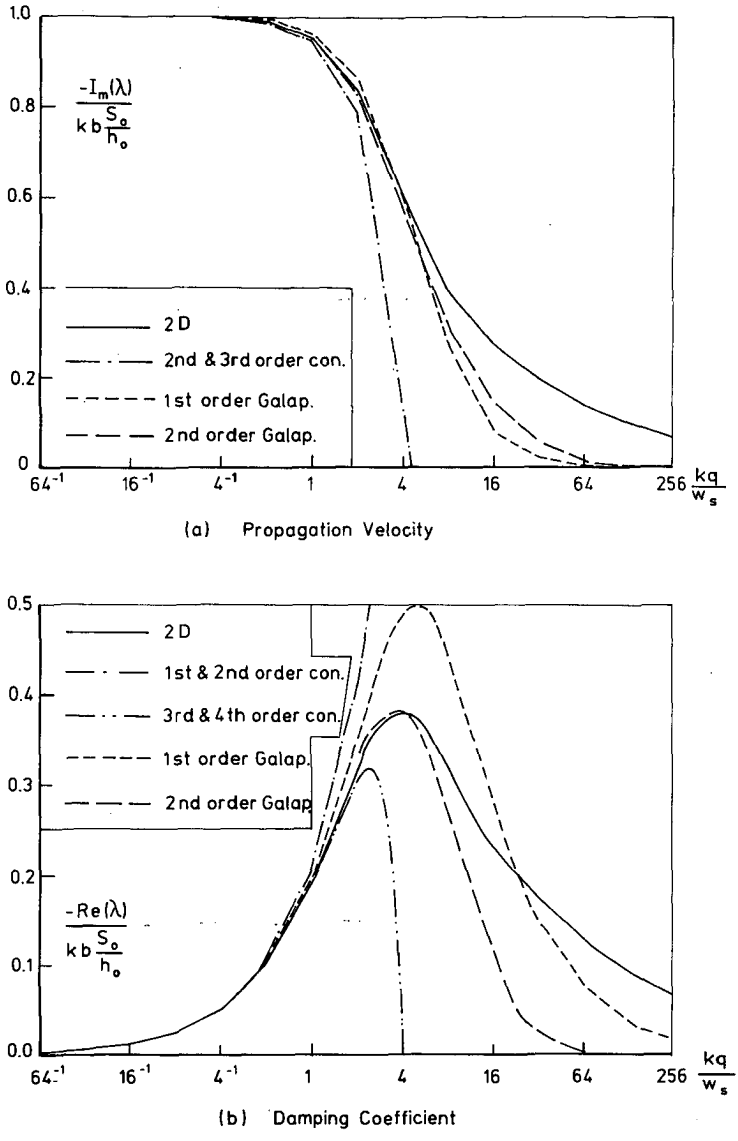

Fig.5.7 Comparison between the models ($\frac{w_s}{u_*} = 0.1$)

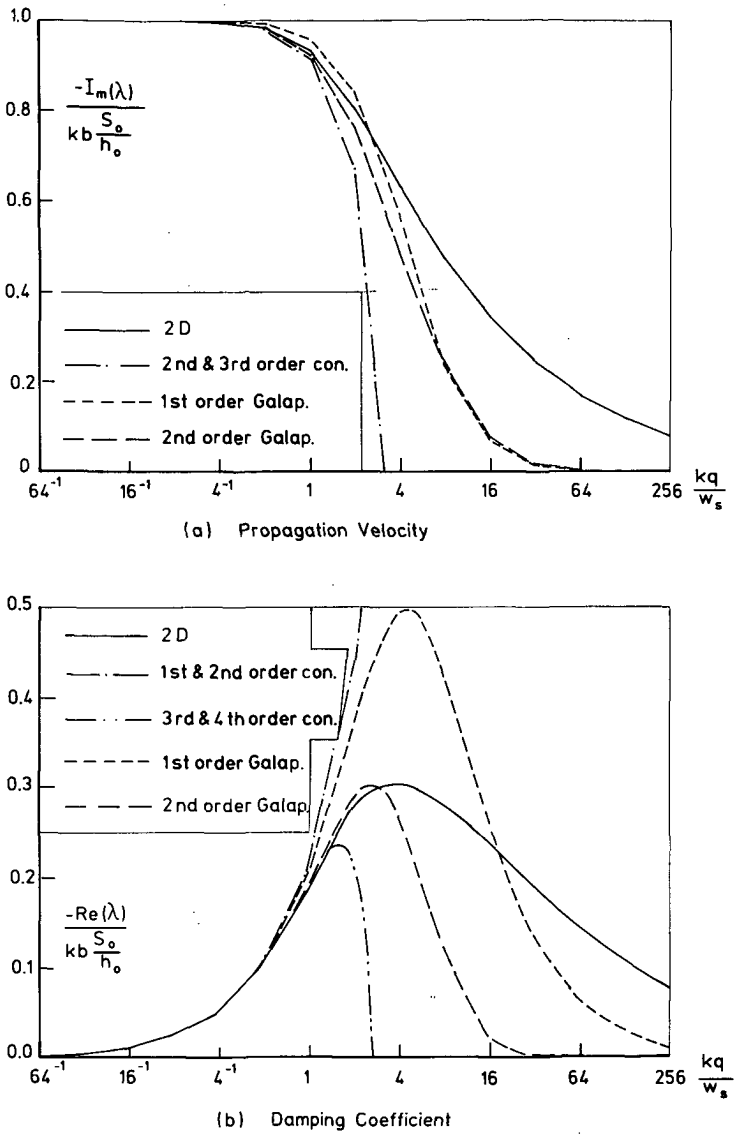

Fig.5.8 Comparison between the models ($\frac{w_s}{u_*} = 0.4$)

$$\lim_{k\to\infty} (-\mathrm{Im}(\lambda)/k) = \frac{\alpha_{22}\gamma_{11}}{\alpha_{11}\gamma_{22}}\, b\, \frac{s_0}{h_0} \tag{5-79}$$

However, this is always negative if the velocity is logarithmically distributed over the depth, although the absolute value is small. This means that a boundary condition at the downstream side is needed for the morphological computation if no bed load transport is present, which is of course physically unrealistic.

This problem is avoided in the present model ($\Phi = (p,\ldots)$). The first order solution for the case under consideration becomes then (see chapter 4)

$$c = c_s \frac{a_{11}}{\alpha_{11}} + \left(a_{22} - \frac{\alpha_{22}}{\alpha_{11}} \frac{a_{11}}{\alpha_{11}}\right) \frac{\partial c_s}{\partial \xi} \tag{5-80}$$

The result of the linear analysis becomes then

$$\lambda = -ik \frac{bs_0}{h_0} \left[\sum_{j=1}^{n+1} \left(\frac{\gamma_{jj}}{\gamma_{11}} - \frac{\alpha_{22}}{\alpha_{11}} \right) \left(ik \frac{q}{w_s} \right)^{j-1} \right]^{-1} \tag{5-81}$$

instead of (5-61). The celerity becomes then

$$\lim_{k\to\infty} (-\mathrm{Im}(\lambda)/k) = 0 \tag{5-82}$$

the same as the exact model. This supports the choice of the first component of the test functions made in the previous chapter.

5.6 Concluding Discussions

The depth-integrated models are developed to fill the gap between the simple transport formula and the complicated three-dimensional model. A depth-integrated model can only be applied if affirmative answers are given on both questions posed in section 5.1:

a) Is the depth-integrated model sufficiently accurate to replace the three-dimensional model?

b) Is it worthwhile to apply the depth-integrated model replacing the simple transport formula?

After the theoretical analysis in the previous sections it is now possible to answer these two questions. Take for example case II considered in the previous section. The morphological behaviour of the different models are clearly shown in fig.5.7. Obviously for $k'=kq/w_s>1$ the application of the simple transport formula will cause significant errors, so it is then worthwhile to apply a more complicated model. From the same figure it can also be observed that the limit on k' below which the depth-integrated models are applicable is much larger than 1. This means that there is indeed a gap between the sophisticated three-dimensional model and the simple transport formula, which can be filled by a depth-integrated model, or in other words there are certainly cases for which both questions posed in the beginning of this chapter have a positive answer.

In the previous chapter it has been shown that a series of depth-integrated models can be developed based on the general asymptotic solution of the convection-diffusion equation. However, when the unsteady three-dimensional problem is concerned only the first order solution can in general be applied since the higher order solutions will be too complicated for application, except the conventional approach. For the conventional model the application of higher order solutions means only to calculate higher order derivatives of $\bar{c}_e(t,s,n)$. As mentioned in the previous chapter the first order solution in the general asymptotic solution is only influenced by the first component in the set of functions Φ. For the two dimensional case the first order solution in the model of Galappatti is an example of the general first order solution with $\phi_1=1$. There are thus only two possibilities remaining to be chosen, viz. the conventional model and the model based on the general first order solution. From the comparisons carried out in the previous section it has been concluded that the first order solution in the model of Galappatti performs much better than the conventional asymptotic solution (see fig.5.4...fig.5.7). Therefore the general first order solution is chosen.

In the comparisons made in the previous section simplifications have been made on the velocity profile and the turbulent diffusion coefficient. The same comparison can also be carried out for the more realistic velocity distribution (logarithmic) and diffusion coefficient(parabolic-constant). The solutions will then also depend on the location of the bed boundary condition (β) and the parameter $\bar{u}/u_*$. The conclusions drawn in the previous section apply also for this comparison, only the influence of the parameter w_s/u_* is now more important. The smaller this parameter the more accurate the model.

Up to now the analysis only concerns the two-dimensional flow case. However, it can be expected that the conclusions drawn from the analysis apply also for the three-dimensional cases.

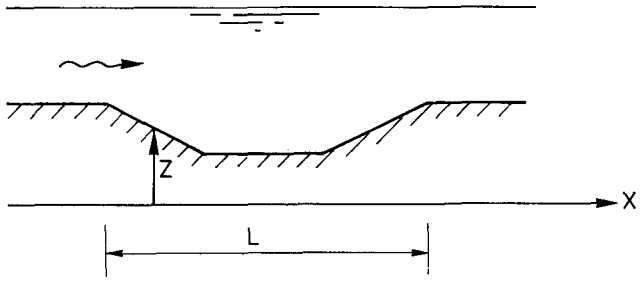

Fig.5.9

In realistic situations the bed level will be irregular, but the result of the linear analysis can still be applied for examining the applicability of a model after a Fourier analysis. As an example the sedimentation of a trench (fig.5.9) is considered. For such a case the bed level $z_b(x)$ can be developed into a Fourier series.

$$z_b(x) = \sum_{j=-\infty}^{\infty} A_j \exp\left[i \frac{j\pi x}{L}\right] \qquad (5\text{-}83)$$

The result of the linear analysis can now be applied to each component in this equation.

For numerical models it should be noted that the shortest wave which can enter the system has the length $2\Delta x$ and the longest wave has the length $2L$, if Δx is the space step and L is the length of the region under consideration. In other words

$$\frac{\pi}{\Delta x} \geq k \geq \frac{\pi}{L} \tag{5-84}$$

Examining the agreement between the depth-integrated and the exact model in the region defined by (5-84) one can thus obtain a good impression about the accuracy of the model.

Examples of applications of the results from the analysis in this chapter are given in chapter 7 and chapter 8.

Chapter 6 NUMERICAL MODELLING

6.1 Introduction

As described in chapter 2, the morphological model considered at present can be divided into three submodels, viz. the flow model, the sediment transport model and the bedlevel model. The flow model used at present is an existing model, therefore only the numerical aspects of the sediment transport model and the bedlevel model are considered in this chapter.

6.2 The concentration Equation

The main numerical problem in the sediment transport model is the solution of the sediment concentration equation (4-147). For convenience this equation is written as

$$\frac{\partial c_s}{\partial t} + U\frac{\partial c_s}{\partial x} + V\frac{\partial c_s}{\partial y} = D\frac{\partial^2 c_s}{\partial x^2} + D\frac{\partial^2 c_s}{\partial y^2} + \frac{c_{se}-c_s}{T_a} \qquad (6\text{-}1)$$

where U = effective velocity in x-direction,
V = effective velocity in y-direction,
D = diffusion coefficient,
T_a = adaptation time.

Two numerical schemes for this equation are considered, one with central space discretization for the convective terms and the other one with upstream discretization.

The Central Scheme

The central scheme is applied in combination with the predictor corrector method (PCM). Thus for the predictor the forward-time central-space (FTCS) scheme is applied while for the corrector the Crank-Nicolson (C-N) scheme is employed. In equation form these schemes read

Predictor

$$\frac{c^{*}_{sjk}-c^{n}_{sjk}}{\Delta t} + U^{n}_{jk}\,\frac{c^{n}_{sj+1,k}-c^{n}_{sj-1,k}}{2\Delta x} + V^{n}_{jk}\,\frac{c^{n}_{sj,k+1}-c^{n}_{sj,k-1}}{2\Delta y} =$$

$$= D^{n}_{jk}\,\frac{c^{n}_{sj+1,k}-2c^{n}_{sjk}+c^{n}_{sj-1,k}}{\Delta x^{2}} + D^{n}_{jk}\,\frac{c^{n}_{sj,k+1}-2c^{n}_{sjk}+c^{n}_{sj,k-1}}{\Delta y^{2}} +$$

$$+ \frac{c^{n}_{sejk}-c^{n}_{sjk}}{T^{n}_{ajk}} \qquad (6\text{-}2)$$

Corrector

$$\frac{c^{**}_{sjk}-c^{n}_{sjk}}{\Delta t} = (1-\theta)\,\frac{c^{*}_{sjk}-c^{n}_{sjk}}{\Delta t} - \theta\left[U^{n+1}_{jk}\,\frac{c^{*}_{sj+1,k}-c^{*}_{sj-1,k}}{2\Delta x} + \right.$$

$$+ V^{n+1}_{jk}\,\frac{c^{*}_{sj,k+1}-c^{*}_{sj,k-1}}{2\Delta y} - D^{n+1}_{jk}\,\frac{c^{*}_{sj+1,k}-2c^{*}_{sjk}+c^{*}_{sj-1,k}}{\Delta x^{2}} +$$

$$\left. - D^{n+1}_{jk}\,\frac{c^{*}_{sj,k+1}-2c^{*}_{sjk}+c^{*}_{sj,k-1}}{\Delta y^{2}} + \frac{c^{n+1}_{sejk}-c^{*}_{sjk}}{T^{n+1}_{ajk}} \right] \qquad (6\text{-}3)$$

This corrector can be applied for a number of times, where c^{*} for every time is the last estimation for c.

This numerical method has already been analysed by Wang (1984) for the one-dimensional case. The analysis for the two-dimensional case discussed here is completely analogous. Therefore the analysis will not be described in detail here, only the important results are summarized below.

For the initial state

$$c_{s}(0,\ x,\ y) = \exp(ik_{x}x + ik_{y}y) \qquad (6\text{-}4)$$

the complex propagation factor is

$$\rho = 1 + \sum_{J=1}^{M} \theta^{J-1} Z^{J} \tag{6-5}$$

with

$$Z = \lambda_x \cos\xi + \lambda_y \cos\eta - \lambda_x - \lambda_y - \beta - i\sigma_x \sin\xi - i\sigma_y \sin\eta \tag{6-6}$$

$$\xi = k_x \Delta x$$

$$\eta = k_y \Delta y$$

$$\lambda_x = \frac{2D\Delta t}{\Delta x^2}$$

$$\lambda_y = \frac{2D\Delta t}{\Delta y^2}$$

$$\sigma_x = \frac{U\Delta t}{\Delta x}$$

$$\sigma_y = \frac{V\Delta t}{\Delta y}$$

$$\beta = \frac{\Delta t}{T_a}$$

M = the number of iterations,

θ = constant coefficient.

The condition for numerical stability

$$|\rho| \leq 1 \tag{6-7}$$

defines a stability domain which can be described by the following two relations.

$$2(\lambda_x + \lambda_y) + \beta \leq f_M(\theta) \tag{6-8}$$

$$\sigma_x^2 + \sigma_y^2 \leq g_M(\theta, \beta, \lambda_x, \lambda_y) \tag{6-9}$$

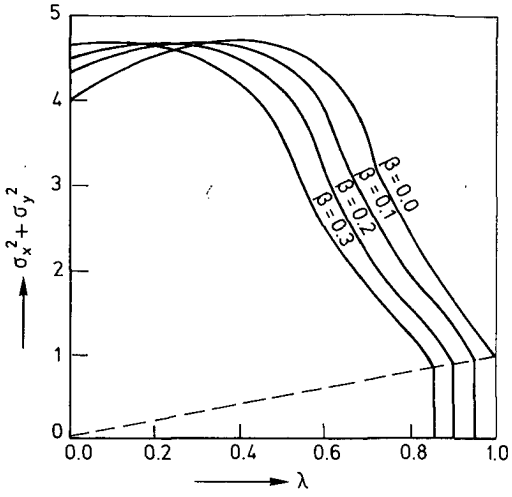

Fig.6.1 Stability domain of PM with three iterations (source term explicit θ=0.5 $\lambda_x=\lambda_y=\lambda$)

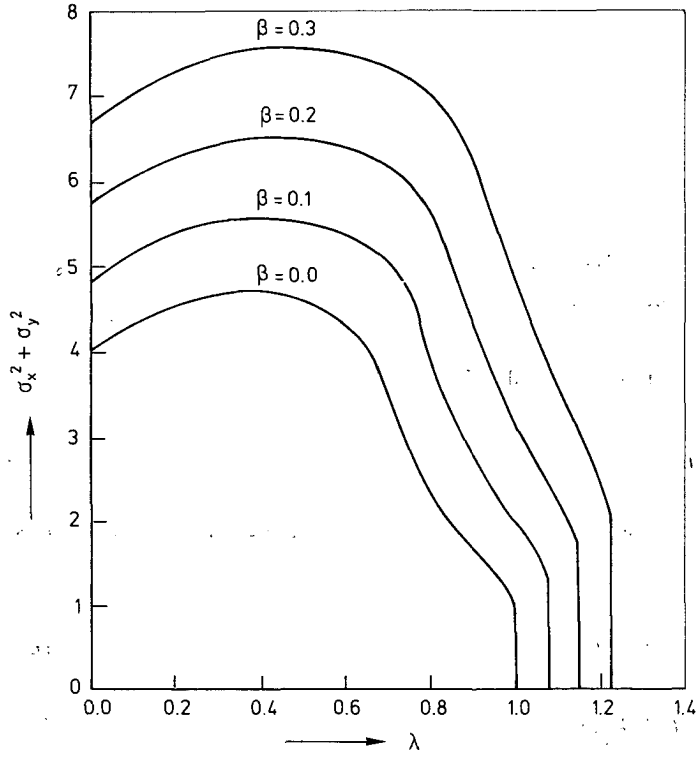

Fig.6.2 Stability domain of PM with three iterations (source term implicit, θ=0.5, $\lambda_x=\lambda_y=\lambda$)

For M>1 the functions f_M and g_M are too complicated to be written in analytical form. It has been shown that M=3 gives the largest stability domain (Wang, 1984). This stability domain is shown in fig.6.1 for θ=0.5 and $\lambda_x=\lambda_y=\lambda$. It can be observed from this figure that the parameter β can give negative influence on the stability when λ is not too small. This can cause serious problems in very shallow water regions where β becomes large. This problem can easily be solved by treating the source term in equation (6-1) implicitly instead of explicitly as in (6-2). The last term in (6-2) and (6-3) becomes then

$$\frac{c_{sejk}^{n+1}-c_{sjk}^{n+1}}{T_{ajk}^{n+1}}$$

The whole scheme remains effectively explicit, but the stability domain is enormously enlarged, as can be seen from fig.6.2.

Another problem with the central scheme is the spatial oscillation. A condition for suppressing oscillation for the one-dimensional flow case is that the cell-Reynolds number should be smaller than 2 (Vreugdenhil,1979).

$$\frac{U\Delta x}{D} < 2 \qquad (6\text{-}10)$$

Suppose that

$$D = \alpha U h$$

then the condition becomes

$$\Delta x < 2\alpha h \qquad (6\text{-}11)$$

Since α has the order of magnitude 1 this condition will in general lead to a unrealistically small Δx. So serious oscillation problems can be expected with the central scheme.

The Upstream Scheme

The upstream scheme introduces such a numerical diffusion that spatial oscillation problem will no more occur. In equation form this scheme reads

$$\frac{c^{n+1}_{sjk}-c^{n}_{sjk}}{\Delta t} + U^{n}_{jk}\,\frac{c^{n}_{sj,k}-c^{n}_{sj-1,k}}{\Delta x} + V^{n}_{jk}\,\frac{c^{n}_{sj,k}-c^{n}_{sj,k-1}}{\Delta y} =$$

$$= D^{n}_{jk}\,\frac{c^{n}_{sj+1,k}-2c^{n}_{sjk}+c^{n}_{sj-1,k}}{\Delta x^{2}} + D^{n}_{jk}\,\frac{c^{n}_{sj,k+1}-2c^{n}_{sjk}+c^{n}_{sj,k-1}}{\Delta y^{2}} +$$

$$+ \frac{c^{n}_{sejk}-c^{n}_{sjk}}{T^{n}_{ajk}} \qquad (6\text{-}12)$$

if U and V are positive. It should be noted that the source term is treated implicitly in order to improve the stability of the scheme. The complex propagation factor for this scheme becomes

$$\rho = \frac{1}{1+\beta}\left(1 - \lambda_x - \lambda_y - |\sigma_x| - |\sigma_y| + (\lambda_x+|\sigma_x|)\cos\xi + \right.$$

$$\left. + (\lambda_x+|\sigma_x|)\cos\eta - i|\sigma_x|\sin\xi - i|\sigma_x|\sin\xi\right) \qquad (6\text{-}13)$$

The stability domain can be described by

$$(|\sigma_x| + |\sigma_y| + |\lambda_x| + |\lambda_y|) \le 1 + 0.5\beta \qquad (6\text{-}14)$$

and is shown in fig.6.3.

The truncation error in the central scheme is of second order while that in the upstream scheme is of first order. Thus the central scheme is in general more accurate than the upstream scheme. However, the spatial oscillation problem makes this scheme unapplicable for most estuary problems, since the space step is in general much larger than the water depth. Therefore most computations in the present study have been carried out with the upstream scheme.

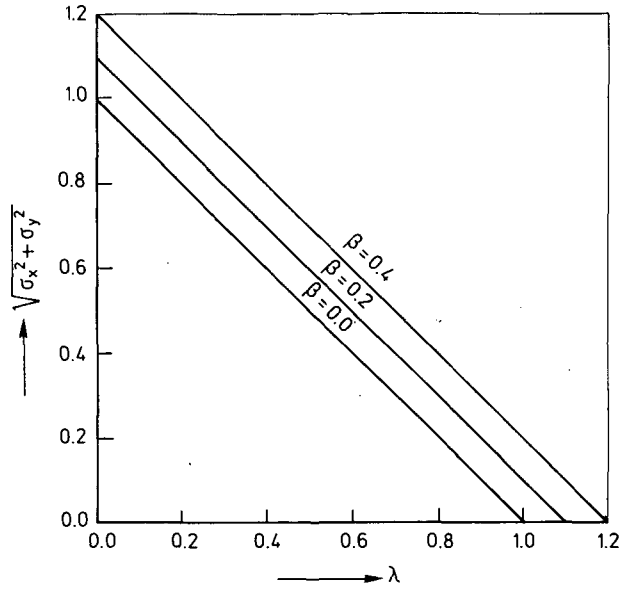

Fig.6.3 Stability domain for the upstream scheme (source term implicit, θ=0.5, $\lambda_x=\lambda_y=\lambda$)

The upstream scheme introduces a substantial numerical diffusion in the computation. However, an analysis on the order of magnitude of terms in the mean concentration equation (Wang, 1984) shows that the source term is dominating. Therefore the upstream scheme is accepted for solving the present mean concentration equation.

6.3 The Bed Level Equation

The bed level in the model is calculated from the integrated sediment transport field as follows

$$(1\text{-}P)\ \frac{z_{jk}^{n+1} - z_{jk}^{n}}{N} + \frac{TX_{j+1/2,k}^{n} - TX_{j-1/2,k}^{n}}{\Delta x} + \frac{TY_{j,k+1/2}^{n} - TY_{j,k-1/2}^{n}}{\Delta y} =$$

$$= \frac{\alpha_x}{2N}\left(z_{j-1,k}^{n} - 2z_{jk}^{n} - z_{j+1,k}^{n}\right) + \frac{\alpha_y}{2N}\left(z_{j,k-1}^{n} - 2z_{jk}^{n} - z_{j,k+1}^{n}\right) \qquad (6\text{-}15)$$

In this equation

P = porosity of the bed,

TX,TY = x- and y- components of the total transport in one tidal period

N = number of tidal period in one morphological step,

α_x, α_y = artificial viscosity in x- and y-direction.

Analysis on this scheme has to be carried out in combination with the sediment transport model. This will be very complicated for a realistic estuary case. Therefore it has been decided to carry out an analysis with the following simplifications.

- The flow is one-dimensional.
- The flow is quasi-steady.
- The sediment transport model can be described as

$$\frac{\partial c_s}{\partial x} = \frac{c_{se} - c_s}{L_a} \tag{6-16}$$

$$S = qc_s \tag{6-17}$$

- The water level remains the same as in the initial state (rigid lid).

For this case the numerical solution for c_s and z follow from

$$\frac{c_{sj} - c_{sj-1}}{\Delta x} = \frac{c_{sej} - c_{sj}}{L_a} \tag{6-18}$$

$$(1-P)\,\frac{z_j^{n+1} - z_j^n}{\Delta t} + \frac{S_{j+1/2}^n - S_{j-1/2}^n}{\Delta x} = \frac{\alpha}{2\Delta t}\left(z_{j-1}^n - 2z_j^n - z_{j+1}^n\right) \tag{6-19}$$

With

$$S_{j+1/2} = q\,\frac{c_{sj} + c_{sj+1}}{2} \tag{6-20}$$

this equation can be written as

$$(1-P)\,\frac{z_j^{n+1} - z_j^n}{\Delta t} + q\,\frac{c_{sj+1}^n - c_{sj-1}^n}{2\Delta x} = \frac{\alpha}{2\Delta t}\left(z_{j-1}^n - 2z_j^n - z_{j+1}^n\right) \tag{6-21}$$

Examine the development of the following disturbance in the bed level

$$Z = \hat{z}\ \exp(ikx) = \hat{z}\ \exp(ik\ j\Delta x) \tag{6-22}$$

where k is the wave number.

Suppose that the equilibrium transport rate can be written as

$$S_e = q\ c_{se} = au^b \tag{6-23}$$

With a linearization it can be shown that the disturbance in the equilibrium concentration c_{se} is

$$C_{se} = \hat{c}_{se}\ \exp(ik\ j\Delta x) \tag{6-24}$$

with

$$\hat{c}_{se} = b\ \frac{c_{se}}{H}\ \hat{z} \tag{6-25}$$

where H is the undisturbed water depth.

From equation (6-18) it can be shown that the disturbance in c_s is

$$C_s = \hat{c}_s\ \exp(ik\ j\Delta x) = \frac{\beta}{1-(1-\beta)\exp(-ik\Delta x)}\ \hat{c}_{se}\exp(ik\ j\Delta x) \tag{6-26}$$

with

$$\beta = \frac{\Delta x}{L_a} \tag{6-27}$$

From (6-20)...(6-27) it can be derived that

$$Z_j^{n+1} = \rho\ Z_j^n \tag{6-28}$$

where ρ is the amplification factor

$$\rho = 1 - \alpha + \alpha\cos\xi - \frac{\sigma\beta^2 i\sin\xi}{1-\beta-\cos\xi+i\sin\xi} \qquad (6\text{-}29)$$

with

$$\sigma = b\,\frac{S_0}{H}\,\frac{\Delta t}{\Delta x} \qquad (6\text{-}30)$$

The stability criterion is again $|\rho|\leq 1$. In contrast with the case with equilibrium transport model the scheme can be stable for $\alpha=0$. For this case the stability condition is

$$\sigma\beta^2 \leq 2 \qquad (6\text{-}31)$$

It is interesting that not only the Courant number is important but also the ratio between the space step and the adaptation length is important for the stability. It should further be noted that for $\xi=\pi$

$$\rho = 1-2\alpha \qquad (6\text{-}32)$$

This means that for $\alpha=0$ waves with length $2\Delta x$ will not be damped.

Although $\alpha=0$ is allowed for the stability according to the analysis above, computations for realistic estuary situations have shown that a small but non zero value of α is required for maintaining stability of the computation. However, a much smaller value is required than in the case of equilibrium transport model. Furthermore a σ value larger than one is allowed in contrast with the equilibrium transport model (see equation 6-31).

Chapter 7 VERIFICATION OF THE MODEL

7.1 Introduction

Any model for sediment transport, mathematical or physical, needs to be verified before it can be applied in practice. The applicability of the present model has already been studied theoretically in chapter 5. In this chapter the model is further verified by comparing it with a more sophisticated three-dimensional model.

Verification of the model for the one-dimensional case has already been carried out by comparison with two-dimensional computations as well as with laboratory experiments (Wang, 1984, Wang and Ribberink, 1986). In these comparisons only uniform flows were considered. In this chapter the verification is extended to the three-dimensional case by considering a more realistic test case.

The present model is a simplification of the three-dimensional model. Therefore a comparison with a three-dimensional model provides a perfect verification of the model if the two models are based on the same basic theories. Van Rijn (1987) reports a three-dimensional computation for a partially closed channel with the SUTRENCH model. This model is based on the same basic theories as described in chapter 4. Therefore this case has been chosen as the test case.

The case concerns a unidirectional flow in a channel of constant width (=1000 m) and a horizontal bed. The channel is partially closed by a dam with a length of 400 m and a width of 100 m as shown in fig.7.1. The discharge is 4000 m^3/s and the water depth at the outlet boundary is 6 m. The bed material is assumed to be sand with d_{50}=200 μm and d_{90}=300 μm.

The case chosen at present is an artificial case rather than a practical case. However, the comparison between the depth-integrated model with the three-dimensional model still can provide useful information about the applicability of the model. It is a step between the theoretical analysis and the test of the model with a case from practice. Together with the

theoretical analysis in chapter 5 this step should help one to distinguish the errors due to the procedure of depth-integrating from other causes.

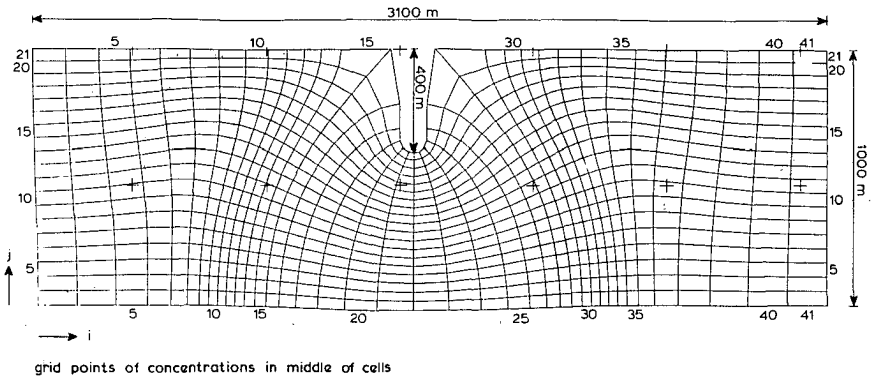

Fig.7.1 Grid schematization of the SUTRENCH computation. After van Rijn and Meijer (1986).

In the following section the applicability of the depth-integrated model for the present case is considered theoretically. This is an application of the results obtained in chapter 5. The comparison between the two models for this case will also provide a verification for the results of the theoretical analysis. In order to keep the computations with the two models comparable with each other, the same flow field should be applied in the two computations. Since the grids in the two models are not the same, a transformation procedure has to be applied in order to obtain the flow field for the present computation. This is considered in section 7.3. In section 7.4 the input parameters and the differences between the two models are summarized. The computational results are reported in section 7.5 and finally section 7.6 summarizes the conclusions drawn from this exercise.

7.2 Theoretical Considerations

Before the computation with the present model is carried out the results of the theoretical analysis can be applied in order to obtain an idea about the validity and applicability of the model for the present case.

A simple examination of the applicability of the model can be made by considering the basic length scales. According to Wang and Ribberink (1986) the depth-integrated model can only be applied when the length scale of the problem is relatively large compared with the length scale $\bar{u}h/u_*$. At present the length of the dam may be considered as the characterizing length scale of the problem, thus L=400 m. The water depth is about 6 m and the roughness hight is k_s=0.25 m, so

$$C = 18 \log \frac{12D}{k_s} = 44.5 \text{ m}^{0.5}/\text{s}$$

$$\frac{\bar{u}}{u_*} = \frac{C}{\sqrt{g}} = 14.2$$

$$\frac{\bar{u}}{u_*} h = 85 \text{ m}$$

$$\frac{Lu_*}{\bar{u}h} \approx 5$$

Based on this consideration it can be concluded that the depth-integrated model should be applicable for the present case but it has to be kept in mind that this schematisation is very rough so the conclusion is not a firm one.

A more detailed consideration can be made by using the result of the analysis presented in chapter 5, with the help of the result from the SUTRENCH computation presented by van Rijn (1987). The equilibrium transport rates along the streamlines B and C (fig.7.3) may be presented in terms of sine functions (via Fourier series). The characterizing wave length for the

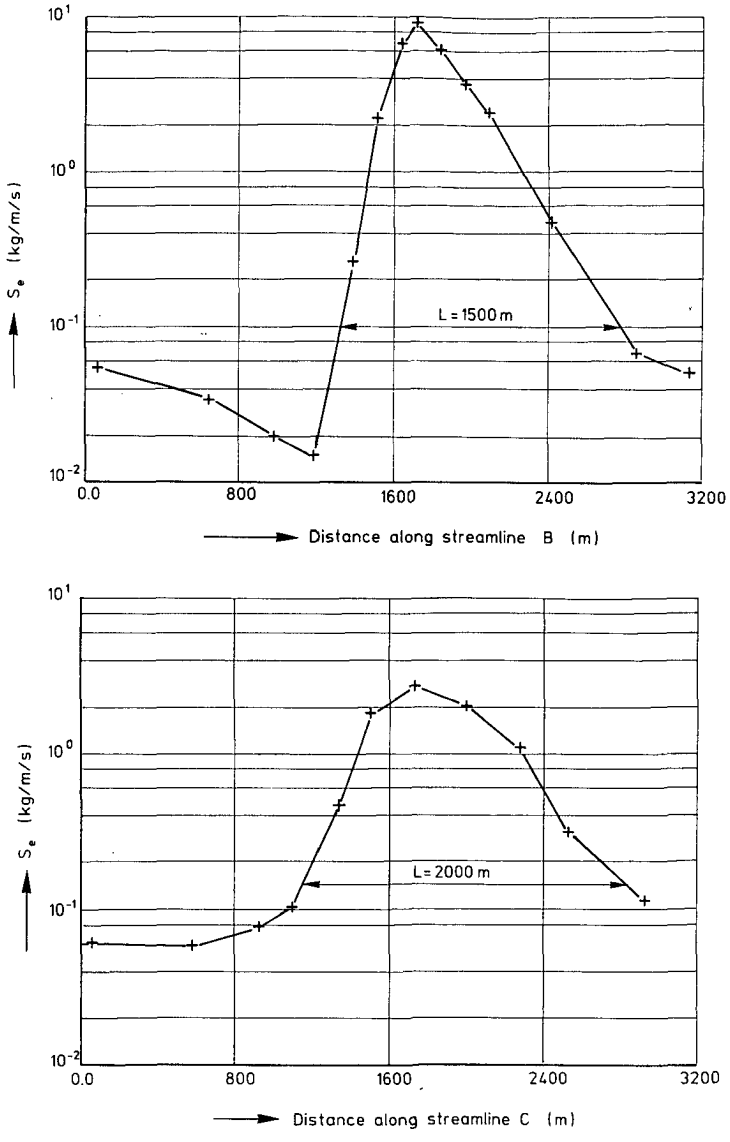

Fig.7.2 Equilibrium transport along Streamline B and C.

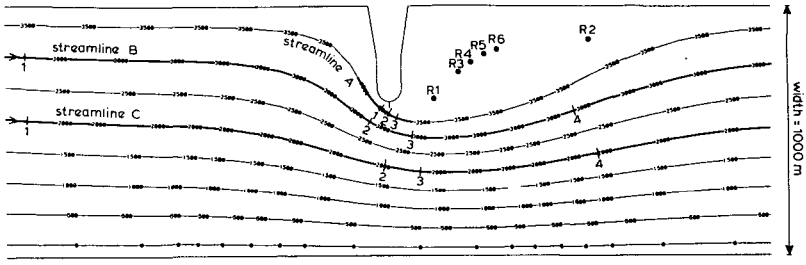

Fig.7.3 Location of the streamlines (after van Rijn and Meijer, 1986)

two streamlines are respectively 1500 m and 2000 m (see fig.7.2). Based on this information the equilibrium concentration may be presented as

$$c_{se} = \hat{c}_{se} \exp(i \frac{2\pi}{L} s) \tag{7-1}$$

or

$$c_{se} = \hat{c}_{se} \exp(ik'\xi) \tag{7-2}$$

with

$$k' = \frac{2\pi}{L} \frac{q}{w_s} \tag{7-3}$$

Equations (5-18) and (5-20) (α=ik') can now be applied to determine the actual concentration, according to the exact solution and the first order solution respectively. Both solutions can be written in the form

$$c_s = \hat{c}_s \exp(ik'\xi - i\theta) \tag{7-4}$$

Compared with the equilibrium concentration (7-2) there is a damping $\hat{c}_s/\hat{c}_{se}$ and a phase lag θ. The damping coefficient and the phase lag according to the exact and the present model are shown in table 7.1. for the two streamlines (fig.7.3).

STREAM-LINE NR.	GENERAL INFORMATION U (m/s)	H (m)	L (km)	w_s/u_*	k'	DAMPING EXACT	ESMOR	PHASE LAG EXACT	ESMOR
B	1.0	6.0	1.5	0.18	2.0	0.574	0.559	0.383	0.475
C	0.9	6.0	2.0	0.20	1.35	0.70	0.715	0.368	0.430

Table 7.1 Analytical Results

The figures in this table show that the present depth-integrated model give similar results as the exact (2DV) model. Therefore it can be concluded with confidence that the model is applicable for the present case.

It should be noted that the damping coefficient can be interpreted as the ratio between the maximum value of the non-equilibrium transport rate and the maximum value of the equilibrium transport rate. The phase lag can be written as

$$\theta = k'\xi = \frac{2\pi}{L}\Delta s \qquad (7\text{-}5)$$

where Δs can be estimated as the distance over which the actual transport is equal to the equilibrium value at a certain site. It is thus also possible to compare the results from the theoretical analysis with the computation results. This will be done in section 7.5 when the computation results are presented.

7.3 Grid Schematisation and the Flow Field Transformation

The grid schematisation of the SUTRENCH computation is shown in fig.7.1.It has 20*40 grid points. The ESMOR model is based on a rectangular staggered grid as shown in fig.3.1. In order to make the computations with the two models comparable with each other, the grid size in the ESMOR computation should be about the same as the minimum grid size in the SUTRENCH computation. Therefore $\Delta x=\Delta y=25m$ is chosen which leads to 41*125 grid points.

Special attention has been paid to the schematisation of the dam. It is not possible to obtain the smooth form of the dam with the ESMOR grid. The schematisation can be seen in e.g. fig.7.4. According to this schematisation the dam is some what too small.

The flow field in the SUTRENCH computation was calculated with the WAQUA model. The ESMOR model is connected with another flow model, viz. the DUCHESS model. In order to keep the two computations comparable it was decided to derive the flow field in the ESMOR grid from the result of the WAQUA model with a transformation procedure.

The flow field transformation is not such an easy problem as it seems to be. The transformation procedure consists of three steps. First the stream function is calculated on the SUTRENCH grid. In the second step the stream function on the present grid is determined via bi-linear interpolation. Finally the flow field is then determined by differentiation. The derived flow field is shown in fig.7.4 together with the original flow field.

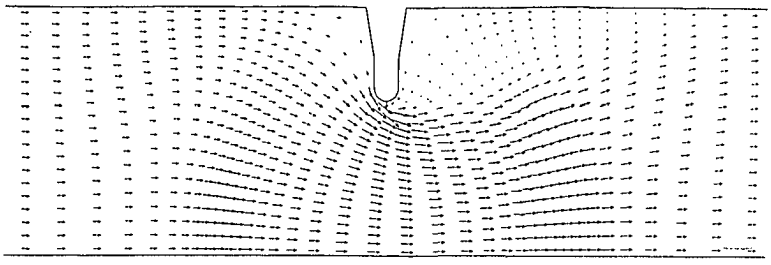

↦ 1.0 m/s

(a) In the SUTRENCH computation.

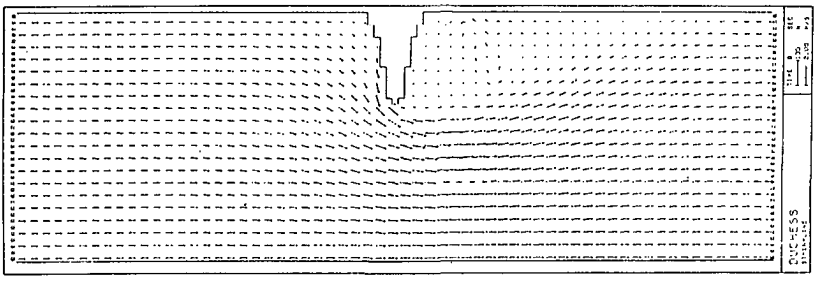

↦

(b) In the ESMOR computation.

Fig.7.4 The velocity field.

7.4 Input Parameters and Differences Between the Two Computations

The basic data in the ESMOR computation are

the flow field h, q_x, q_y as described in the previous section,		
roughness	k_s	= 0.25 m,
particle size of the bed material	d_{50}	= 200 μm,
	d_{90}	= 300 μm,
particle fall velocity of suspended material	w_s	= 0.0125 m/s,
relative density of sediment	Δ	= 1.65,
constant of von Karman	κ	= 0.4,
horizontal diffusion coefficient	ϵ_x	= 0.5 m^2/s,
porosity of bed material	P	= 0.4,
location of the bed boundary	β	= 0.0082,
time step	Δt	= 10 s.

Further the coefficients in the ESMOR model have been calculated with exactly the same vertical diffusion coefficient and the flow velocity profile as in the SUTRENCH computation.

The following differences can be detected between the two models.

1. The upstream boundary condition

SUTRENCH $\quad c = c_e$

ESMOR $\quad \frac{\partial \bar{c}}{\partial t} = \frac{\bar{c}_e - \bar{c}}{T_a}$

This difference is not significant since for the eventually steady case $\partial \bar{c}/\partial t = 0$, so $\bar{c} = \bar{c}_e$.

2. The closed and the outlet boundaries

SUTRENCH $\quad c = c_e$

ESMOR $\frac{\partial \bar{c}}{\partial N} = 0$

The present condition is more realistic but van Rijn has shown that this condition does not influence the results very much.

3. The location of the bed boundary

SUTRENCH $z_a = 0.05$ m

ESMOR $\beta = z_a/h = 0.05/6.09 = 0.0082$

The difference is negligible since the water depth only varies from 6.00 m to 6.18 m.

4. The vertical velocity

SUTRENCH included

ESMOR excluded

The vertical flow velocity is not large so this difference will not be very important

5. Initial condition

SUTRENCH $c(t=0) = c_e$

ESMOR $c(t=0) = 20$ ppm = constant

This difference is insignificant since only the steady situation is of interest.

7.5 Computational Results

Concentration

The ESMOR model is a depth-integrated model, so it does not produce concentration profiles as in the *SUTRENCH* model. It gives only the transport concentration which is defined as

$$c_s = \int_0^1 p(\zeta)\, c(\zeta)\, d\zeta \qquad (7\text{-}6)$$

The contour lines of c_s as well as its equilibrium value c_{se} are shown in fig.7.5. It can be observed from this figure that there is clear damping and phase lag. Further the small disturbances present in c_{se} have been damped out in c_s.

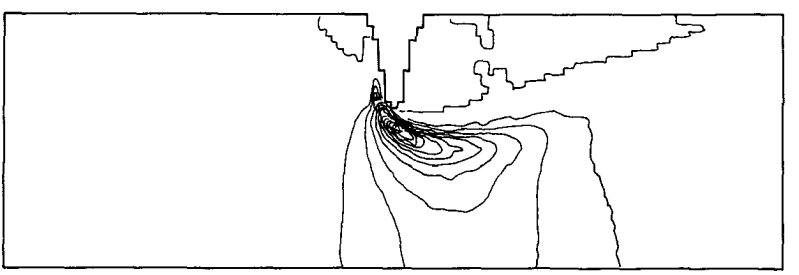

(a) Equilibrium (interval = 40 ppm)

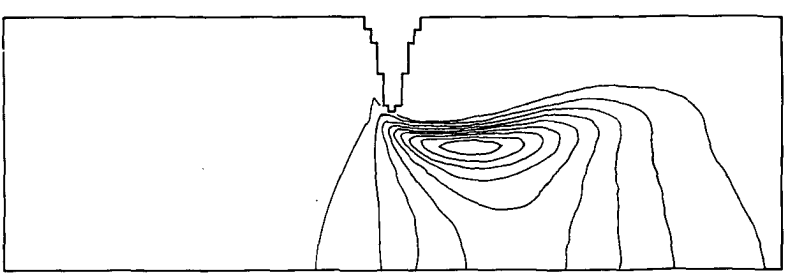

(b) Non-equilibrium (interval= 20 ppm)

Fig.7.5 The computed sediment concentration field.

It should be noted that c_s is not equal to $\bar{c}$. This makes the comparison with the SUTRENCH model rather difficult. However, the comparison can perfectly be carried out for the transport rate and the bedlevel change rate.

Transport Rate

The sediment transport field from the present computation as well as from the SUTRENCH computation are shown in fig.7.6. Comparison between the two computations based on this figure is difficult because of the different plot routines used in the two computations. However, a close examination on the numerical output shows that the agreement between the two computations is quite good. Only in the direct vicinity of the dam head the ESMOR computation seems to give a too small transport rate. This is at least partly caused by the fact that the dam in the ESMOR computation is too small and the velocity at the dam head is therefore too small.

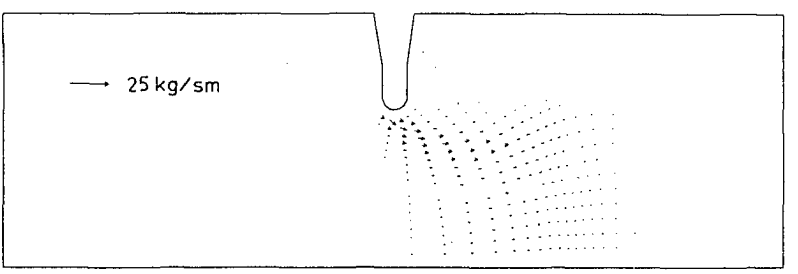

(a) The SUTRENCH model.

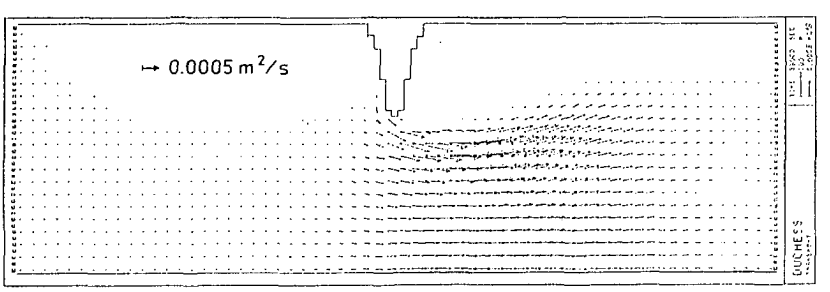

(b) The ESMOR model.

Fig.7.6 The computed sediment transport field.

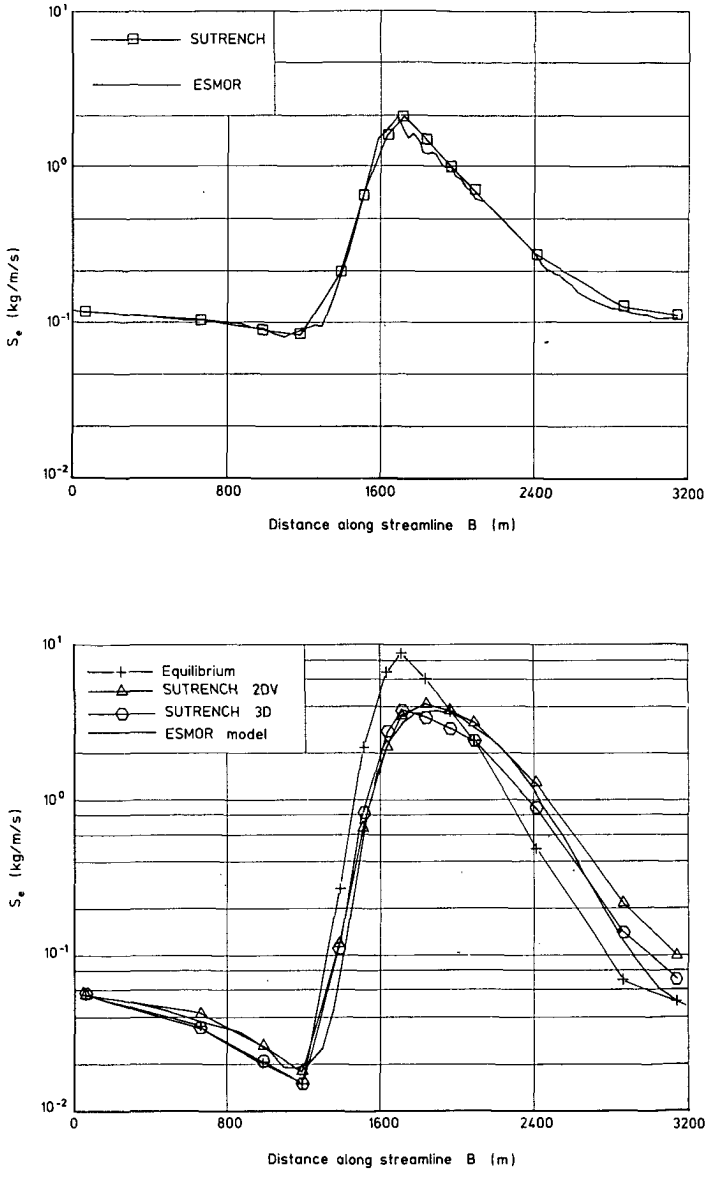

Fig.7.7 Velocity and transport along streamline B

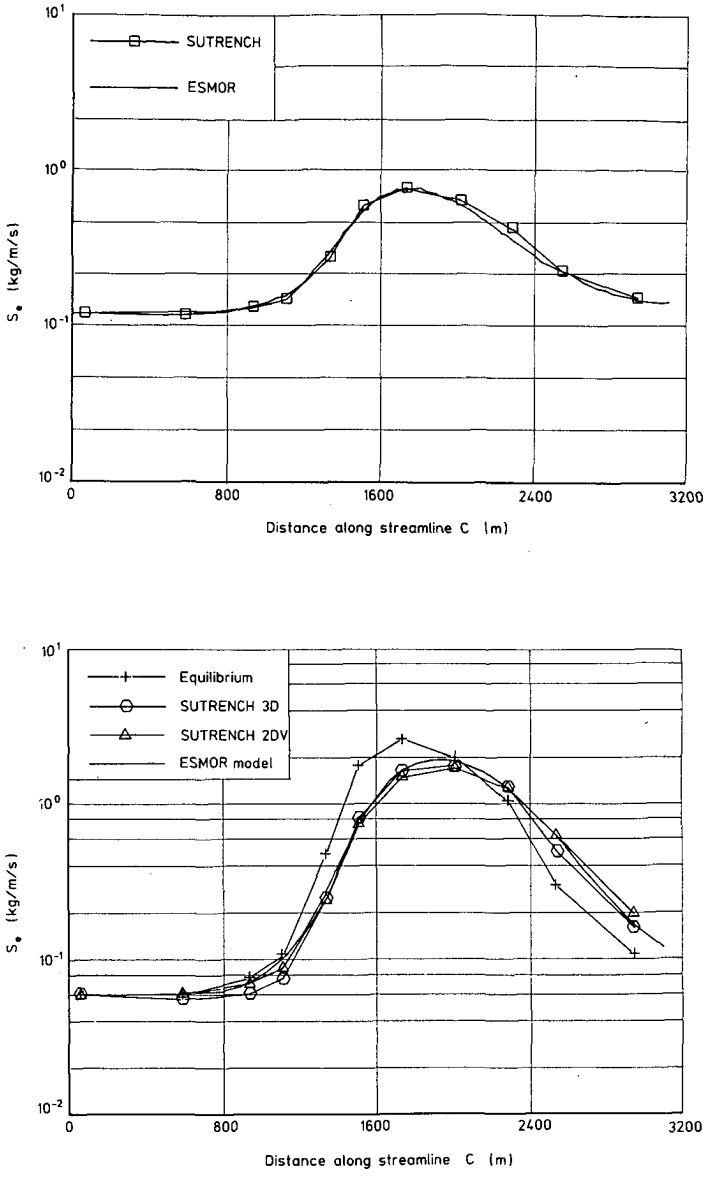

Fig.7.8 Velocity and transport along streamline C.

A better comparison can be made for the transport rate along a particular streamline. In fig.7.7 this is done for streamline B(see fig.7.3). In this figure the 2DV SUTRENCH computation is also presented in addition to the 3D SUTRENCH and the ESMOR computation. The 2DV computation is based on the two-dimensional model along the streamline. According to van Rijn(1987) the 2DV and 3D computations should give almost the same result since the horizontal diffusion for the present case is not very important. Fig.7.7 shows that the difference between the ESMOR computation and the 3D computation has the same order of magnitude as the difference between the 2DV and 3D computations. This means that the agreement between the ESMOR model and the SUTRENCH model is almost perfect. The same applies also for streamline C as shown in fig.7.8.

In table 7.2 the different computations are evaluated in terms of damping coefficient and phase lag (see section 7.2). The phase lag from the computations is the averaged value at the increasing part and at the decreasing part. Although the schematisation of the equilibrium transport rate as a sine function of the distance along the streamline is a very rough one, the analytical results agree with the computation results quite well. The present case gives thus not only a test for the depth integrated model, it also provides a verification for the theoretical analysis.

STREAM-LINE		ANALYSIS 2DV	COMPUTED 3D SUTRENCH	COMPUTED 2DV	ANALYSIS 1DH	COMPUTED 2DH ESMOR
B	DAMPING	0.547	0.42	0.47	0.559	0.42
B	PHASELAG	0.383	0.28	0.40	0.475	0.36
C	DAMPING	0.700	0.65	0.64	0.715	0.73
C	PHASELAG	0.368	0.28	0.40	0.430	0.36

Table 7.2 Comparison between analytical results and computations

Bedlevel Change Rate

The bedlevel change rate from the ESMOR computation is shown with contour lines in fig.7.9. The result of the SUTRENCH model is represented in fig.7.10. The erosion as well as the sedimentation pattern from the two computations agree very well with each other. By examining the numerical output it has been found that the maximum erosion rate is 43 mm/h and the maximum sedimentation rate is 10.5 mm/h. The values reported by van Rijn are respectively 100 mm/h and 25 mm/h. This large difference is only present in the direct vicinity of the dam head. It is probably partly due to the disturbance in the flow field introduced during transformation and partly due to the error introduced by the depth integrated modelling.

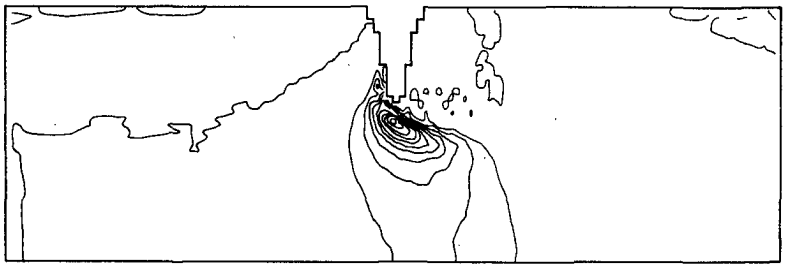

(a) Erosion (interval = 4 mm/h)

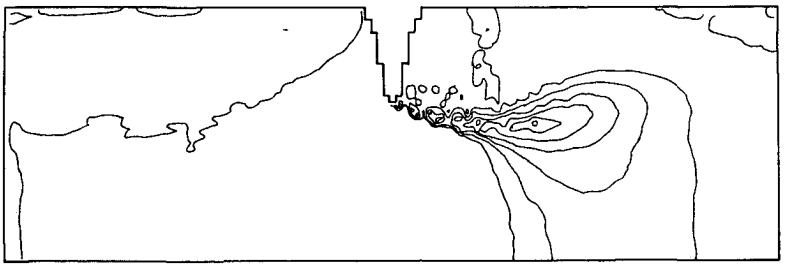

(b) Sedimentation (interval = 2 mm/h)

Fig.7.9 Bed level change calculated from the ESMOR model

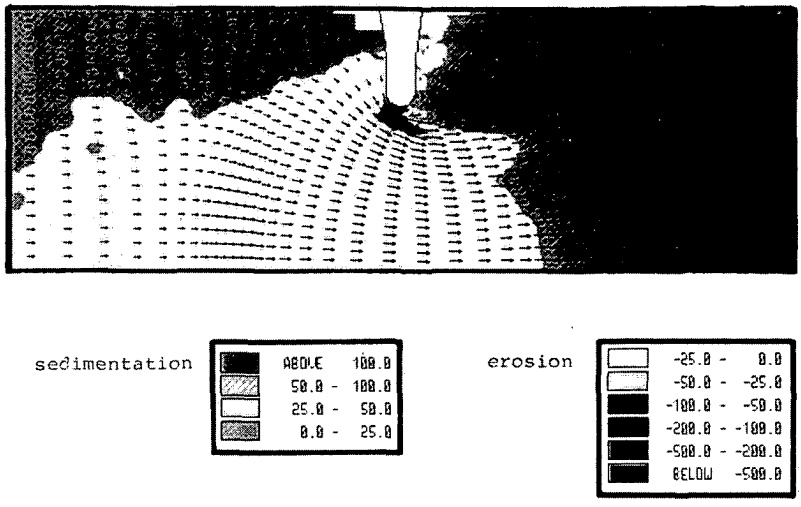

Fig.7.10 Bed level change calculated from the SUTRENCH model

Computation time

SUTRENCH: CPU time for the 40x20(x10) grid is about 90 s for 100 time steps on a CDC CYBER 855 computer (van Rijn, 1987).

ESMOR : CPU time for the 125x41 grid is about 90 s for 200 time steps on a IBM 3083-JX1 computer.

The two computers mentioned above have about the same computation speed. apparently the ESMOR model will be about 10 times faster than the SUTRENCH model if they are both used on a same horizontal grid. This is logical because the SUTRENCH computation uses 10 grid points in the vertical direction.

7.6 Summary and Conclusions

A computation has been carried out with the ESMOR model for a partially closed channel which has already been calculated with the SUTRENCH model. A comparison between the two models has been perfectly possible since they have exactly the same theoretical background. Before the computation is carried out the results of the theoretical analysis have been applied with some schematizations. The conclusions from the theoretical analysis are verified with the computation results.

The main findings from this study are summarized in the following conclusions

* Transformation of the flow field from one grid to another grid is not such an easy problem. It should be done via the stream function when ever possible.

* The theoretical analysis shows that the depth-integrated model is applicable for the present case. The conclusions of the theoretical analysis are supported by the computation results.

* The agreement between the results from the depth-integrated model and the SUTRENCH model is quite good.

* The computation cost of the ESMOR computation is much lower than that of the SUTRENCH computation if the two models are both used on a same horizontal grid. The ratio between the computation costs depends on the number of grid points in the vertical direction in the SUTRENCH computation.

Chapter 8 A PRACTICAL APPLICATION OF THE MODEL

8.1 Introduction

After the verification of the morphological model in the previous chapter it is logical to test the model further for field conditions. Testing the model by applying it for a practical problem is not such a easy task. For the application of the model a lot of field data are required which are often not available. Special adjustment to the model and assumptions have to be made for the absent data. It should also be noted that the model cannot be applied to every estuary due to the simplification made. In fact the model can only be applied for well-mixed estuaries because the density flow effect is not taken into account. This makes the choice of a test problem even more difficult. Despite these difficulties attempts are made in this chapter to apply the model to a estuary. For this purpose the Yantze estuary is chosen. In section 8.2, it is argued that the model is applicable for that case.

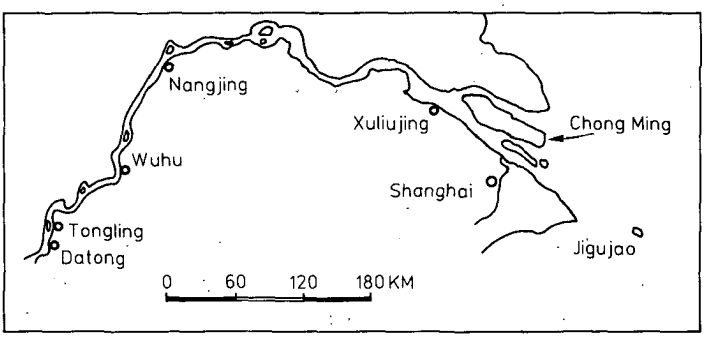

Fig.8.1 The tidal region of the Yantze River.

The Yantze River (Changjiang in Chinese), with a length of 6380 km and a catchment area of 1.8 million km^2, is the largest and the most important river in China. It flows into the East China Sea north of Shanghai. The river mouth is situated at Jigujiao which forms the natural downstream boundary of the estuary. The tidal influence can reach up the river as far as Tongling and Wuhu in the dry season during spring tide. Datong located 640 km from the river mouth is the most downstream tide free hydrologic station (see fig.8.1). In order to have clearly defined upstream boundary

conditions, a study on the Yantze estuary should start from this station although Xuliujing is usually considered as the upstream boundary of the estuary.

The Yantze estuary is of great economic importance to China. It is the entrance to Shanghai harbour and also the main waterway for seagoing ships. Without this estuary the Shanghai Economic Zone would probably never have been developed. At present various enterprises are being constructed along the south bank of the estuary. The most important one is the Baoshan Steel Mill with a total planned output of six million tons of steel in 1990. Another important one is the Shidongkou Thermal Power Plant with a total installed capacity of 2400 MW, which will start operation in 1992. Especially for these enterprises, jetties are built along the south bank of the estuary for the sea going transport of raw material, fuel and products. Further, the Luojing harbour with a total yearly transport of 24,000,000 tons and Qiyakou harbour with a total yearly transport of 60,360,000 tons are planned along the south bank of the estuary. For these harbours and jetties it is very important to keep the navigation channels in good order. Therefore, investigation of the morphological development in the estuary is of great importance.

The Yantze estuary is divided by islands and sand banks in a regular way. Downstream of Xuliujing the estuary is first divided into the south and north branches by the Chongming island. The south branch is then subdivided into the south and north channels by the Changxing and Hengsha islands. The south channel is further divided into south and north passage by the Jiuduan sandbank. Corresponding to these ordered regular divisions the development of the estuary seems also to happen in a systematic way. Every division is initiated by an underwater sandbank. The sandbank becomes an island as the division develops. The division will finally disappear when the island joins the north bank of the estuary. At the same time a new division somewhere downstream will start to develop. This systematic process has already repeated itself several times in history although the period of the process is considerable (Chen et al, 1982). At present, the north branch is decreasing its volume due to sedimentation. It is expected that the Chongming island will join the north bank in the near future.

At present (1989) the Yantze estuary seems to be too large to be included in the ESMOR model. It is certainly impossible to consider the whole region from Datong to Jigujiao (640 km) because of the large area covered, although it would be ideal to do so for the boundary conditions of the morphological model. Even when Xuliujing instead of Datong is considered as the upstream boundary the model will cover an area of about 100 km * 100 km^2. This will not only lead to too many grid points but the available data for such a model will also be very restricted since extensive measurements have not been carried out in all parts of the estuary. As mentioned above, the south branch is the main waterway at present while the north branch is silting up. Most enterprises under construction or in planning stage are located along the south bank of the south branch. The south branch has become the most interesting part of the estuary for research. Most measurements are also carried out in the south branch. Therefore it is decided to take the south branch for the study. As upstream boundary the cross section at Xinjian is chosen and as downstream boundary the Hengsha cross section in the south channel and the Gongqingwei cross section in the north channel, (see fig.8.2).

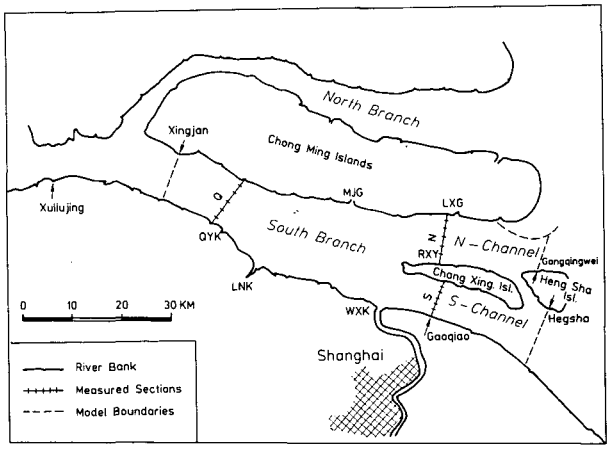

Fig.8.2 The Yantze Estuary.

In the following section the collected data are described and analyzed. The calibration of the flow as well as the sediment transport model is carried out in section 8.3 followed by a simulation of a one week measuring period in 8.4. The long term morphological computations are described in section 8.5 followed by some sensitivity analysis in section 8.6. Finally in section 8.7 the conclusions from the study are summarized.

8.2 The Field Data

8.2.1 General Features of the Estuary

Before the ESMOR model is applied the general features of the estuary have to be examined in order to see whether the model is applicable for the estuary.

The most important feature of an estuary is the type of mixing which is determined by the ratio between the river inflow and the tidal prism of the estuary.

At the Datong hydrologic station the following data are derived from the measurements in the period 1947 to 1983.

long term annual runoff	$912*10^9$ m^3
long term averaged discharge	28900 m^3/s
maximum discharge	92600 m^3/s
minimum discharge	4620 m^3/s

The tide in the Yantze estuary is semi-diurnal, with a period of 12 h 25 min. At the mouth the maximum tidal range is 4.62 m, the average tidal range is 2.66 m, and the minimum tidal range is 0.17 m. In different seasons, depending on the tidal range, the tidal prisms of the estuary are:

flood season, spring tide	$5.3 * 10^9$ m^3
dry season, spring tide	$3.9 * 10^9$ m^3
flood season, neap tide	$1.6 * 10^9$ m^3
dry season, neap tide	$1.3 * 10^9$ m^3

The type of mixing of an estuary can be characterized by the mixing number M which is the ratio between the fresh water inflow (QxT) and the tidal prism (Simmons and Brown, 1969). According to Officer (1975) an estuary is stratified if $M \geq 1$, well-mixed if $M \leq 0.01$ and partially mixed if $0.01 \leq M \leq 1.0$. The type of mixing of the Yantze estuary has been studied by Huang and Zhong (1986). Under the long term mean fresh water inflow and average tide M is determined to be 0.29, So on the whole the partially mixed type is predominant in the Yantze estuary. However, in the flood season during neap tide (M=2.6), stratified flow may occur, while in the dry season during spring tide (M=0.05) the estuary may become well mixed. At the long term flood season mean discharge, 45500 m^3/s, the 'null point' which indicates the upper limit of the salt intrusion, is located at Tongsha, where the mouth bar is formed. This is located just outside the modelling region at present. Therefore the density flow effect at present can be neglected although the estuary as a whole is not well-mixed.

At the Datong hydrologic station data are also collected for the sediment transport.

flood season averaged sediment concentration	1.0	kg/m^3
dry season averaged sediment concentration	0.1	kg/m^3
annual averaged sediment concentration	0.544	kg/m^3
averaged annual sediment load	$486*10^9$	kg

Especially the annual sediment load is very important for the calibration of the morphological model since it determines the morphological time scale of the estuary.

The sediment in the estuary is quite fine. It consists mostly of silt. For such fine material, flocculation can be important when the salinity is above a certain level. Cohesive sediment particles in the Yantze estuary consists mainly of illite (70 to 77%) while the percentage of montmorillonite is only 3.5-7.5% (Shen et al, 1986). According to Dyer (1979) flocculation of illite and kaolinite is complete above a salinity of 0.4% if adequate particle concentration is present. Therefore, it can be expected that the flocculation can be important when the salinity is above 0.4%. Measurements

from August 28, 1984 to September 4, 1984 show that fresh water dominates in the upstream part of the region under consideration. The salinity at the Qiyakou (Q) cross section is below 0.16%. In the downstream part of the region the salinity is much higher. In the south channel (S) and north channel (N) the salinity varies between 0.6 to 1.7% in the same period. This means that the flocculation in the upstream part of the region can be neglected while in the downstream part it can be important. Little is known about the flocculation of sediment in the Yantze estuary. In the present study the flocculation effect is not taken into account. This shortcoming of the model has to be kept in mind when computational results are interpreted.

8.2.2 Data Required for the Study

For the morphological computation with the present model the following data are required.

Geometry and topography

Detailed information on the geometry and bed level in the area under consideration at the initial state is required.

Roughness of the bed

The Chezy coefficient in the whole area has to be known.

Boundary condition for the flow

For the ideal boundary condition for the flow the water level at the downstream boundary has to be specified while at the upstream boundary the discharge has to be given.

Properties of the sediment

The grain sizes of the bed material as well as the suspended material have to be known. For the suspended material the fall velocity has also to be known. For the bed composition the porosity has to be known.

Boundary condition for the sediment transport

For the ideal boundary conditions the transport rate at the upstream boundary during ebb and the sediment concentration at the downstream boundary during flood have to be specified.

The data mentioned up to now are the necessary data to run the model. In order to calibrate and to verify the model the following additional data are required.

- Water level measured in some stations within the model area.
- Flow velocity measured within the region under consideration.
- Sediment concentration or transport rate in the region under consideration.
- Bed level of the whole area at different times.

8.2.3 Collected Data

The collected data are mostly from three sources, the annual sounding of the bed level in the estuary, the records of the hydrologic and tidal stage record stations, and the 1984 hydrologic survey conducted in the period between 28 August and 4 September. Among these sources the 1984 hydrologic survey is the most important one. In the following the required data listed in the previous section are examined one by one in order to see if they are satisfied. If this is not the case a solution is suggested.

Geometry and Topography

This information has been obtained from a large scale (1:50000) navigation map. The navigation map is updated every year with measurements (soundings) usually conducted from April to October of the year. The bed levels indicated on the map are thus not measured at one certain time. The topography of the years 1984 and 1985 is selected for the present study.

Roughness of the bed

No field data concerning the bed roughness is available. However, various tidal flow computations have been carried out for the estuary, so some experience about the resistance to the flow has been gained. An often used value of n in the Manning formula for the region under consideration is 0.013, thus

$$C = \frac{D^{\frac{1}{6}}}{0.013} \qquad (8\text{-}1)$$

where D = water depth in m,
C = Chezy coefficient in $m^{0.5}/s$.

In the ESMOR model the Chezy coefficient is calculated as

$$C = A \log\frac{12D}{k_s} \qquad (8\text{-}2)$$

Table 8.1 shows that a satisfactory agreement between equation (8-1) and (8-2) is achieved for A = 40 and k_s = 0.18 m with the water depth varying from 1 to 34 m.

WATER-DEPTH	EQUATION (8-1)	EQUATION (8-2)	WATER-DEPTH	EQUATION (8-1)	EQUATION (8-2)
1.0 m	76.9	72.9	4.0 m	96.9	97.0
7.0 m	106.4	106.7	10.0 m	112.9	112.9
13.0 m	118.0	117.5	16.0 m	122.1	121.1
19.0 m	125.7	124.1	22.0 m	128.8	126.6
25.0 m	131.5	128.8	28.0 m	134.0	130.8
31.0 m	136.3	132.6	34.0 m	138.5	134.2

Table 8.1 Comparison between equations (8-1) and (8-2)

A value k_s of 0.18 m is realistic for a bed with sediment transport, but an A value of 40 certainly needs some explanation.

It should be noted that

$$A = \frac{\sqrt{g}}{\kappa \log e} \qquad (8\text{-}3)$$

where κ is the von Karman constant. For κ =0.4 the usual value A = 18 is obtained. According to Einstein and Chien (1954) κ value can be decreased by the presence of the suspended sediment in the flow. Einstein and Chien (1954) relate the κ value to the relative energy required to keep the sediment in suspension (see fig.8.3). It is difficult to apply this theory directly to a tidal flow since the energy slope i is then not well defined. However, using the Chezy equation the relative energy may be modified as follows for a single fraction of sediment

$$\Sigma \frac{\Delta c w_s}{ui} = \Delta c \frac{w_s}{u} \frac{C^2 D}{u^2} \qquad (8\text{-}4)$$

For Δ=1.65, c = 1000 ppm, w_s = 1 mm/s, u = 1 m/s, D = 10 m, C = 112 $m^{0.5}/s$ this equation becomes

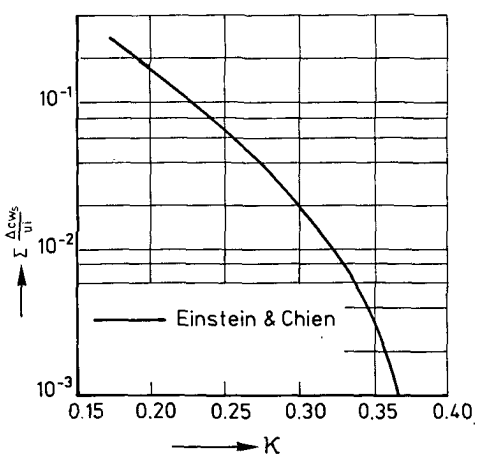

Fig.8.3 Relation between von Karman constant and relative energy

$$\Sigma \frac{\Delta cw_s}{ui} = 0.21 \qquad (8\text{-}5)$$

From fig.8.3 it follows that $\kappa = 0.18$, which may explain the value A=40.

In the final computation the A value is determined by calibration. The value given here is used as reference.

Boundary condition for the flow

The boundaries of the region are chosen such that at each boundary a tidal stage record station is present. So the downstream boundary condition is satisfied but for the upstream boundary condition the required discharge record is not available.

Mathematically it is no problem to give water level boundary conditions at both sides of the model, but it can be dangerous from a accuracy point of view. Specifying the water levels at both sides means that the water surface gradient is given. A small error in the water levels can cause a large error in the gradient, especially when the difference between the water levels is small. A large error in the gradient means a large error in the velocity. Furthermore computations have shown that this type of upstream boundary condition can give numerical problems. Special measures have to be taken to assure stability of the computation as described in the following section.

In the short term computations including those for calibration and the simulation of the measuring period, the measured water level at the upstream boundary is used as boundary condition. In the long term morphological computations a flow computation of one tidal period has been carried out first, and the computed discharge at the upstream boundary during this period is used as boundary condition for further computation.

Properties of the sediment

During the 1984 hydrologic survey the grain size of bed material at 10 locations in total in the south channel and north channel cross section has been determined. These data are shown in table 8.2

VERTICAL	d_{50}	VERTICAL	d_{50}
S1	15.5	N1	53.0
S2	12.0	N2	50.5
S3	62.5	N3	90.0
S4	105.0	N4	125.0
S5	43.0	N5	27.5

Table 8.2 Grain size of the bed material in μm

d_{50} in μm at the south channel cross section			
VERTICAL	SPRING TIDE	average tide	NEAP TIDE
S1	14.2	13.5	6.7
S2	12.0	13.3	7.7
S3	13.0	11.9	8.6
S4	11.6	13.5	6.6
S5	11.8	11.1	6.3
d_{50} in μm at the north channel cross section			
N1	12.2	8.9	7.3
N2	13.7	11.4	7.0
N3	16.6	10.1	10.4
N4	16.5	12.4	9.7
N5	17.2	11.6	8.8
$\bar{d}$ in μm at the Qiyakou cross section			
Q	13.5	18.3	9.25

Table 8.3 Grain size of the suspended material

The grain size of the bed material appears to vary strongly from site to site, but the area covered by the measurement points is too restricted to draw a conclusion about the distribution of the bed material needed to calculate the bed load transport. However, the bed load transport can be neglected with respect to the suspended transport as will be shown in section 8.6. Therefore this will not cause serious problem for the computation.

The grain size of the suspended material was also measured in 3 cross sections during the 1984 hydrologic survey (see table 8.3).

The suspended material appears to be more homogeneous in the region than the bed material but it clearly depends on the amplitude of the tide. The fall velocity is not measured. It might be estimated from the grain size as follows

$$w_s = \frac{1}{18} \frac{\Delta g}{\nu} d^2 \qquad (8\text{-}6)$$

With this formula it can be shown that the fall velocity is in the order of 0.1 mm/s. It should be noted that the fall velocity may also be influenced by the flocculation. Reliable data for w_s can only be obtained from field measurement. Therefore it is decided to consider w_s as a calibration parameter.

No information about the porosity of the bed is available. In the computations it is assumed to be 0.4, which is probably not exact, especially in regions with fine bed material.

Boundary Condition for Sediment Transport

No sediment concentration or transport rate measurement was conducted at the boundaries. Therefore assumptions have to be made for the boundary conditions. At the downstream boundary during flood the dynamical equilibrium concentration from the single point model is applied in all computations.

$$\frac{\partial c_s}{\partial t} = \frac{c_{se} - c_s}{T_a} \qquad (8\text{-}7)$$

The same has been done for the upstream boundary during ebb in the short term computations. It should be noted that for the case of steady flow this condition is equivalent to applying the equilibrium transport rate at the upstream boundary. For the long term morphological computations this condition alone is not sufficient for the upstream boundary condition for the morphological model. Therefore in the long term computations the problem is solved analogously as for the flow computation. A computation of one tidal period is carried out first and the computed transport rate at the upstream boundary is used as boundary condition in further computation.

Water level in the region

The tidal records of the six tidal stage stations present in the region (fig.8.2) are collected. These records can be used for the calibration and verification of the flow model.

Flow velocity in the region

During the 1984 hydrologic survey flow velocities at 15 verticals have been measured during spring tide, average tide as well as neap tide. These data are used for the calibration and verification of the flow model.

Sediment concentration

During the 1984 hydrologic survey also the sediment concentration has been measured in the 15 verticals. These data can be used for calibrating and verifying the sediment transport model.

Bed level at different times

The bed levels of 1984 and 1985 have been collected. The bed level measured in 1984 is used as the initial bed level while that of 1985 is used for testing the morphological model.

8.2.4 Theoretical Considerations on the Applicability of the Model

Based on the collected field data the result from the theoretical analysis as presented in chapter 5 can be applied to examine the applicability of the model.

Basic parameters

$$\frac{\bar{u}}{u_*} = \frac{C}{\sqrt{g}} \approx 30$$

$$\bar{u} \sim 1 \quad m/s$$

so $u_* \sim 0.03$ m/s

$w_s \sim 0.001$m/s

so $$\frac{w_s}{u_*} \sim 0.03$$

The convergence radius of the asymptotic solution of Galappatti (1983) e.g. can now be determined. For $w_s/u_*=0.03$, $R_\alpha \approx 33$. (see section 5.3).

Time Variation

The characterizing time scale for the present problem is the tidal period

$$T = 44700 \text{ s.}$$

so the α value characterizing the time variation is

$$\alpha = i \frac{2\pi}{T} \frac{h}{w_s}$$

For h=10 m and w_s=0.001 m/s $|\alpha|=1.4$ which is much smaller than R_α. Therefore the model will certainly be applicable regarding to the time variation.

Spatial variation

As pointed out in chapter 5 the wave number k characterizing the bed level variation in a numerical model is always in the range

$$\frac{\pi}{\Delta x} \leq k \leq \frac{\pi}{L}$$

where Δx is the space step and L is the length of the region under consideration. At present Δx=1 km and L=80 km, so the magnitude of

$$\alpha = ik \frac{q}{w_s}$$

varies from 0.4 to 32 for q=10 m^2/s. Thus the spatial variation is also within the convergence domain of the model of Galappatti (1983). Therefore it can be concluded that the model is certainly applicable for the present case.

8.3 Basic Parameters and Calibration of the model

8.3.1 Basic Parameters

The region under consideration has a length of about 80 km and a width of about 15 km. For the computational grid (fig.8.4) the space steps are chosen as Δx=Δy=1 km. The time step should be restricted by the stability as well as the accuracy requirement.

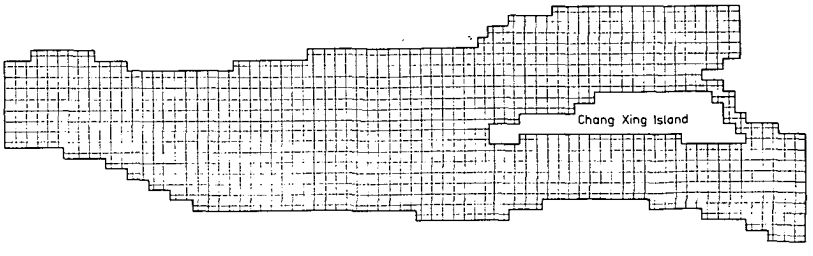

Fig.8.4 The computational grid

In the flow model the ADI method is applied for the numerical computation, which is theoretically unconditionally stable. According to Stelling et al (1987) the ADI method can only be accurate if

$$\Delta t \sqrt{gd\left[(0.5\Delta x)^{-2} + (0.5\Delta y)^{-2}\right]} \leq 4\sqrt{2} \qquad (8\text{-}8)$$

For $\Delta x=\Delta y=1000$m and $\sqrt{gD}$ = 10 m/s this gives $\Delta t \leq 200$ s. Therefore $\Delta t=200$ s is chosen for the computation. Computations have also been carried out with other time steps. The influence of the time step on the accuracy is discussed in section 8.6.

The time step for the concentration computation is chosen the same as that for the flow computation. The time step for the transport rate is chosen larger than that of the flow computation.

The geostrophic force is determined by the latitude θ of the region, which is about 31^0 N, so

$$f = 2\Omega \sin\theta = 7.49 * 10^{-5}\ s^{-1}$$

The horizontal eddy viscosity has been chosen as

$$E = 0.03\ \bar{u}_s D \qquad (8\text{-}9)$$

This is about $u_* D$ for C=110 $m^{0.5}/s$.

8.3.2 Calibration of the Flow Model

The calibration of the flow model is carried out with a computation using the field data measured during the first tidal period of the 1984 hydrologic survey. Only one calibration parameter is used, i.e. the Chezy coefficient. Two computations have been carried out one with

$$C = 40 \log \frac{12D}{0.18}$$

and the other with

$$C = 30 \log \frac{12D}{0.18}$$

From the comparison between the results of the two computations the following conclusions have been drawn.

* The Chezy coefficient does not have significant influence on the computed water level. The agreement with the measurements is quite good in both computations.

* The influence of the Chezy coefficient on the flow velocity is much more important. The second computation agrees better with the measurement than the first computation. In the first computation the Chezy coefficient seems to be too large while in the second computation it seems to be too small. For further computations it has been decided to use

$$C = 33 \log \frac{12D}{0.18} \qquad (8\text{-}10)$$

In the calibration computations the water level has been specified at both the upstream and downstream boundary as boundary condition. This appears to cause some serious numerical problems in the flow model DUCHESS. The problem occurs at the boundary region, especially during an inflow period. At the boundary a circulation occurs and its strength grows in time, eventually causing 'overflow' in the inflow discharge. This is apparently due to the numerical schematization at the water level boundaries. In order to avoid this problem the inflow velocity is smoothed along the boundary after each time step with

$$v_i^{new} = \left[v_i + \alpha(v_{i-1} - 2v_i + v_{i+1})\right]^{old} \qquad (8\text{-}11)$$

where i is the grid number along the boundary. Physically this means that a extra viscosity of $\alpha\Delta x^2/\Delta t$ is added to the water at the boundary. Therefore the α value should be chosen as small as possible. Computations show that α = 0.05 is sufficient to maintain stability of the computation.

8.3.3 Calibration of the Sediment Transport Model

Two parameters are used for calibrating the sediment transport model, the fall velocity and the bed boundary condition.

The gradient type bed boundary condition is applied in the computation with the equilibrium concentration computed from

$$c_{se} = A \frac{\bar{u}_s^2}{D} \tag{8-12}$$

where A is a coefficient with dimension $T^2 L^{-1}$ to be determined via the calibration. This equation is applied only because it is often used for the Yantze estuary (see e.g. Huang, 1986) as well as for the Qiantang estuary (Lin et al, 1981) of which the sediment is mostly from the Yantze estuary (Lin, 1984). At present (1989) the obtained data is too restricted to verify this formula.

The fall velocity w_s is the key parameter in the model. It is the only parameter determining the adaptation time when the flow field is known. The adaptation time is the most important parameter determining the phase lag and the damping of the sediment concentration compared with the equilibrium concentration. The other calibration parameter, the coefficient A has also strong influence on the amplitude of the concentration but it does not influence the phase lag. Therefore the agreement for the phase lag with the measurement is used as a criterion for determining w_s.

Four computations have been carried out for the calibration of w_s, respectively with w_s=0.0001, 0.0005, 0.001 and 0.002 m/s. The best agreement has been found for w_s= 0.001 m/s.

It should be noted that the concentration equation is linear, so the calibration with the coefficient A is quite easy when w_s is already determined. The best value for A can be found by extrapolation. However, it appears that good agreement between the measurement and computation can only be obtained if the coefficient A varies in the region. The eventually used value (in s^2/m) is

$$A = 0.030 \qquad \text{for flood} \qquad (8\text{-}13a)$$

$$A = \begin{cases} 0.030 & \text{for } y>50\text{km} \\ 0.0525 & y<41\text{km} \\ [1.75\ (50-y)/9 + (y-41)/9]*0.03 & 41<y<50 \end{cases} \qquad \text{for ebb} \qquad (8\text{-}13b)$$

where y is the distance in km measured from the upstream boundary. No proper explanation can be given for equation (8-13b). The final conclusion on the formula for the equilibrium concentration will be given in the following section after the simulation of the whole measuring period.

8.4 Simulation of the Measuring Period

From August 28 to September 4, 1984 a hydrologic survey was organized in the estuary. This one week measuring period, in the flood season of the Yantze river, was chosen such that spring tide, average tide as well as neap tide were covered. During the survey the flow velocity, sediment concentration, water temperature and salinity were measured in five cross sections distributed in the whole estuary, among which three sections are located in the region under consideration (see fig.8.2). In each cross section data were collected in five verticals with five measuring points in each vertical. A part of the data collected in this survey has already been used for calibrating the model described in the previous section. In this section a simulation of the whole measuring period is described.

The simulation has two aims.

1) It provides a verification of the calibrated model.

2) It gives information about the influence of the spring-neap tide cycle. This information is useful for determining the standard tide in the morphological computation.

The important input parameters in this computation are

$w_s = 0.001$ m/s
$\Delta x = \Delta y = 1000$ m

$\Delta t_f = \Delta t_c = 298$ s
$\Delta t_s = 4 * 298 = 1192$ s
$\Delta t_m = 89400$ sec = 24 h 50 min.

The Chezy coefficient, bed boundary condition, upstream and downstream boundary conditions for the flow as well as for the sediment transport are as described in the previous two sections. In fig 8.5 the applied water level at the boundaries are shown. Neither secondary flow nor bed load transport is included in this computation. Their influence will be discussed in section 8.6.

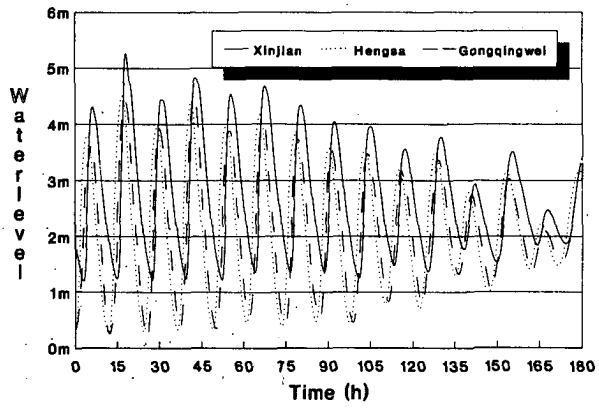

Fig.8.5 Boundary conditions for the flow.

In order to restrict the computation time, the time step for the flow computation Δt_f and for the concentration computation Δt_c has been chosen larger than the value mentioned in the previous section. The influence of the time step will be discussed in the sensitivity analysis in section 8.6. Δt_s is the time step for the transport rate computation. It can be chosen larger than Δt_c because it is not restricted by any stability requirement. It has only to be small enough for an accurate integration of the transport rate over the tidal period.

Δt_m is the morphological time step. At present it is chosen as two times the tidal period, which means that the bed level in the model is adjusted every day. This time step is relatively small. It is chosen to ensure an real simulation of the measuring period.

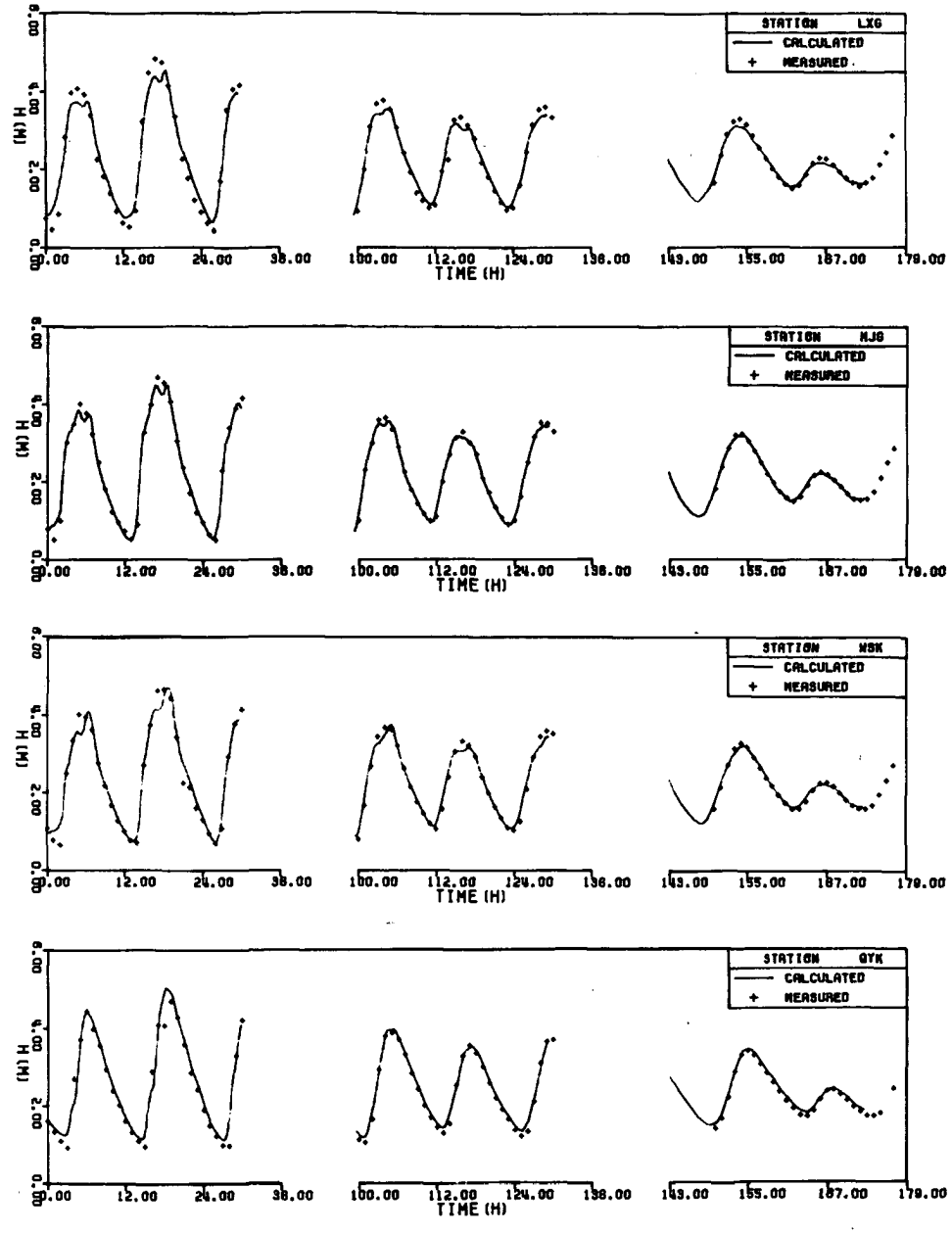

Fig.8.6 Calculated and measured water level.

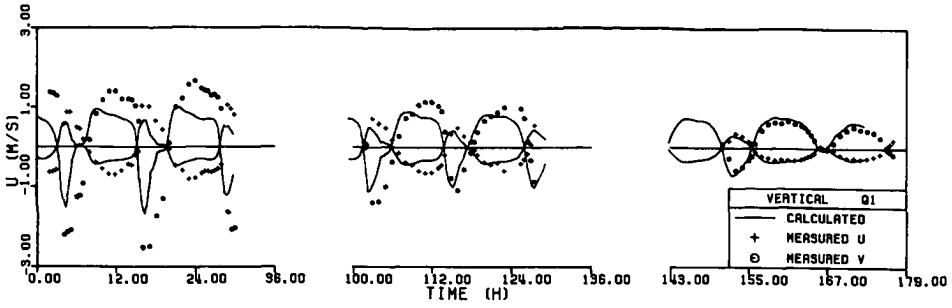
U (M/S)
3.00
1.00
-1.00
-3.00
0.00
12.00
24.00
36.00
100.00
112.00
124.00
136.00
143.00
155.00
167.00
179.00
TIME (H)
VERTICAL Q1
CALCULATED
MEASURED U
MEASURED V

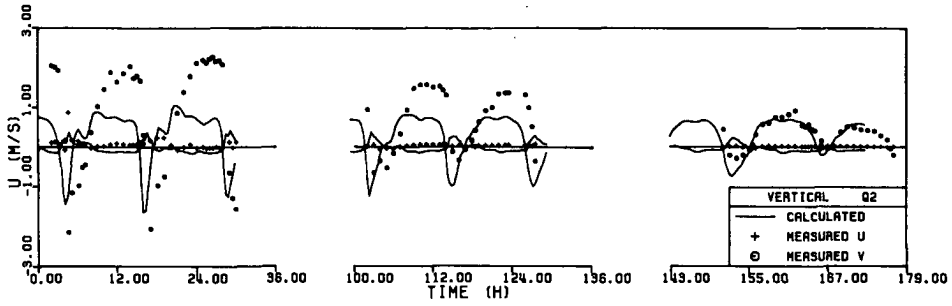
U (M/S)
3.00
1.00
-1.00
-3.00
0.00
12.00
24.00
36.00
100.00
112.00
124.00
136.00
143.00
155.00
167.00
179.00
TIME (H)
VERTICAL Q2
CALCULATED
MEASURED U
MEASURED V

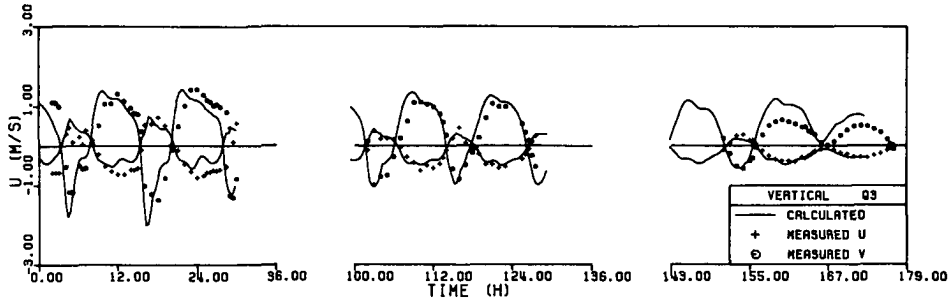
U (M/S)
3.00
1.00
-1.00
-3.00
0.00
12.00
24.00
36.00
100.00
112.00
124.00
136.00
143.00
155.00
167.00
179.00
TIME (H)
VERTICAL Q3
CALCULATED
MEASURED U
MEASURED V

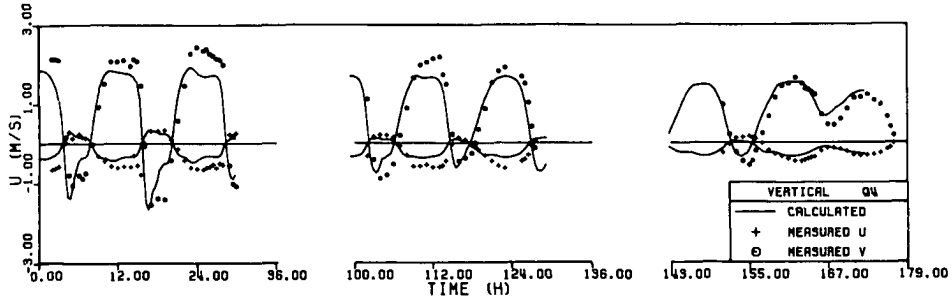
U (M/S)
3.00
1.00
-1.00
-3.00
0.00
12.00
24.00
36.00
100.00
112.00
124.00
136.00
143.00
155.00
167.00
179.00
TIME (H)
VERTICAL Q4
CALCULATED
MEASURED U
MEASURED V

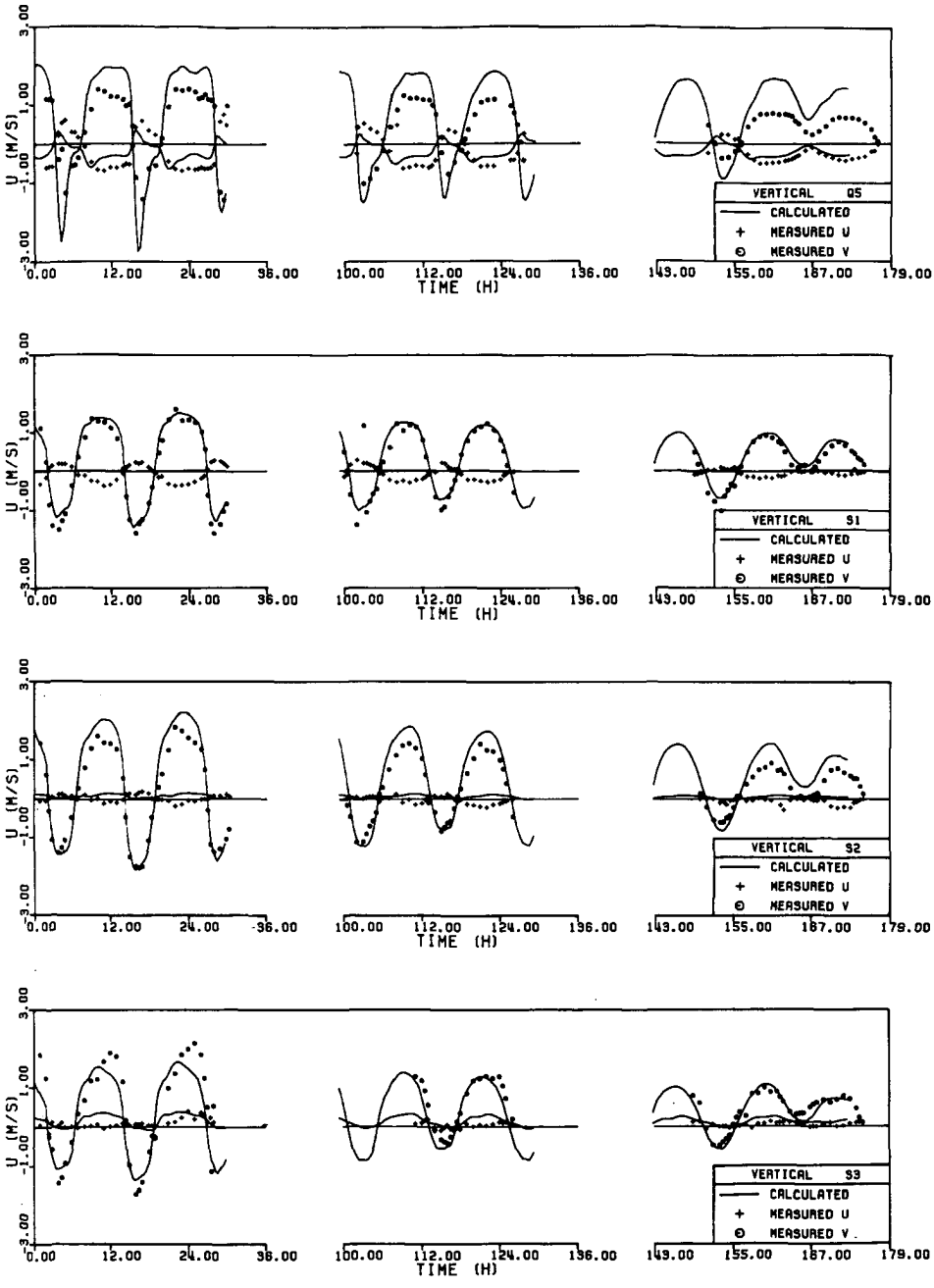
U (M/S)
3.00
1.00
-1.00
-3.00
0.00
12.00
24.00
36.00
100.00
112.00
124.00
136.00
143.00
155.00
167.00
179.00
TIME (H)
VERTICAL 05
CALCULATED
MEASURED U
MEASURED V
VERTICAL 01
CALCULATED
MEASURED U
MEASURED V
VERTICAL 02
CALCULATED
MEASURED U
MEASURED V
VERTICAL 03
CALCULATED
MEASURED U
MEASURED V

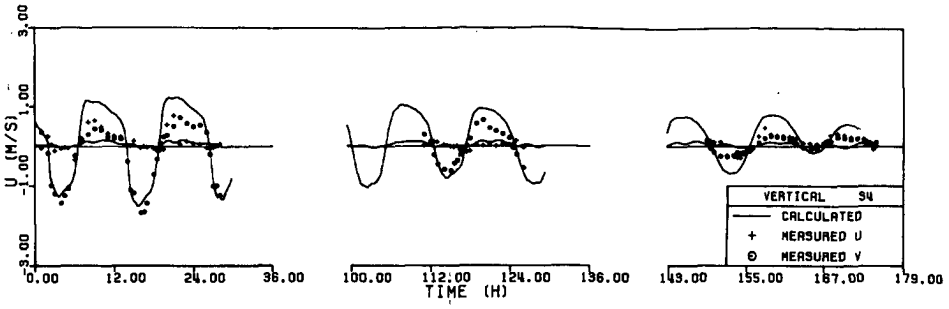
U (M/S)
3.00
1.00
-1.00
-3.00
0.00
12.00
24.00
36.00
100.00
112.00
124.00
136.00
143.00
155.00
167.00
179.00
TIME (H)
VERTICAL S4
CALCULATED
+ MEASURED U
⊖ MEASURED V

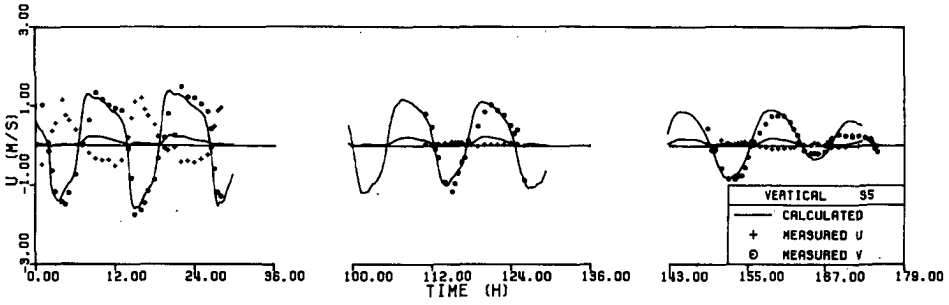
U (M/S)
3.00
1.00
-1.00
-3.00
0.00
12.00
24.00
36.00
100.00
112.00
124.00
136.00
143.00
155.00
167.00
179.00
TIME (H)
VERTICAL S5
CALCULATED
+ MEASURED U
⊖ MEASURED V

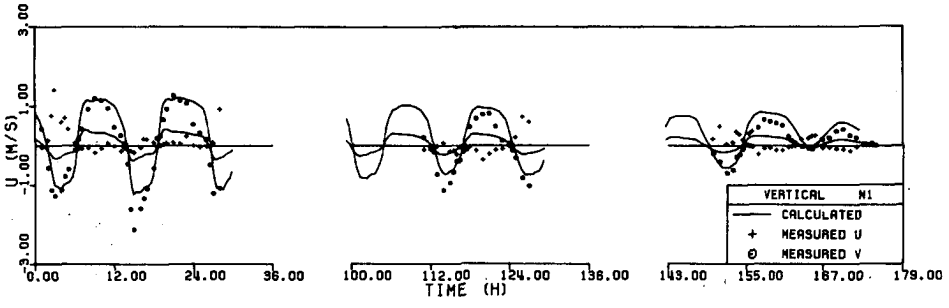
U (M/S)
3.00
1.00
-1.00
-3.00
0.00
12.00
24.00
36.00
100.00
112.00
124.00
136.00
143.00
155.00
167.00
179.00
TIME (H)
VERTICAL N1
CALCULATED
+ MEASURED U
⊖ MEASURED V

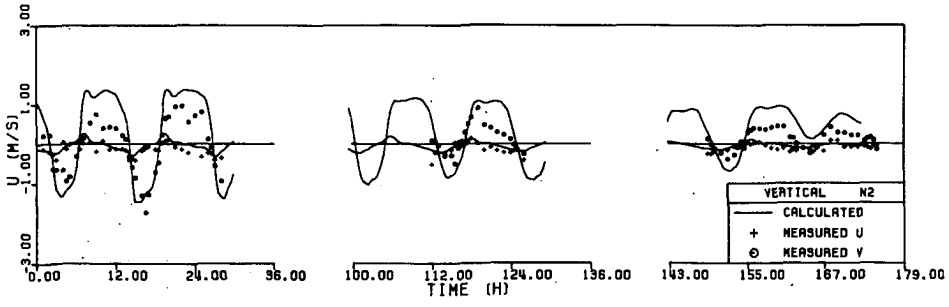
U (M/S)
3.00
1.00
-1.00
-3.00
0.00
12.00
24.00
36.00
100.00
112.00
124.00
136.00
143.00
155.00
167.00
179.00
TIME (H)
VERTICAL N2
CALCULATED
+ MEASURED U
⊖ MEASURED V

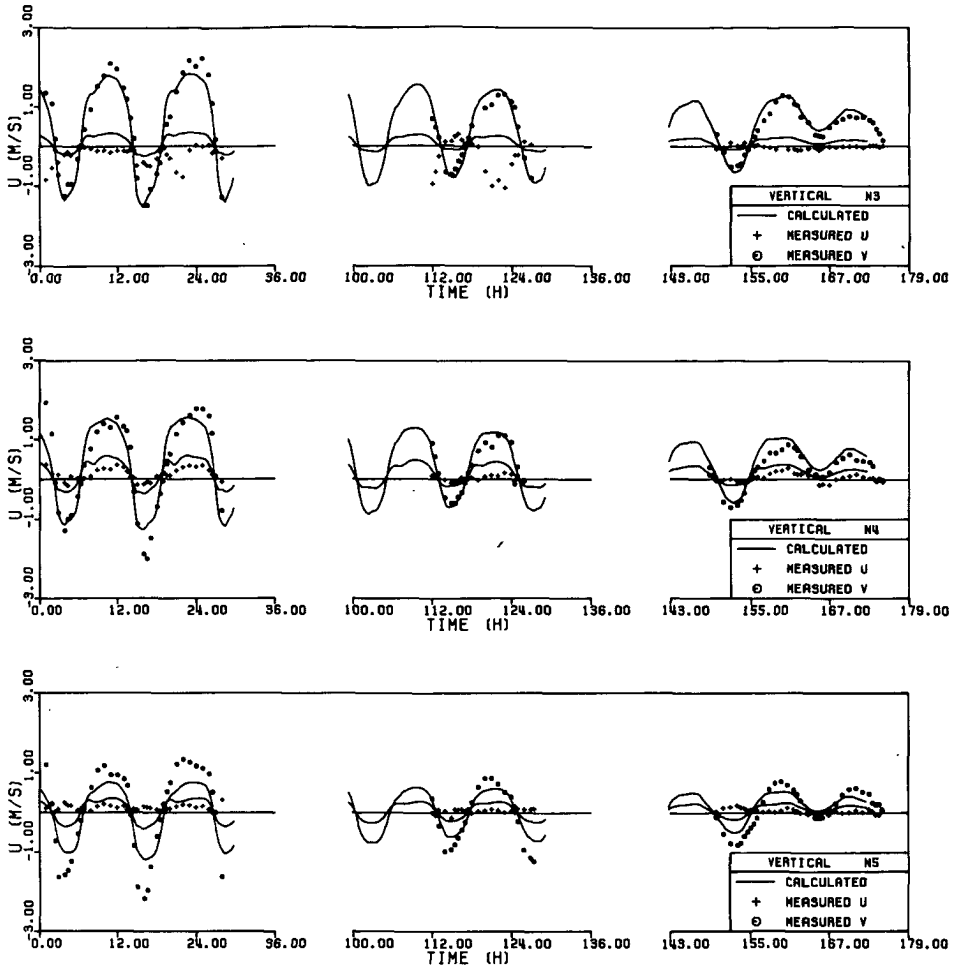

Fig.8.7 comparison between calculated and measured velocity in the 15 verticals.

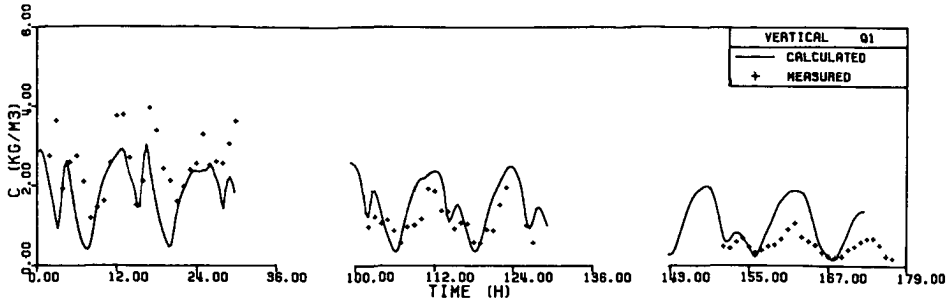
VERTICAL Q1
CALCULATED
MEASURED
C (KG/M3)
0.00
2.00
4.00
6.00
0.00
12.00
24.00
36.00
100.00
112.00
124.00
136.00
143.00
155.00
167.00
179.00
TIME (H)

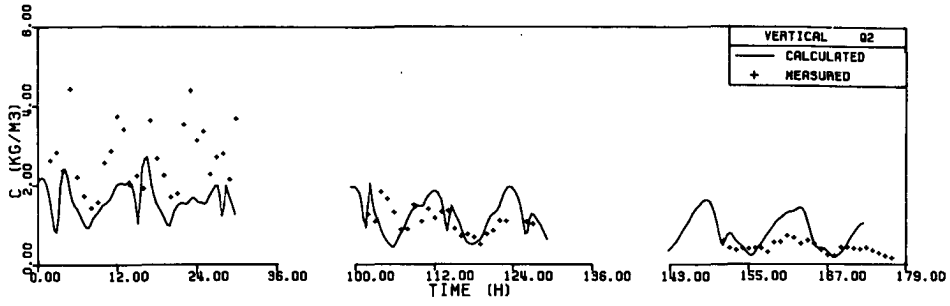
VERTICAL Q2
CALCULATED
MEASURED
C (KG/M3)
0.00
2.00
4.00
6.00
0.00
12.00
24.00
36.00
100.00
112.00
124.00
136.00
143.00
155.00
167.00
179.00
TIME (H)

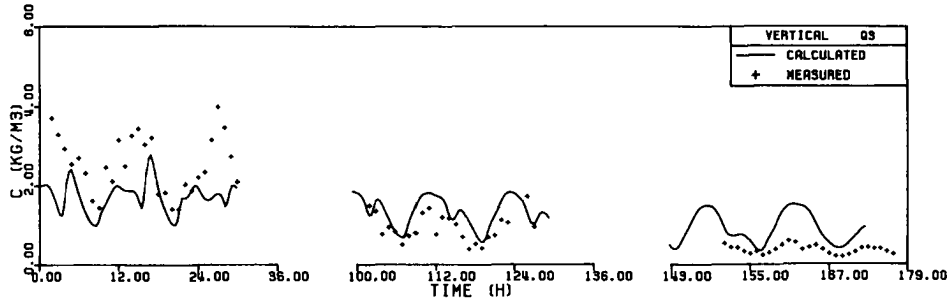
VERTICAL Q3
CALCULATED
MEASURED
C (KG/M3)
0.00
2.00
4.00
6.00
0.00
12.00
24.00
36.00
100.00
112.00
124.00
136.00
143.00
155.00
167.00
179.00
TIME (H)

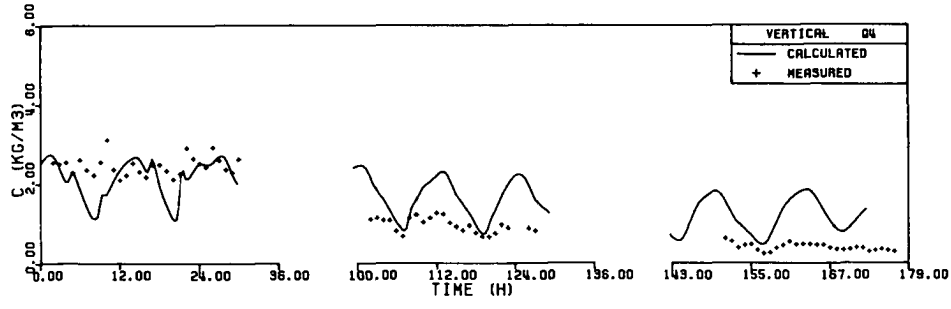
VERTICAL Q4
CALCULATED
MEASURED
C (KG/M3)
0.00
2.00
4.00
6.00
0.00
12.00
24.00
36.00
100.00
112.00
124.00
136.00
143.00
155.00
167.00
179.00
TIME (H)

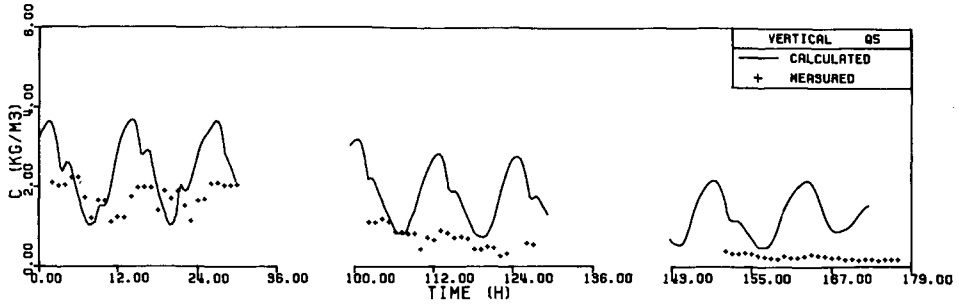
VERTICAL Q5
CALCULATED
MEASURED
C (KG/M3)
0.00
2.00
4.00
6.00
0.00
12.00
24.00
36.00
100.00
112.00
124.00
136.00
143.00
155.00
167.00
179.00
TIME (H)

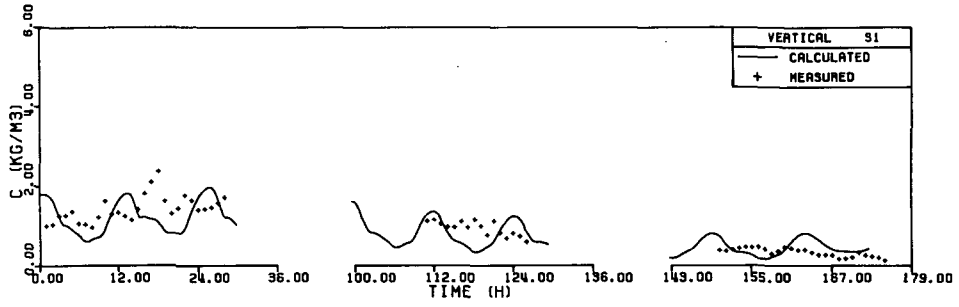
VERTICAL S1
CALCULATED
MEASURED
C (KG/M3)
0.00
2.00
4.00
6.00
0.00
12.00
24.00
36.00
100.00
112.00
124.00
136.00
143.00
155.00
167.00
179.00
TIME (H)

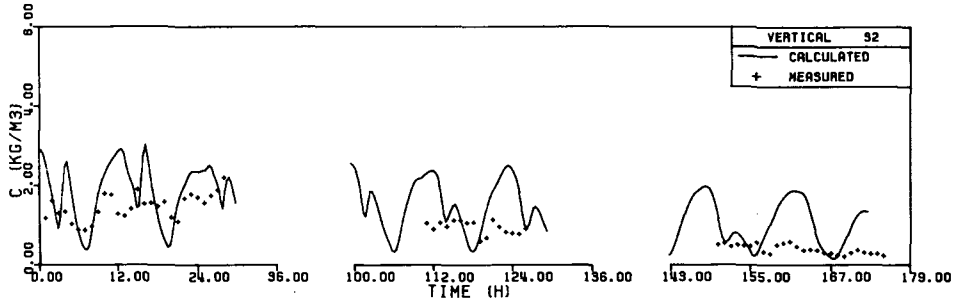
VERTICAL S2
CALCULATED
MEASURED
C (KG/M3)
0.00
2.00
4.00
6.00
0.00
12.00
24.00
36.00
100.00
112.00
124.00
136.00
143.00
155.00
167.00
179.00
TIME (H)

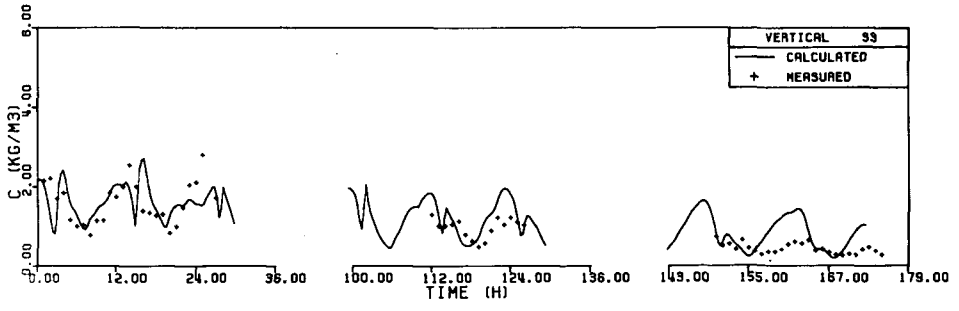
VERTICAL S3
CALCULATED
MEASURED
C (KG/M3)
0.00
2.00
4.00
6.00
0.00
12.00
24.00
36.00
100.00
112.00
124.00
136.00
143.00
155.00
167.00
179.00
TIME (H)

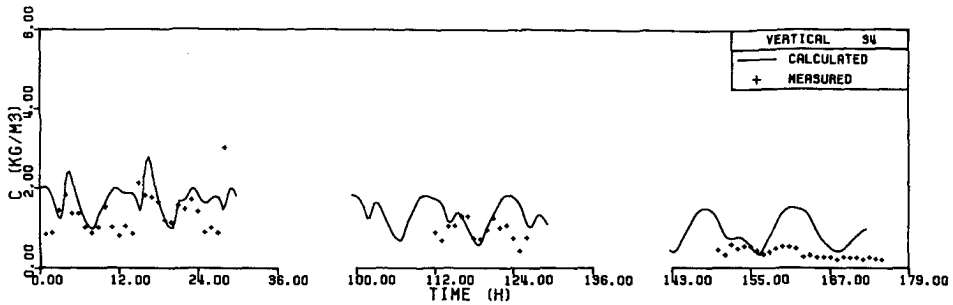
VERTICAL S4
CALCULATED
MEASURED
C (KG/M3)
8.00
4.00
2.00
0.00
0.00
12.00
24.00
96.00
100.00
112.00
124.00
136.00
143.00
155.00
167.00
179.00
TIME (H)

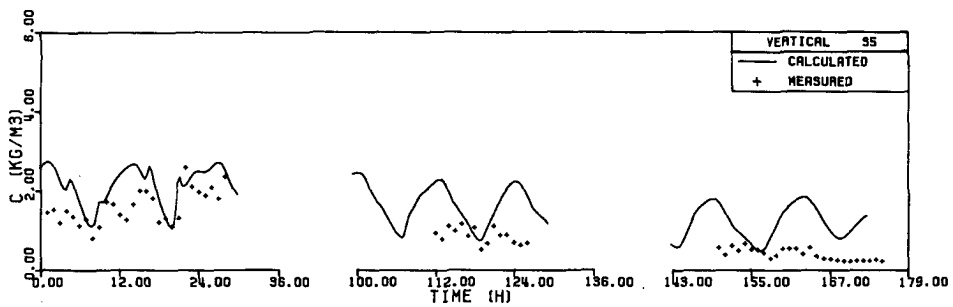
VERTICAL S5
CALCULATED
MEASURED
C (KG/M3)
8.00
4.00
2.00
0.00
0.00
12.00
24.00
96.00
100.00
112.00
124.00
136.00
143.00
155.00
167.00
179.00
TIME (H)

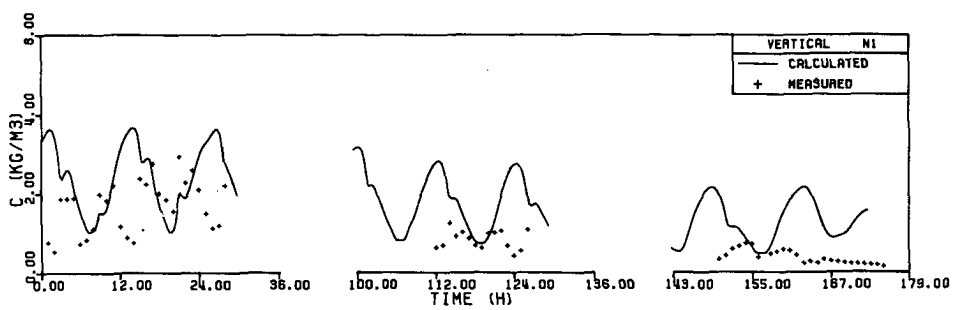
VERTICAL N1
CALCULATED
MEASURED
C (KG/M3)
8.00
4.00
2.00
0.00
0.00
12.00
24.00
96.00
100.00
112.00
124.00
136.00
143.00
155.00
167.00
179.00
TIME (H)

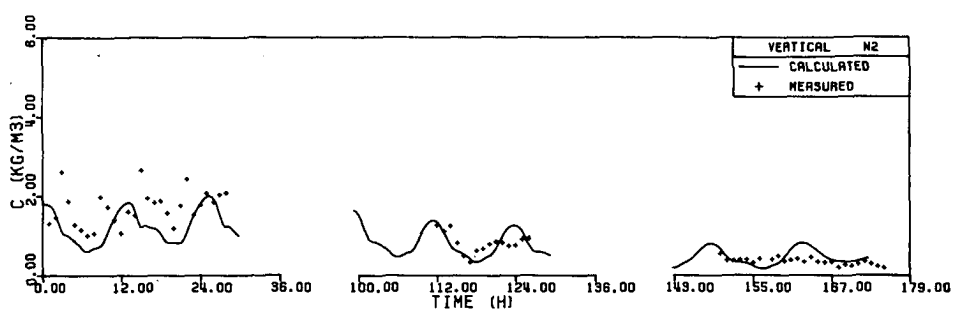
VERTICAL N2
CALCULATED
MEASURED
C (KG/M3)
8.00
4.00
2.00
0.00
0.00
12.00
24.00
96.00
100.00
112.00
124.00
136.00
143.00
155.00
167.00
179.00
TIME (H)

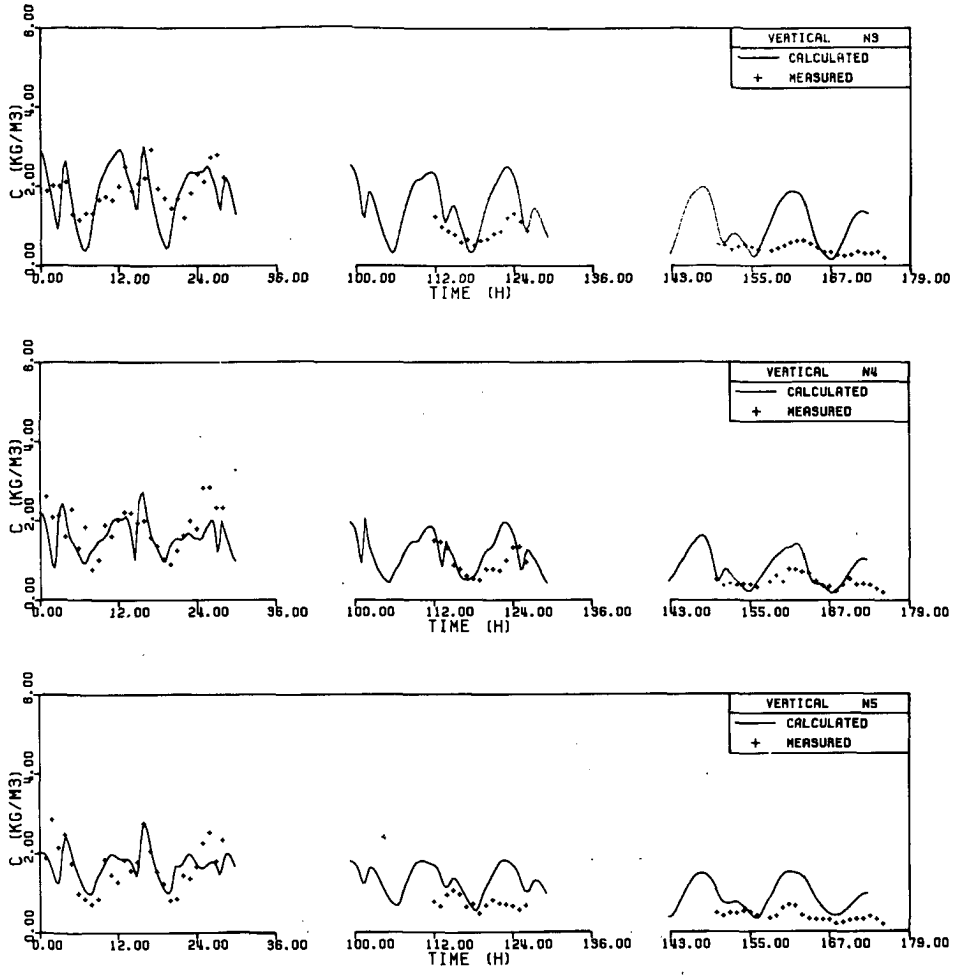

Fig.8.8 Comparison between calculated and measured mean concentration in the 15 verticals.

The results from the flow model are presented in fig.8.6 and fig.8.7. Fig.8.6 shows the measured and calculated water level at different stations during spring tide, average tide and neap tide. The agreement between the computation and the measurements is good in the whole period. The comparison between the computed and measured flow velocities in the 15 verticals is carried out in fig.8.7. The agreement for most verticals is reasonable in the whole period, although in some verticals especially those near the river bank (Q2, Q5, S4, N2, N5) considerable deviations between the measurement and the computation are present. In general it can be concluded that the calibration of the flow model has been satisfactory.

Fig.8.8 shows the comparison between the measured and calculated sediment concentration in the 15 verticals. From this figure it can be observed that:

* The results in all Q-verticals are not satisfactory. Especially during neap tide the concentration is overestimated. This is probably due to the fact that the A coefficient in equation (8-13) is too large.

* The results in the S- and N-verticals are better, but still not really satisfactory. However, for these regions it seems to be impossible to make the agreement between the measurements and the calculations better by modifying the two calibration parameters.

* The results during the average tide are reasonable in most verticals.

Fig.8.9 shows the transport rate in the three cross sections. The agreement between the measurement and the calculation is reasonable, but during the averaged and neap tide the transport is considerably overestimated by the computation, especially in the cross section Q. The same conclusion is drawn from fig.8.10 where the dayly total flood- and ebb-transport through the three cross sections is shown. It seems thus that the calibration of the sediment transport model has not been very satisfactory. However, with the available field data it is not possible to improve the agreement between the computation and the measurement very much by changing the calibration parameters. The A coefficient given in equation (8-13) is estimated under spring tide condition. It is too large for average tide and neap tide,

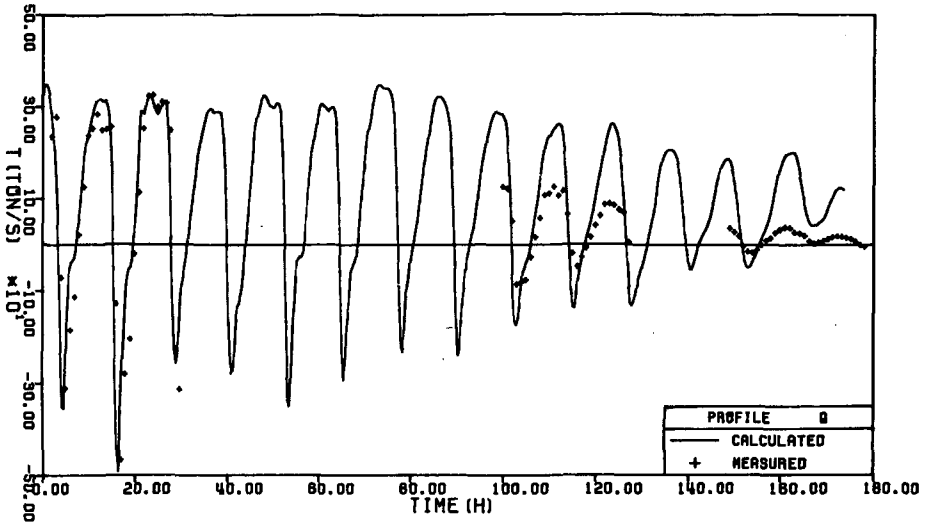

Fig.8.9a Calculated and measured sediment transport through cross section Qiyakou.

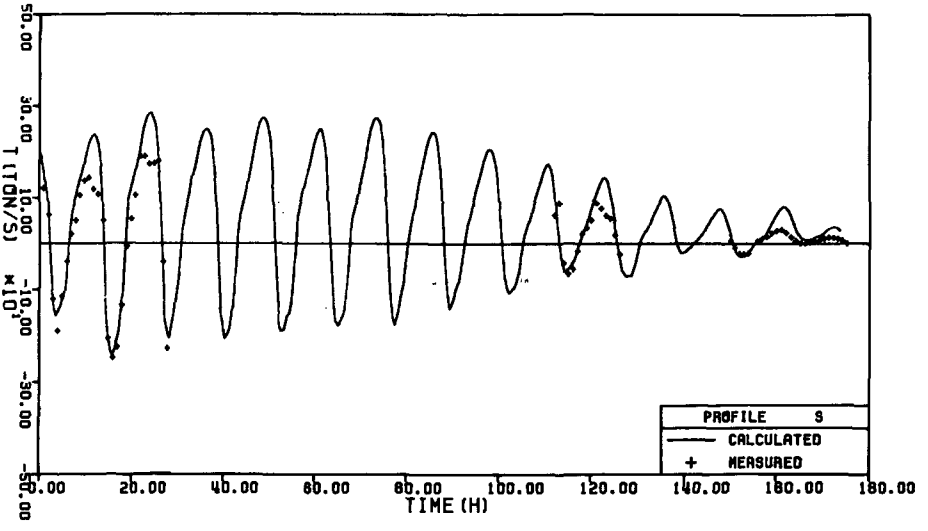

Fig.8.9b Calculated and measured sediment transport through cross section South Channel.

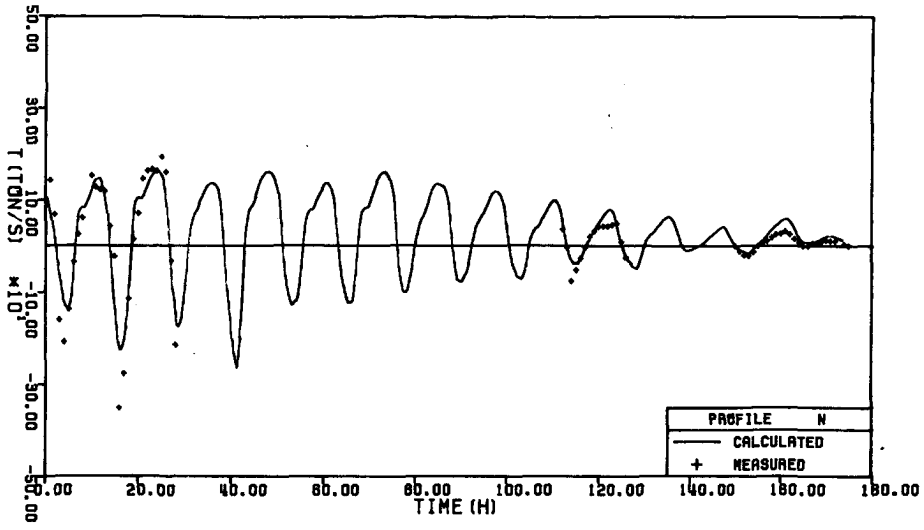

Fig.8.9c Calculated and measured sediment transport through cross section North Channel.

especially during ebb. It seems to be better to take A = constant = 0.030 s^2/m instead of (8-13b) which is determined only based on computations during the spring tide.

The net transport field and the calculated bed level change during spring tide, average tide and neap tide are respectively shown in fig.8.11 through fig.8.13. All three figures show similar patterns of erosion and sedimentation. Therefore it seems to be perfectly possible to carry out the morphological computation with a properly chosen standard tide.

The choice of the standard tide should be based on the net transport during the tidal period. The net transport in the standard tide has to be about the averaged net transport in the spring-neap tide cycle. Computational results in all three measured cross sections show that the averaged net transport is reproduced by the average tide (fig.8.10). The same conclusion is also drawn from the measurements. Therefore the average tide will be chosen as the standard tide in the morphological computations.

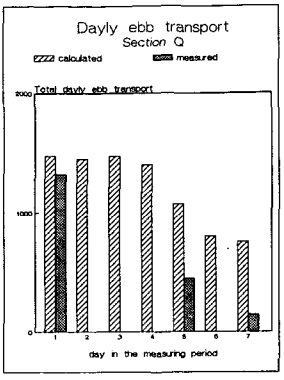

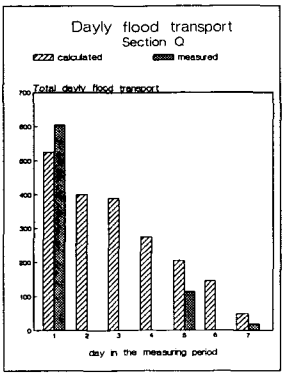

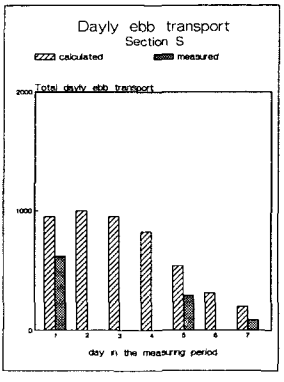

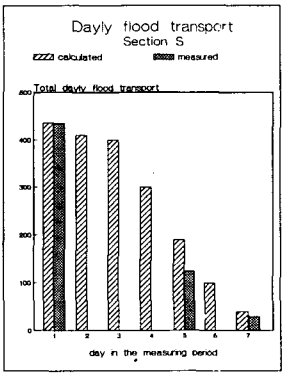

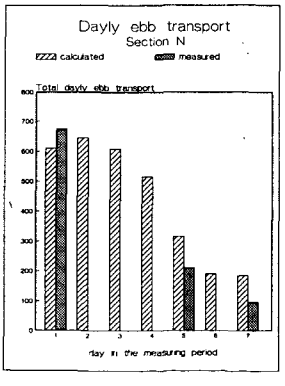

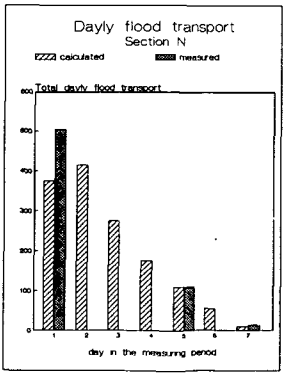

Fig.8.10 Total ebb- and flood transport through the three cross sections (in 10000 tons)

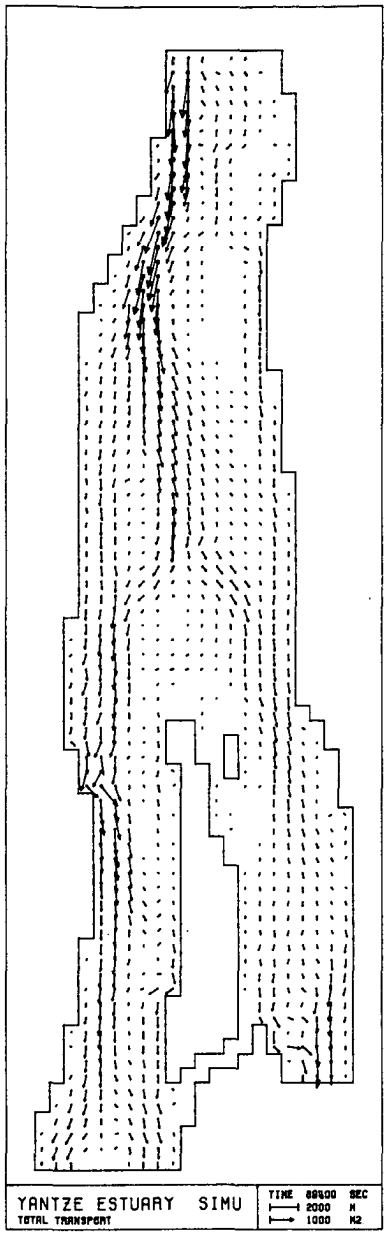

Fig.8.11a Calculated total transport field during the spring tide.

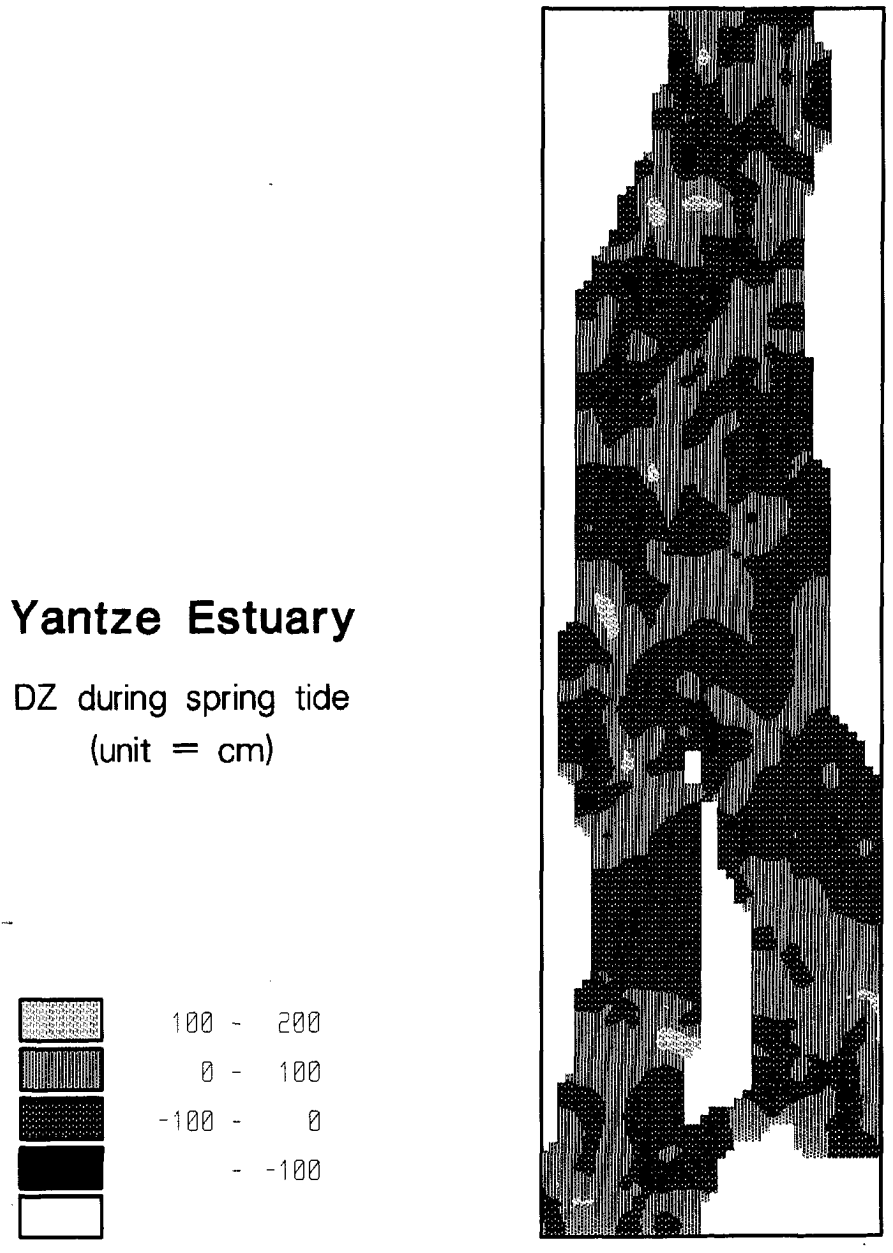

Fig.8.11b Calculated bed level change during the spring tide.

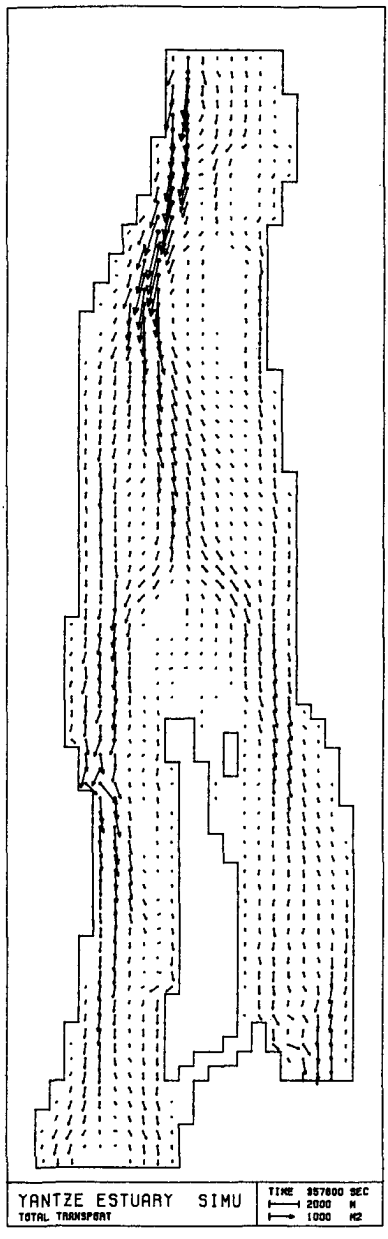

Fig.8.12a Calculated total transport field during the average tide.

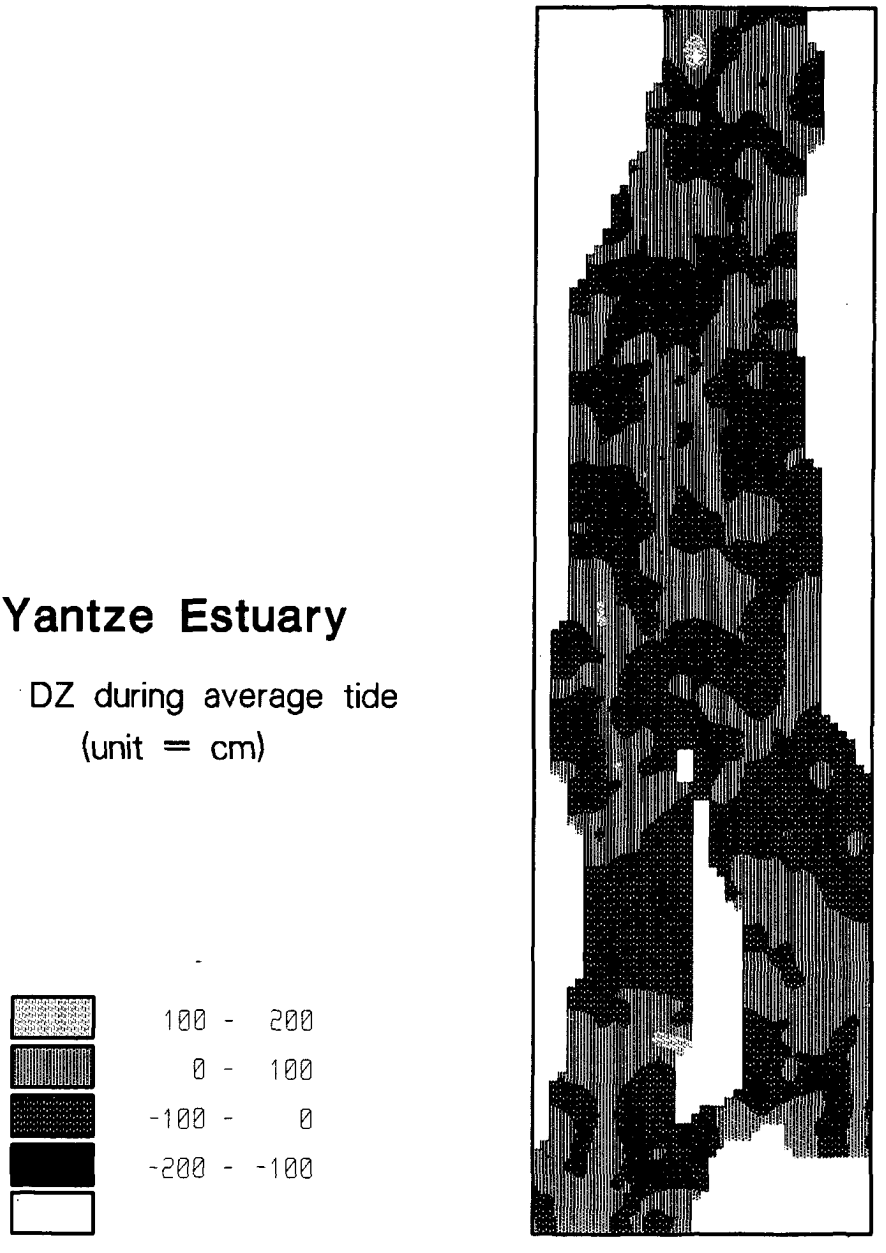

Fig.8.12b Calculated bed level change during the average tide.

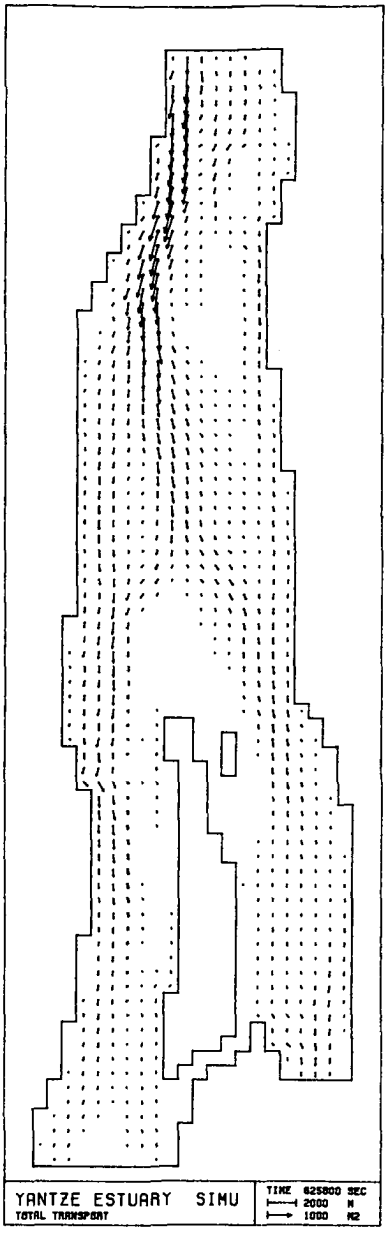

Fig.8.13a Calculated total transport field during the neap tide.

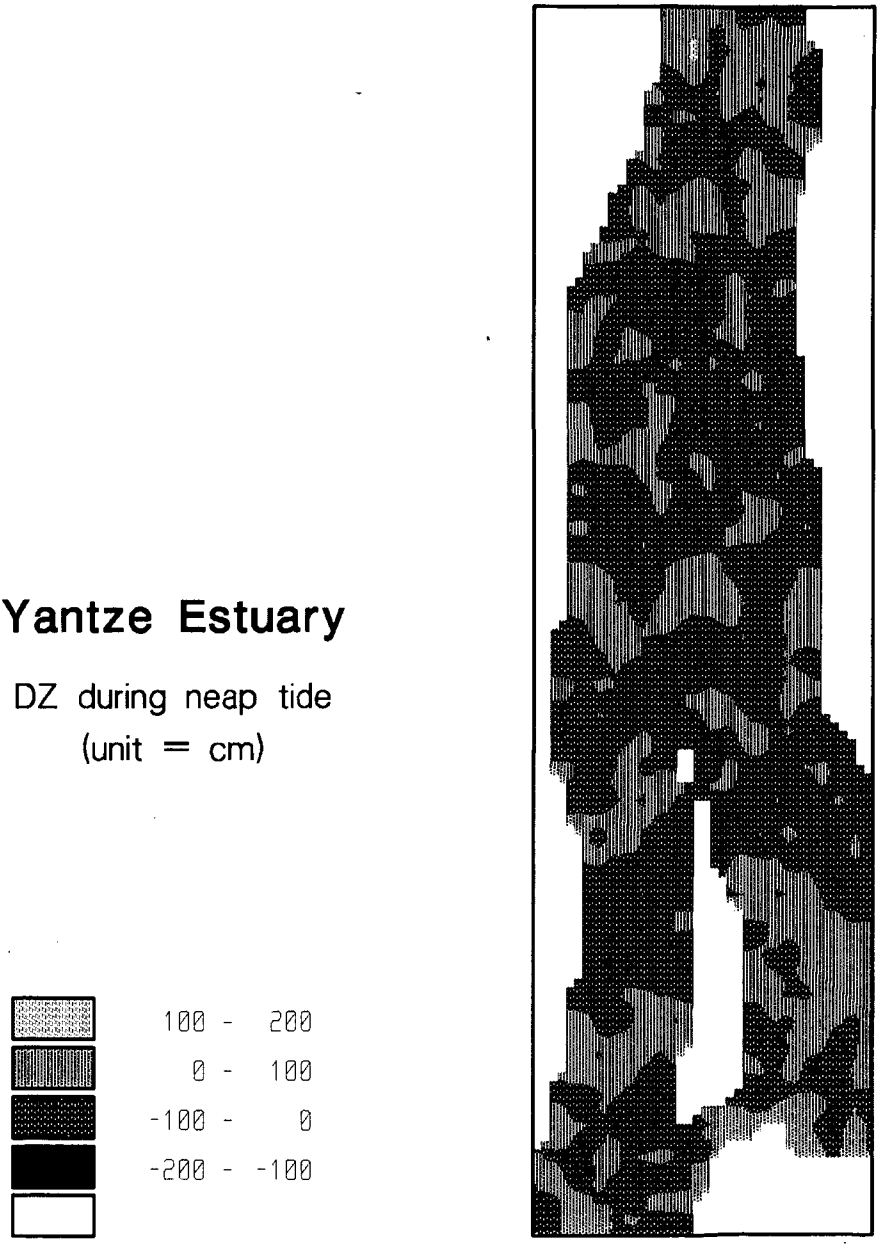

Fig.8.13b Calculated bed level change during the neap tide.

8.5 Long Term Morphological Computation

In the previous section a standard tide has been derived for the morphological computation after studying the spring-neap tide cycle. However, the morphological process is also influenced by the seasonal variation of the upstream river flow. The measuring period was in the flood season, during which the sediment transport rate is relatively high. As no information is available about the seasonal variation it is decided to adjust the coefficient A in equation (8-12) such that the morphological time scale is correctly reproduced. In order to reproduce the correct morphological time scale the annual sediment transport through the estuary has to be reproduced correctly. The computed total transport through the estuary with the standard tide with $A=0.030\ s^2/m$ appears to be about four times the averaged transport measured at Datong station. Therefore it has been decided to use $A=0.0075\ s^2/m$ in the morphological computation. It should be noted that the adjustment implies the assumption that in the river reach from Datong station to the estuary no significant sedimentation and/or erosion takes place. This river reach has a length of about 500 km and a width of about 1 km. A averaged bed level change of 1 cm in the reach will thus lead to a sedimentation or a erosion of about 10×10^9 kg of sediment, which is about 2% of the annual sediment transport measured at the Datong station. So the assumption is certainly a reasonable one.

The other parameters in the model are

$$\Delta t_f = \Delta t_c = 196.05 \text{ s},$$
$$\Delta t_s = 4 * 196.05 = 784.2 \text{ s},$$
$$\Delta t_m = 40T = 1788000 \approx 20 \text{ days},$$
$$M_r = 3,$$
$$\alpha_x = 0, \quad \alpha_y = 0.10,$$

The parameter M_r is the number of time steps of morphological computations after each flow computation. This means that M_r-1 continuity corrections are carried out instead of a complete tidal flow computation each time. At present the complete tidal computation is carried out after every 3 morphological time steps, i.e. about two months.

The α_x and α_y are the smoothing coefficients in the bed level model in x- and y-direction respectively (see equation 6-15). The channels in the estuary are mostly in the y-direction, so α_x has been chosen as zero in order to avoid severe "numerical sedimentation" of the channels. A small non zero α_y value appears to be necessary for maintaining the stability of the computation. This is in contradiction with the conclusion drawn in chapter 6 from an analysis of the simplified case. However, the value of α_y needed is much smaller than in the case of bed load transport.

The other parameters have the same value as in the simulation of the measuring period described in the previous section.

The computation is carried out for 5 years. The computed result is shown in fig.8.14 and fig.8.15. Fig.8.14 shows the bed topography at different times while in fig.8.15 the bed level change after every 2 years is presented. From these figures the following general features of the morphological development of the region can be observed

* There are three morphologically active regions, the south and the north channel and the region near the upstream boundary. In the middle region upstream of the Changxing island relatively less morphological changes take place.

* In the north channel erosion is dominating while in the south channel sedimentation is relatively more important.

* The deep channel in the south channel is shifting to the south.

The computed result after one year (fig.8.15a) can also be compared with the measurement which is shown in fig.8.16. The following conclusions can be drawn from the comparison.

* The time scale of the morphological development is correctly reproduced by the model. The calculated erosion and sedimentation are of the same order of magnitude as the measured ones.

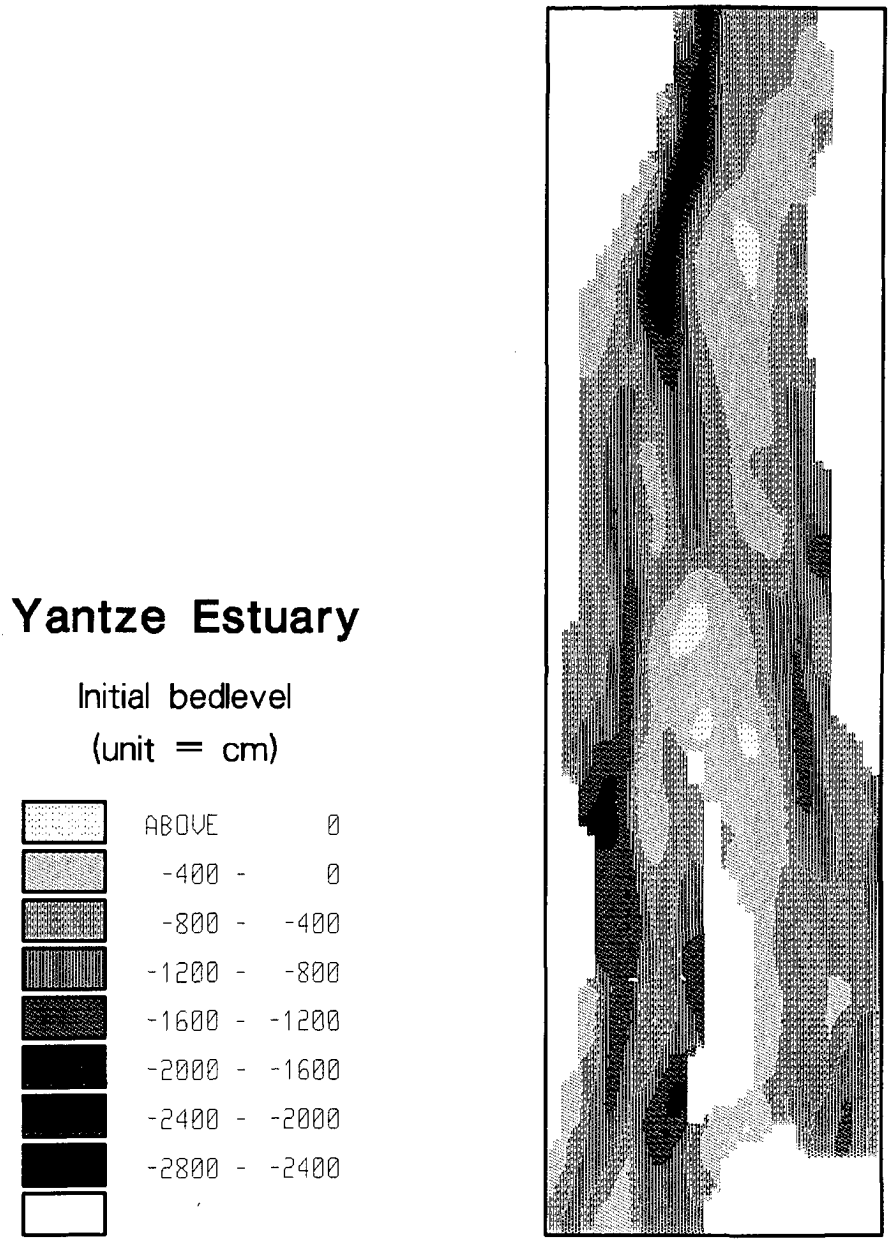

Fig.8.14a The initial bed topography.

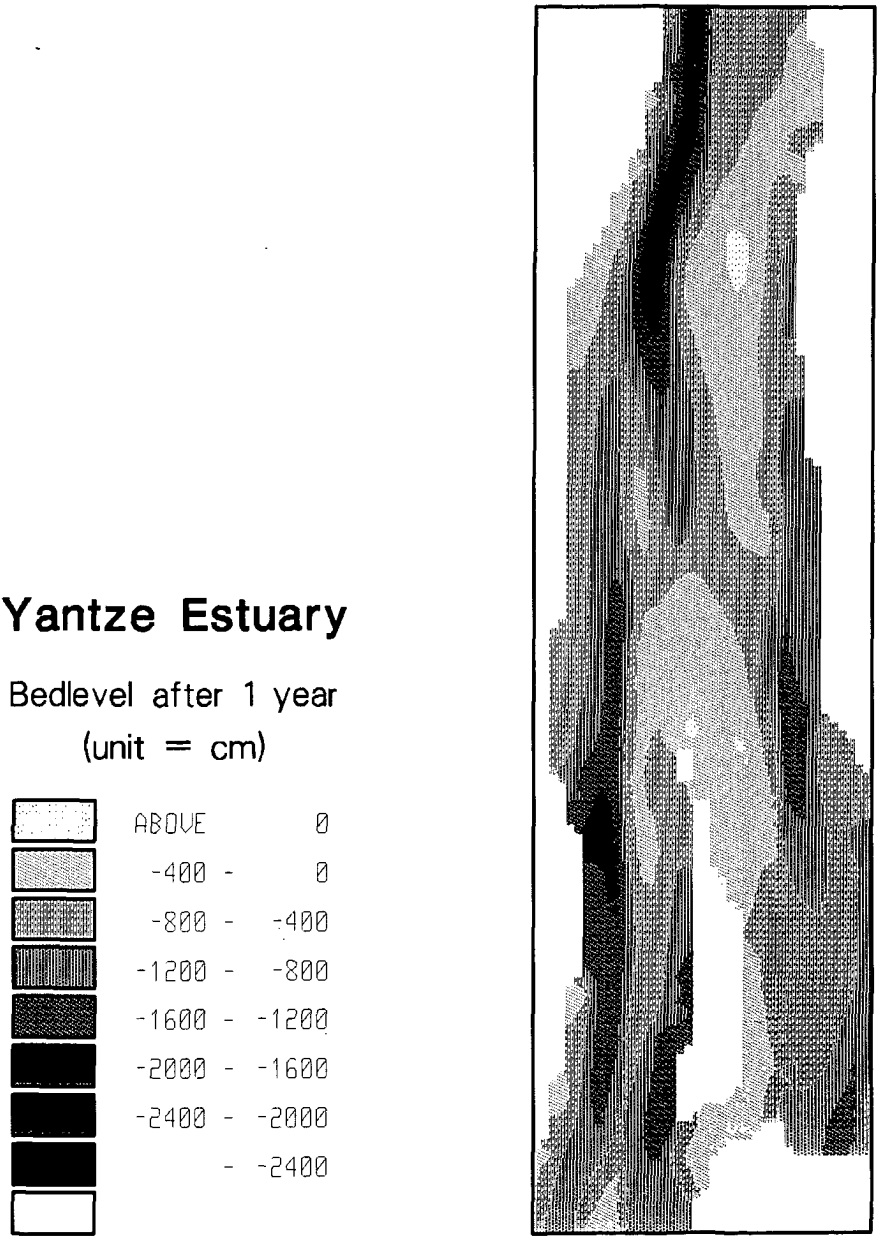

Fig.8.14b Calculated bed topography after 1 year.

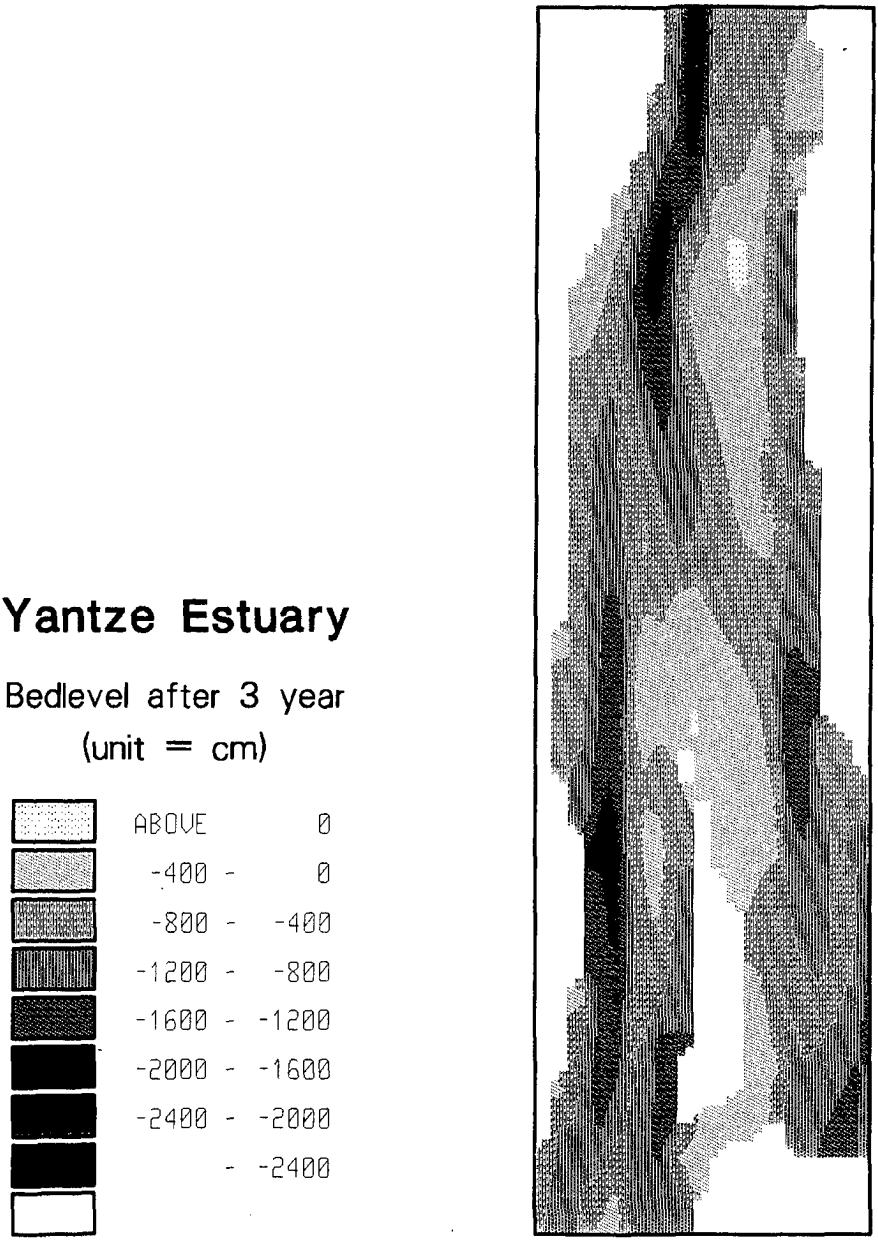

Fig.8.14c Calculated bed topography after 3 year.

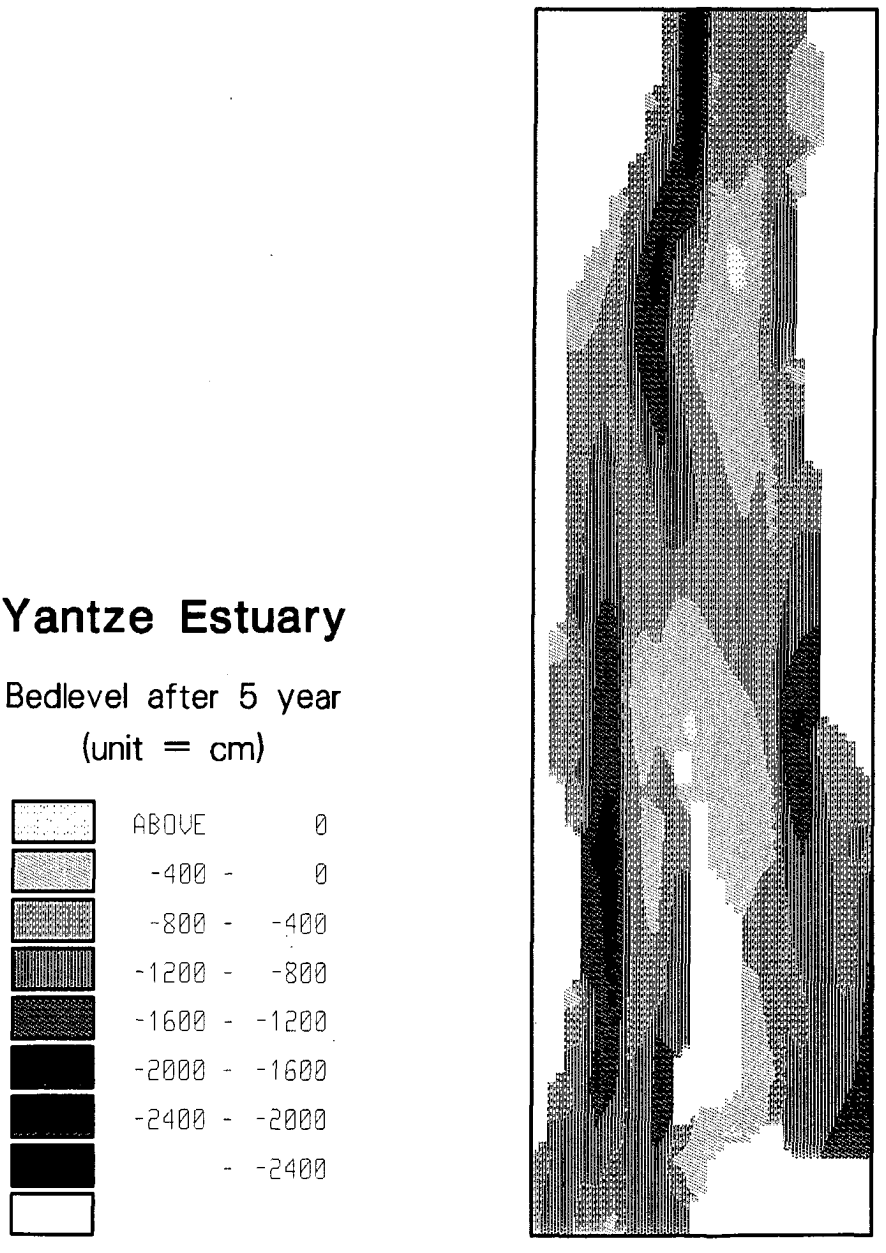

Fig.8.14d Calculated bed topography after 5 year.

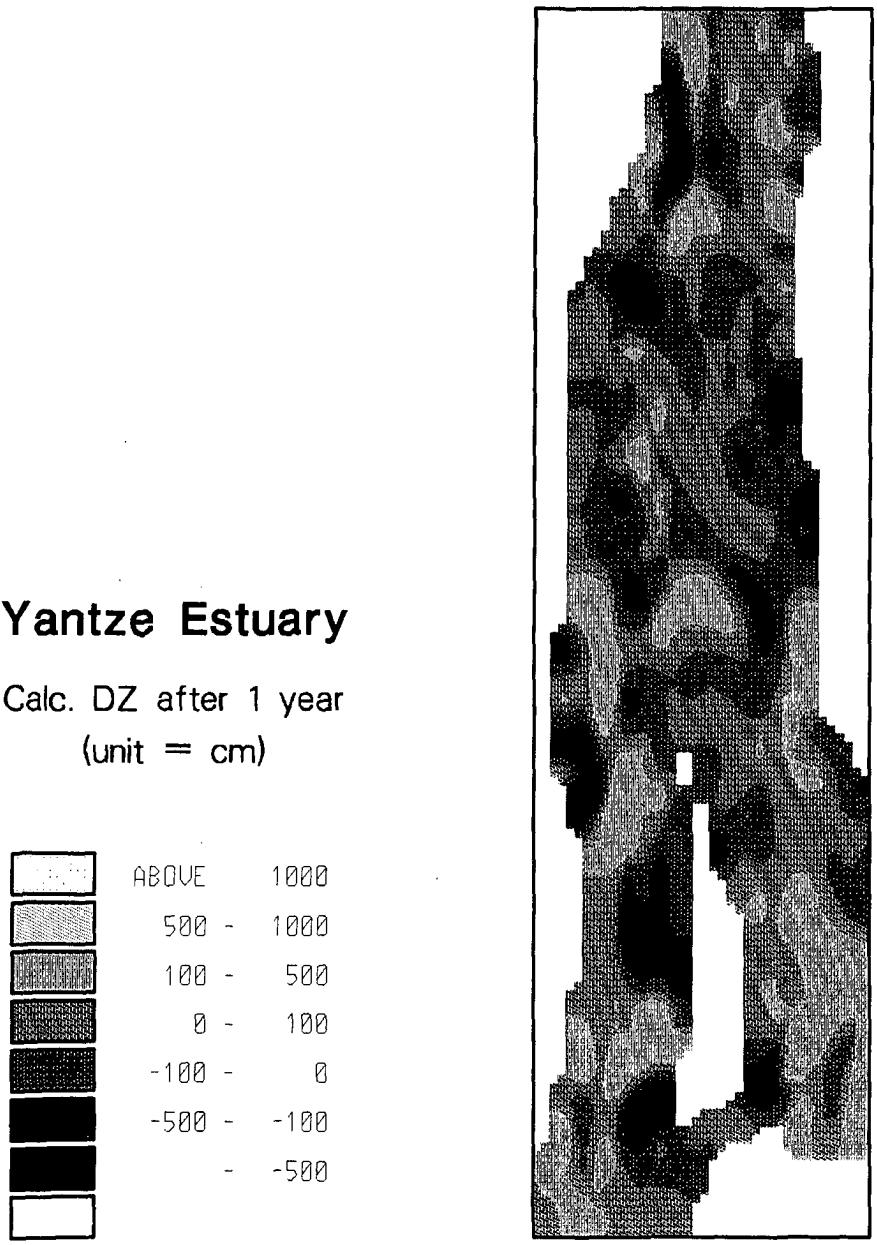

Fig.8.15a Calculated bed level change after 1 year.

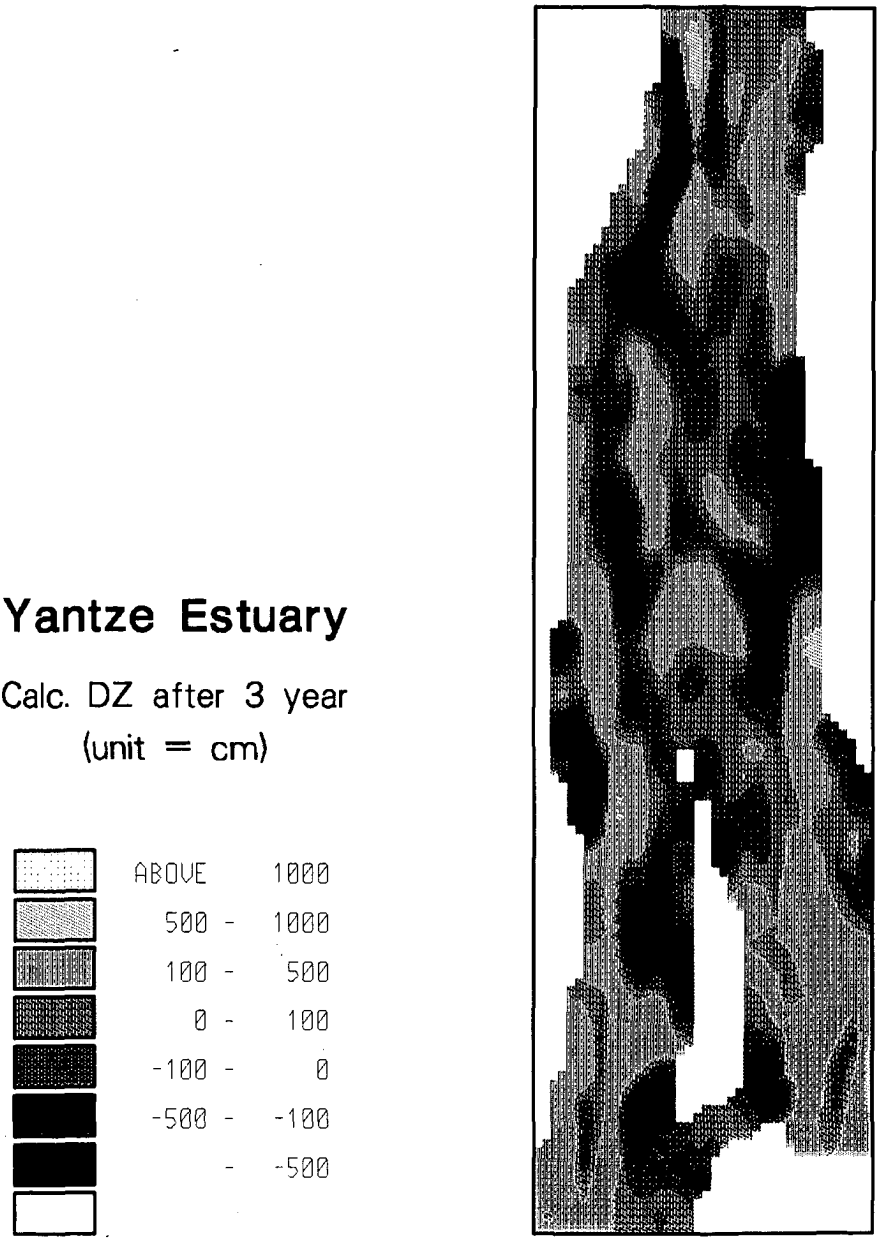

Fig.8.15b Calculated bed level change after 3 year.

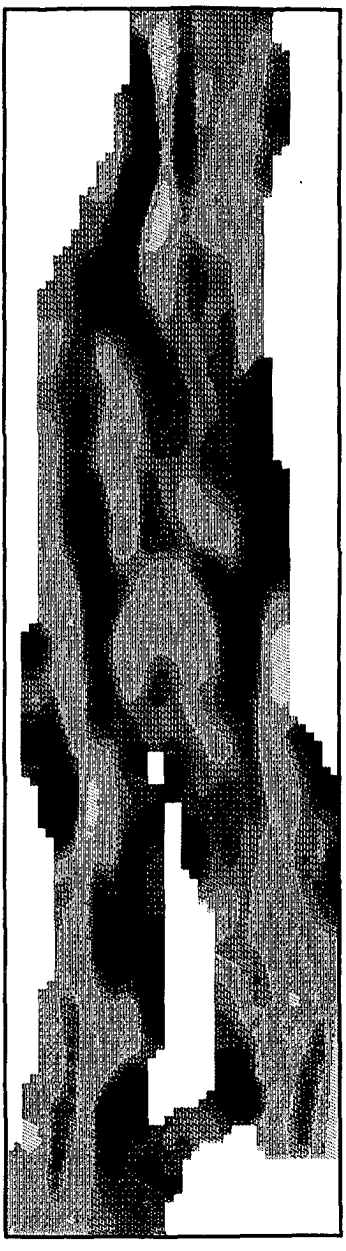

Fig.8.15c Calculated bed level change after 5 year.

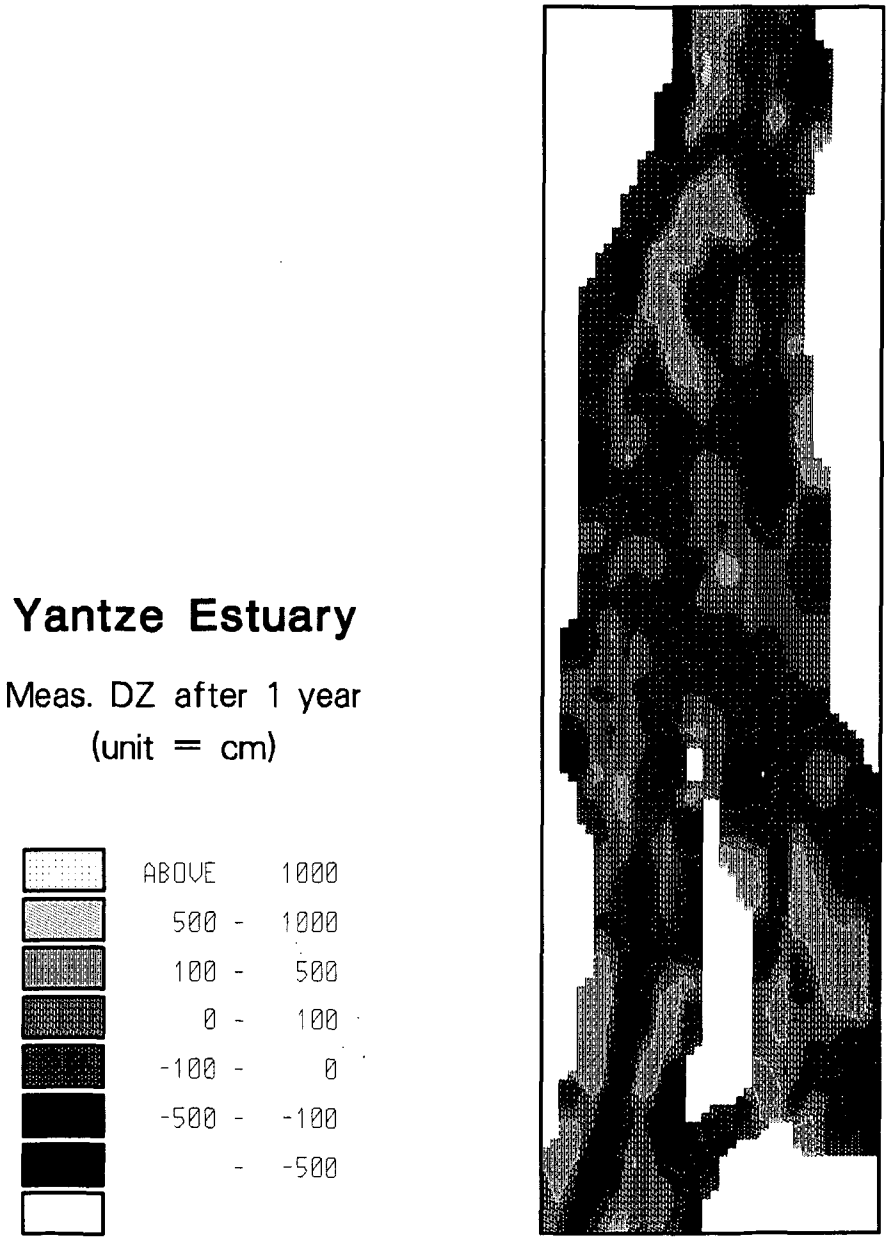

Fig.8.16 Measured bed level change after 1 year.

* The locations of the important erosion and sedimentation areas are reasonably reproduced in the north and the south channel. In the upstream region only areas where strong erosion or sedimentation occur are correctly reproduced in the computation.

* In the middle region where no significant morphological changes occur the erosion and sedimentation areas are poorly reproduced.

* The forms and extent of the erosion and sedimentation areas are not exactly reproduced.

With the quantity and quality of the available field data in mind it is concluded that the obtained agreement between the measurement and computation is reasonable. The result of the whole computation is encouraging.

The CPU time for this computation on a IBM 3083-JX1 computer is about two hours.

8.6 Sensitivity Analysis

Sensitivity analysis is aimed to examine the influence of the parameters in the model. It is very important for morphological computations because many uncertainties exist about the parameters in the model (de Vries, 1982).

The following parameters are considered in the present analysis.

* The secondary flow
* The bed load transport
* The fall velocity w_s
* The morphological time step Δt_m
* The number of continuity corrections M_r
* The time step for the flow and concentration computation Δt_f.

A distinction should be made between the physical parameters and the model parameters. For the model parameters (the latter three) the sensitivity

analysis helps to make an optimal choice of them such that sufficient accuracy is obtained with minimal computational efforts. For the physical parameters (the former three) the sensitivity analysis helps to understand the influence of the uncertainty in the parameters on the final results.

Influence of the secondary flow and the bed load transport

The influence of the secondary flow and the bed load transport is examined with three computations over one tidal period as shown in the following table. As reference (G0) the result of the simulation of the measuring period during the first period is chosen.

Run	sec.flow	bed load
G0	excl.	excl.
G1	incl.	excl.
G2	excl.	incl.
G3	incl.	incl.

No significant difference in the net sediment transport with the reference computation has been found in any of the three computations. Therefore it is concluded that neither the bed load nor the secondary flow is important in the present problem.

Influence of the fall velocity

The influence of w_s on the transport field has already been considered during the calibration of the model. Three computations over 6 months with w_s=0.0005 m/s, 0.001 m/s and 0.002 m/s respectively are carried out to examine the influence on the long term morphological development.

The input parameters in the computations are

Run	w_s	Δt_c	Δt_m	M_r	α_y	T_{end}
G4	0.001	300	20T	3	0.05	6 months
G5	0.0005	300	20T	3	0.05	6 months
G6	0.002	300	20T	3	0.05	6 months

The comparison between the computations is made in terms of the bed level changes, see fig.8.17...fig.8.19. These figures show that the computation result is very sensitive to the value of w_s. It can be observed that the larger the value of w_s the faster the morphological development. This can be explained by the fact that the larger the value of w_s the smaller the adaptation time, the weaker the damping and the larger the transport rate. In addition to this systematic difference between the computations a great scatter in the figures can be observed, which means that the computed sedimentation-erosion pattern will be affected. It is thus very important to use the correct value of w_s in the computation.

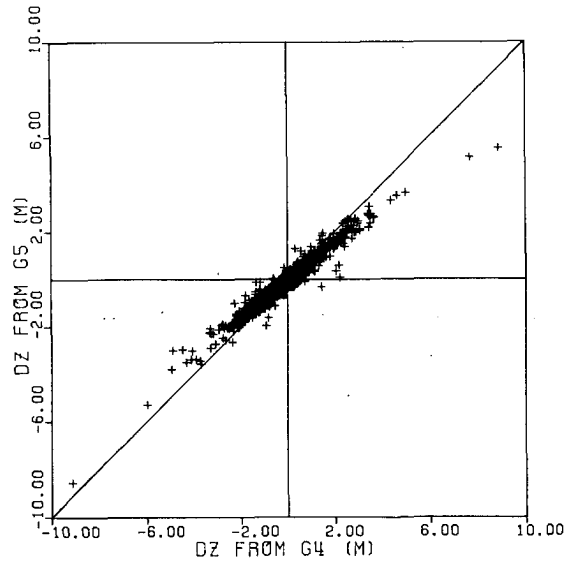

Fig.8.17 Influence of the fall velocity.
Comparison between G4 and G5.

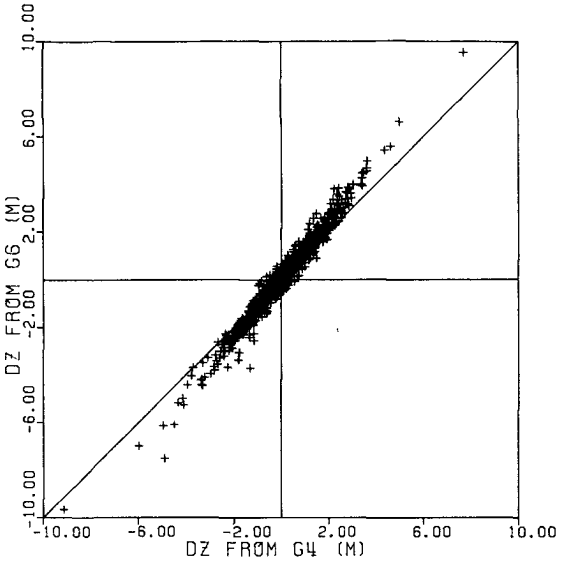

Fig.8.18 Influence of the fall velocity. Comparison between G4 and G6.

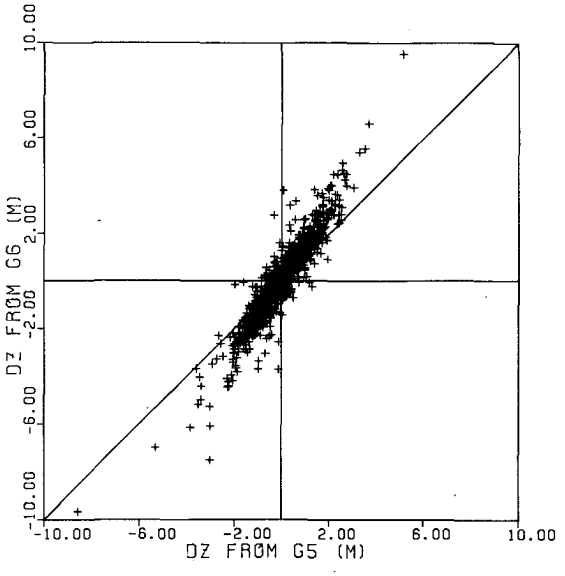

Fig.8.19 Influence of the fall velocity. Comparison between G5 and G6.

The influence of Δt_m

The influence of the morphological time step is examined with the following computations.

Run	Δt_m	M_r	α_y	Δt_f	t_{end}
G4	20T	3	0.05	300 s	6 months
G7	10T	3	0.025	300 s	6 months
G8	40T	3	0.10	300 s	6 months

The α_y value is adjusted to Δt_m in order to ensure that the effective diffusion coefficient

$$E = \frac{1}{2} \alpha \Delta x^2 / \Delta t \qquad (8\text{-}14)$$

is the same in all computations.

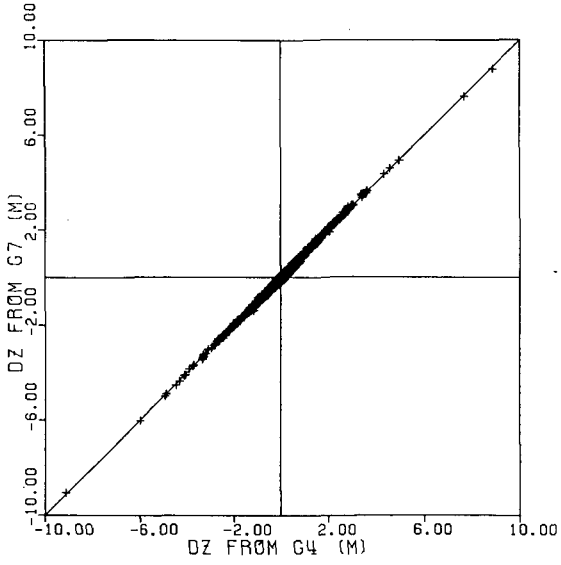

Fig.8.20 Influence of the morphological time step. Comparison between G4 and G7.

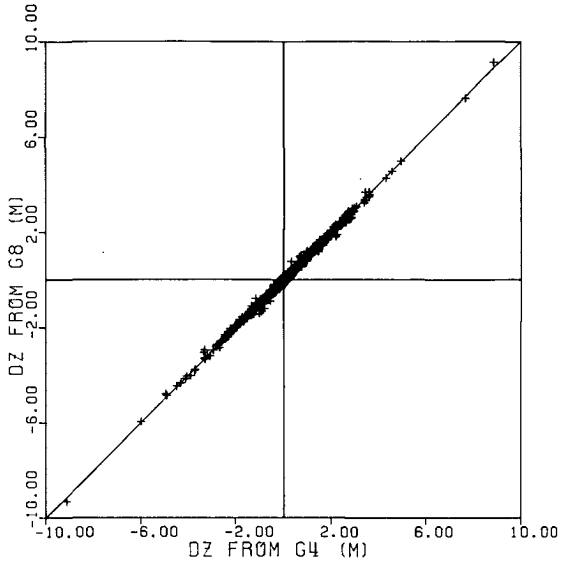

Fig.8.21 Influence of the morphological time step. Comparison between G4 and G8.

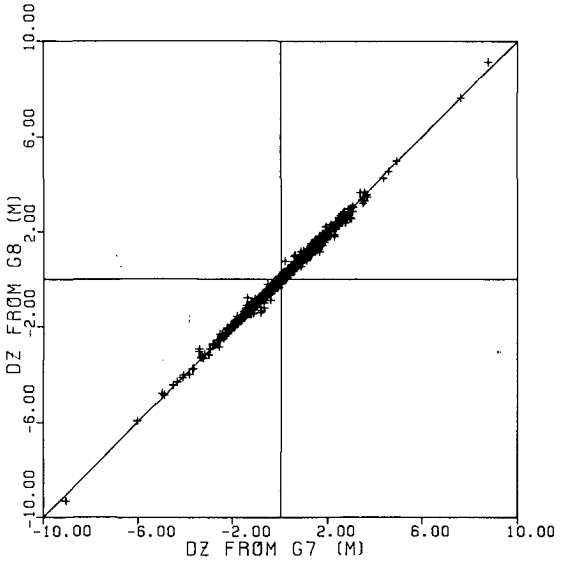

Fig.8.22 Influence of the morphological time step. Comparison between G7 and G8.

The results of the computations are compared in fig.8.20...fig.8.22. The differences between the three computations are small. Even the difference between G7 and G8 is acceptable. Therefore it can be concluded that Δt_m can be enlarged to 40T, but it is expected that this is about the limit.

The influence of M_r

The influence of the continuity corrections is analysed by the following computations.

Run	M_r	Δt_m	α_y	Δt_f	T_{end}
G8	3	40T	0.10	300	6 months
G9	1	40T	0.10	300	6 months

M_r=1 in G9 means that the tidal flow field is recalculated after each morphological time step.

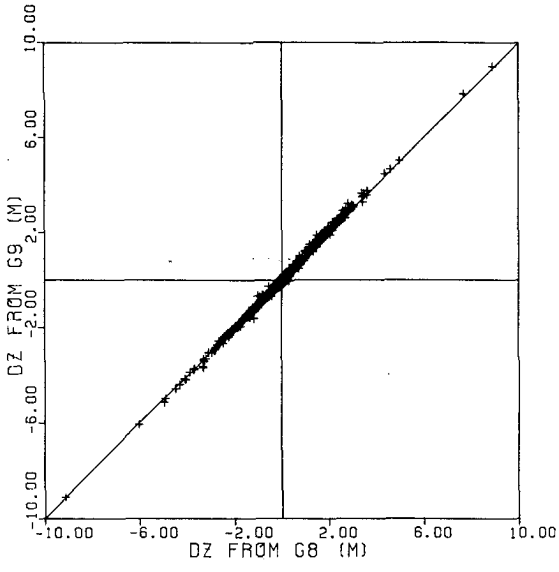

Fig.8.23 Influence of the continuity correction. Comparison between G8 and G9.

The two computations are compared in fig.8.23, which shows that the difference between the two computations is acceptable. This means that computation with M_r=3 is allowed. Moreover, the continuity correction seems to cause some small systematic error, especially for erosion regions. The complete computation G9 gives higher erosion rates. Thus larger values for M_r would not be allowed.

The influence of Δt_f

The influence of the time step in the flow computation and the concentration computation ($\Delta t_f = \Delta t_c$) is examined with the following computations.

Run	Δt_f	Δt_m	M_r	α_y	T_{end}
G8	300	40T	3	0.10	6 months
G10	150	40T	3	0.10	6 months

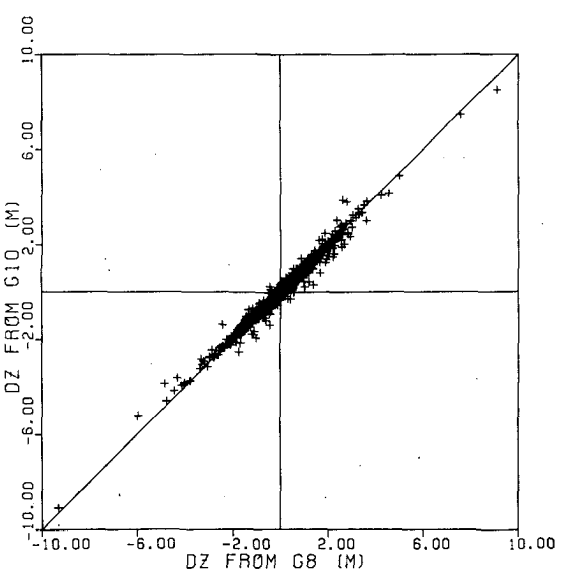

Fig.8.24 Influence of the time step.
Comparison between G8 and G10.

The results of the two computations are compared in fig.8.24. It is clearly shown by this figure that $\Delta t_f = 300$ s is too large. The large difference between the two computations is probably caused by the difference in the computed flow fields. The adaptation time is about $h/w_s \approx 10/0.001 = 10000$ s, so $\Delta t_c/T_a \approx 0.03$. It seems that this must be small enough.

8.7 Discussion and Conclusions

The analysis of the collected data has shown that they are actually not sufficient for calibrating, verifying and testing the morphological model. The most serious problem is concerned with the properties of the sediment, especially the fall velocity which is a key parameter in the model. Moreover, too little is known about the sediment transport mechanism to specify a realistic bed boundary condition for the suspended sediment transport model. The upstream boundary condition is another problem. This is mainly caused by the fact that the present model covers only a part of the estuary. To avoid this problem the upstream boundary should be situated at the Datong hydrologic station, which is located 640 km from the river mouth. At present this is impossible since the available data and the computer capacity are too restricted. The present study is mainly based on the data collected during one hydrologic survey. This is obviously much too restricted because no information is available about the long term variation of the flow in the estuary such as the seasonal variation. In the hydrologic survey the sediment concentration is only measured during a typical spring tide, average tide and neap tide. This is also an important shortcoming of the data. However, with the present measuring technique and the available financial means it seems to be impossible to improve the field data significantly in the near future. Nevertheless the following suggestions are made for the collection of data.

* More hydrologic surveys should be organized in a year. The surveys should thus not only be carried out during flood seasons.

* The surveys should cover a larger area than in 1984. Especially the region upstream of Xuliujing should also be covered by the surveys.

* The measurements during a survey should be continued in the whole period, thus not only during a restricted number of tidal periods.

* Special attention should be paid to the measurements of the sediment properties and the sediment transport. Especially the fall velocity of the sediment particles should be measured in the field extensively.

A simulation of the 1984 survey has been carried out after calibrating the flow and sediment transport model using a part of the data collected during this survey. The following conclusions have been drawn from the results of the simulation.

* The agreement between the measured and calculated water level in the region is very good.

* The agreement between the measured and calculated flow velocity is good.

* The agreement between the measured and calculated sediment concentration is fair.

* The agreement between the measured and calculated sediment transport through the three cross sections is reasonable.

* The average tide can be used as the standard tide for the morphological computation representing the spring-neap tide cycle.

A long term (5 year) morphological computation has been carried out. Only the result after one year can be compared with the measurement. The following conclusions have been drawn from the comparison.

* The general features and the time scale of the morphological development are reasonably reproduced by the model.

* The agreement between the measured and calculated bed level change is better in regions with strong morphological changes than in regions with small changes.

* The agreement in the downstream region (South and North Channel) is better than in the upstream region.

An extended sensitivity analysis for the model has been carried out concerning physical parameters as well as model parameters. From the analysis the following conclusions are drawn.

* The secondary flow and the bed load transport seem to be not very important for the case under consideration.

* The computational result is very sensitive to the value of the fall velocity w_s. Therefore it is very important to make accurate estimates for w_s.

* The maximum morphological time step allowed is about 40 times the tidal period, i.e. about 20 days.

* The continuity correction method can be applied to restrict the computational efforts. At present this method can be applied at least two times after each complete tidal flow computation.

* The time step for the flow computation should not be too much larger than 150 s in order to assure sufficient accuracy of the morphological computation.

Chapter 9 SUMMARY AND CONCLUSIONS

In this study a two-dimensional morphological model for estuaries (ESMOR) has been developed. The ESMOR model is aimed at well mixed estuaries, because the density flow effect is not taken into account. Further the influence of wind and short waves is not included. The model should thus still be considered as in developing stage.

The ESMOR model consists of four submodels, the main flow model, the secondary flow model, the sediment transport model and the bed level model. Special attention is paid to the formulation of the sediment transport model, especially for the suspended load transport. A depth-integrated model has been developed based on an asymptotic solution of the convection-diffusion equation governing the sediment concentration. This asymptotic solution is a generalization of the one presented by Galappatti (1983, also see Galappatti and Vreugdenhil, 1985).

A series of depth-integrated models can be developed based on the general asymptotic solution by choosing different sets of test functions. Although not all mathematically proved, examples of various models based on the general asymptotic solution lead to the following statements.

* The conventional asymptotic solution as well as the solution of Galappatti are included in the presented general asymptotic solution. These solutions can be derived from the general solution by making certain choices for the test functions.

* More sophisticated solutions than the conventional solution or the solution of Galappatti may be obtained by choosing proper test functions.

* The asymptotic solution can only converge to the complete solution of the convection-diffusion equation if the test functions together form a complete system.

* The convergence rate of the asymptotic solution depends on the linear dependence between the test functions. The optimal convergence seems to be obtained when the test functions form an orthogonal system.

Extensive theoretical analysis has been carried out for the depth integrated model for suspended sediment transport. Good insight into the validity and the applicability of the model have been gained from the analysis. The following conclusions have been drawn.

* For each asymptotic solution a convergence domain can be determined. It depends on the properties of the test functions.

* For the one-dimensional case the convergence domain is a circle. For the multi-dimensional cases the convergence domain is a cylinder in the multi-dimensional space.

* The convergence radius of an asymptotic solution is an important indicator for the validity and applicability of the model. The larger the convergence radius the better the solution is.

* The convergence radius of the solution of Galappatti (1983) is larger than the one of the conventional solution.

* Within the convergence domain the higher order solution is always better than the lower order solution, but outside the convergence domain this is not always the case.

* Concerning the overall agreement between the depth-integrated models and the models based on direct solution of the convection-diffusion equation the first order solution of the model of Galappatti and the first order solution proposed in this study are quite good.

* In the one-dimensional cases the difference between the non-equilibrium concentration field and the equilibrium concentration field can be characterized by a damping coefficient and a phase lag. This difference

causes a decrease of the propagation velocity as well as a damping of the bed forms.

After the theoretical analysis the model has been verified with a comparison between the present model and the three-dimensional SUTRENCH model. The comparison between the two models is perfectly possible because they are based on exactly the same basic theories. The flow field in the computation with the ESMOR model is derived from that in the SUTRENCH computation with a interpolation procedure. The following conclusions have been drawn from this exercise.

* The agreement between the ESMOR model and the SUTRENCH model for the present test problem is very good.

* The applicability of the model for the present case can be well analyzed with the results from the theoretical study. The exercise provides also a verification for the analytical results.

Finally the ESMOR model has been applied to a real estuary, the Yantze estuary. Despite many difficulties the model has been applied to simulate a survey period of one week and to predict the morphological development of the region in 5 year time. The following conclusions have been drawn from the application.

* Despite of the large effort spent in the measurements, the available data are insufficient for the calibration, verification and test for the model, concerning both the amount and the quality of the data. More measurements covering larger region are required for these purposes. Special attention should be paid to the properties of the sediment in the estuary, both the bed material and the suspended material. For the suspended material the fall velocity of the particles is extremely important since it is a key parameter in the model. Field measurements for this parameter should be carried out.

* Reasonable agreement has been achieved between the measured and calculated concentration as well as sediment transport. Concerning the

morphological development the comparison between the measured and calculated bed level change after one year shows a reasonable agreement in regions with significant changes while in regions with minor changes the agreement is worse.

This study has shown that long term morphological computations in estuaries can be realized with the present computer facilities. The ESMOR model presented here forms a good basis for further development in mathematical modelling of morphological processes in estuaries. To improve the model much more work has to be carried out. Especially the influences of the density flow effect, wind and short waves, flocculation of cohesive sediment, etc., which are not taken into account here, should be reconsidered. However, this study has provided a good insight into the behaviour for the sediment transport model, especially the depth-integrated model for the suspended sediment transport.

MAIN SYMBOLS

Symbol		Dimension
A	Coefficient	(-)
c	sediment concentration	(-)
C	Chezy coefficient	$(L^{0.5}T^{-1})$
$\bar{c}$	depth averaged concentration	(-)
c_i	ith order term in the asymptotic solution	(-)
$\bar{c}_e$	mean equilibrium concentration	(-)
d	grain size	(L)
D	water depth	(L)
f	coefficient of geostrophic acceleration	(T^{-1})
g	gravity acceleration	(LT^{-2})
h	water depth ($=D-z_a$)	(L)
i	gradient	(-)
I	intensity of the secondary flow	(LT^{-1})
I_b	intensity of the secondary flow due to curvature	(LT^{-1})
I_c	intensity of the secondary flow due to geostrophic effect	(LT^{-1})
k	wave number	(L^{-1})
k_s	resistance hight of Nikuradse	(L)
L	length scale	(L)
n	coordinate in the normal direction to the streamline	(L)
N	coordinate normal to the boundary	(L)
p	normalized velocity profile	(-)
q	normalized secondary velocity profile	(-)
q_x	discharge in x-direction per unit length	(L^2T^{-1})
q_y	discharge in y-direction per unit length	(L^2T^{-1})
Q	discharge in the flow direction per unit length	(L^2T^{-1})
R_s	radius of curvature of the main flow streamline	(L)
R_α	convergence radius	(-)
s	coordinate in the main flow direction	(L)
S	sediment transport	(L^2T^{-1})
S_s	sediment transport in the flow direction	(L^2T^{-1})
S_n	sediment transport in the normal direction	(L^2T^{-1})
S_{tot}	total sediment transport in a tidal period	(L^2)

t	time	(T)
T	tidal period	(T)
u	flow velocity in x-direction	(LT^{-1})
$\bar{u}$	depth averaged flow velocity in x-direction	(LT^{-1})
u_n	secondary flow velocity	(LT^{-1})
u_s	main flow velocity	(LT^{-1})
$\bar{u}_s$	depth averaged main flow velocity	(LT^{-1})
v	flow velocity in y-direction	(LT^{-1})
w	flow velocity in z-direction	(LT^{-1})
w_s	fall velocity of sediment particles	(LT^{-1})
x	horizontal coordinate	(L)
y	horizontal coordinate	(L)
z	vertical coordinate	(L)
z_a	location of the bed boundary	(L)
z_b	bed level	(L)
α	coefficient	(-)
α_{jk}	coefficients	(-)
β	z_a/h	(-)
β_{jk}	coefficients	(-)
γ_{jk}	coefficients	(-)
δ	delta function	(-)
δ_{jk}	coefficients	(-)
Δ	relative density of the sediment	(-)
Δt	time step	(T)
Δx	space step in x-direction	(L)
Δy	space step in y-direction	(L)
ϵ_s	diffusion coefficient in s-direction	(L^2T^{-1})
ϵ_n	diffusion coefficient in n-direction	(L^2T^{-1})
ϵ_z	diffusion coefficient in z-direction	(L^2T^{-1})
ϵ'	normalized diffusion coefficient	(-)
ϕ	profile function	(-)
ϕ_j	test functions	(-)
Φ	collection of test functions	(-)
κ	von Karman constant	(-)
τ	dimensionless time	(-)
ξ	dimensionless coordinate in s-direction	(-)

η	dimensionless coordinate in n-direction	(-)
ζ	dimensionless coordinate in z-direction	(-)
λ	exponential coefficient	(-)
μ	coefficient	(-)
ρ	density of the fluid	(ML^{-3})
σ	Courant number	(-)
θ	coefficient	(-)
ψ	coefficient	(-)
χ	coefficient	(-)

REFERENCES

Bagnold, R.A.(1956), The flow of cohesionless grain in fluids, Proc. Royal Soc., London, Vol. 249, 1956.

Bendegom, L. van(1947), Some considerations about river morphology and river improvement (in Dutch), De Ingenieur, 59, 4, B & W, pp. B1-B12.

Booij, R. and Kalkwijk, J.P.Th.(1982), Secondary flow in estuaries due to the curvature of the main flow and rotation of the earth and its development, Report no. 9-82, Delft University of Technology, Dept. of Civil Eng.

Chen, J.Y., Yu, C.X. and Xu, H.G.(1982), The model of development of the Changjiang estuary during the last 2000 years, estuarine comparison, Edited by Kennedy, Academic press, 1982, pp. 655-666.

Coleman, N.L.(1970), Flume studies of the sediment transfer coefficient, Water Resources Research, Vol. 6, No. 3, June, 1970.

Davies, A.M.(1986), On extracting current profiles from vertical integrated numerical models, JONSMOD paper, 1986.

DuBoys, M.P.(1879), Le Rhone et les rivieres a lit affouilable, Mem. Doc. Am. Pont et Chaussees, ser. 5, Vol. XVIII.

DUT (1983), FLOWS user's guide, Delft University of Technology, Dept. of Civil Eng.

DUT (1986), DUCHESS program documentation, Delft University of Technology, Dept. of Civil Eng.

DUT (1987), DUCHESS user's guide, Delft University of Technology, Dept. of Civil Eng.

Dyer, K.R.(Ed.) (1979), Estuarine hydrology and sedimentation, Cambridge University Press, London.

Einstein, H.A.(1950), The bedload function for sediment transportation in open channel flows. Tech. Bull. no. 1026, US Dept. for Agriculture, Washington D.C.

Elder, J.W.(1959), The dispersion of marked fluid in turbulent shear flow, J. of Fluid Mech., 5, 544-560.

Engelund, F. and Hansen, E.(1967), A monograph on sediment transport in alluvial streams, Teknisk Forlag, Copenhagen.

Galappatti, R.(1983), A depth integrated model for suspended transport, Report no. 83-7, Delft University of Technology, Dept. of Civil Eng.

Galappatti, R. and Vreugdenhil, C.B.(1985), A depth integrated model for suspended sediment transport, J. of Hydr. Res., Vol. 23, no. 4.

Hauguel, A.(1978), Utilization des modeles mathematiques pour L' etude du transport solide sous L' action des courants de Maree, Report E42/78.41, EDF, Direction des Etudes et Recherches.

Holz, K.P. and Crotogino, A.(1984), simulation of sediment process in estuaries, Proc. 4th Int. Conf. Applied numerical modelling, Taiwan, pp. 247-282.

Huang, S.(1986), The evolution characteristics of the Chang Jiang estuary (in Chinese), J. of Sed. Res., no. 4, 1986.

Huang, S. and Zhong, X.J.(1986), The classification and process characteristics of estuaries in China, Proc. of the 3rd Symp. on river sedimentation, Mississippi, USA.

Jansen, P.Ph.(ed.) (1979), Principles of river engineering, Pitman, London.

Kalkwijk, J.P.Th. and Booij, R.(1986), Adaptation of secondary flow in nearly horizontal flow, J. of Hydr. Res., Vol. 24, no. 1.

Kalkwijk, J.P.Th. and de Vriend H.J.(1986), Computation of the flow in shallow river bends, J. of Hydr. Res., Vol. 18, No. 4.

Lin, C.K.(1984), A study on the source and quantity of sediment at the Yantze River estuary (in Chinese), J. of Sed. Res., No. 2, 1984.

Kerssens, P.J.M.(1974), Adaptation lengths of suspended sand verticals (in Dutch), Delft University of Technology, Dept. of Civil Eng.

Kerssens, P.J.M.(1977), Morphological computations for suspended sediment transport, Report S 78-VI, Delft Hydr. Lab., Delft, the Netherlands.

Lin, Pin-nam, Huang J. and Li, X.(1981), Mathematical model of suspended sediment transport by tidal flow in Qiantang estuary (in Chinese), J. of Sed. Res., No. 2, 1981.

Lin, Pin-nam, Huang J. and Li, X.(1981), Unsteady transport of suspended load at small concentrations, J. of Hydr. Eng., Vol. 109, No.1.

Lin, Pin-nam, and Shen, H.(1984), Two-D flow with sediment by characteristic method, J. of Hydr. Eng., Vol. 110, no. 5.

McAnally, W.H., Letter, J.V. and Thomas, W.A.(1986), Two and three-dimensional modelling systems for sedimentation, Proc. 3rd Int. Symp. river sedimentation, Jackson, Mississippi, pp. 115-148.

Meyer-Peter, E. and Muller, R.(1948), Formulas for bed load transport, Proc. 2nd Congr. IAHR, Stockholm, Vol. 2, Paper 2, pp. 39-64.

Nayfeh, A.H.(1973), Perturbation methods, Wiley, New York, 1973.

Officer, C.R.(1975), Physical oceanography of estuaries, New York, 1975.

Olesen, K.W.(1987), Bed topography in shallow river bends, Doctoral thesis, Delft University of Technology.

Ribberink, J.S.(1986), Introduction to a depth integrated model for suspended transport, Report no. 6-86, Delft University of Technology, Dept. of Civil Eng.

Rijn, L.C. van(1984a), Sediment transport, Part I: Bed load transport, J. of Hydr. Eng., Vol. 110, no. 10.

Rijn, L.C. van(1984b), Sediment transport, Part II: Suspended load transport, J. of Hydr. Eng., Vol. 110, no. 11.

Rijn, L.C. van(1987), Mathematical modelling of morphological processes in case of suspended sediment transport, Doctoral thesis, Delft University of Technology.

Rijn, L.C. and Meijer, K.(1986), Three-dimensional modelling of suspended sediment transport for currents and waves, Report Q250/Q422/H461, Delft Hydr. Lab., Delft, The Netherlands.

Rozovskii, I.L.(1961), Flow of water in bends of open channels, Israel Progr. for scientific transl., Jerusalem (orig. publ. 1957).

Schmidt, W.(1925) Der Massennautausch in freier Luft und verwandte Erscheinungen, Probleme der kosmischen Physik, vol. 7, Hamburg.

Shen, H.T., Li, J.F. and Zhu, H.F.(1986), Transport of the suspended sediment in Chang Jiang estuary (in Chinese), J. of Sed. Res., no. 1, 1986.

Simmons, H.B. and Brown, F.R.(1969), Salinity effects on estuarine hydraulics and sedimentation, IAHR, Proc of the 13th Congr.

Stelling, G.S.(1983), Construction of computational methods for shallow water flow problems, Doctoral thesis, Delft University of Technology, Delft, The Netherlands.

Stelling, G.S. Wiersma, A.K. and Willemse, J.B.T.M.(1986), Practical aspects of accurate tidal computations, J. of Hydr. Eng., Vol. 112, no. 9.

Struiksma, N., Olesen, K.W., Flokstra, C. and de Vriend, H.J.(1985), Bed deformation in curved alluvial channels, J. of Hydr. Res., Vol. 23, no. 1.

Taylor, G.I.(1954), The dispersion of matter in turbulent flow through a pipe, Proc. Roy. Soc. A, 223, pp. 446-468.

Vermaas, H.(1984), Private communication.

Vreugdenhil, C.B.(1979), Hydraulic computations (in Dutch), Delft University of Technology, Dept. of Civil Eng., Lecture notes, b84.

Vreugdenhil, C.B.(1982), Finite difference schemes for bottom change computations in which the celerity needs not to be known (in Dutch), Informatie X61, Delft Hydr. Lab., Delft, The Netherlands.

Vreugdenhil, C.B. and de Vries, M.(1967), Computations of non-steady bedload transport by a pseudo viscosity method, Proc. IAHR, Fort Collins.

Vriend, H.J. de(1976), A mathematical model of steady flow in curved shallow channels, Report no. 76-1, Delft University of Technology, Dept. of Civil Eng.

Vriend, H.J. de(1977), A mathematical model of steady flow in curved shallow channels, J. of Hydr. Res., Vol. 15, no. 1.

Vriend, H.J. de(1981), Steady flow in shallow channel bends, Doctoral thesis, Delft University of Technology, Delft, The Netherlands.

Vriend, H.J. de(1984), Compound 2DH mathematical models in coastal morphology, Report no. R1747-I, Delft Hydr. Lab., Delft, The Netherlands.

Vriend, H.J. de(1985), Flow formulation in mathematical models for 2Dh morphological Changes, Report no. R1747-5, Delft Hydr. Lab., Delft, The Netherlands.

Vriend, H.J. de(1986), Two and three-dimensional mathematical modelling of coastal morphology, Report no. H284-2, Delft Hydr. Lab., Delft, The Netherlands.

Vries, M. de(1959), Transients in bed-load transport (Basic considerations), Report no. R3, Delft Hydr. Lab., Delft, The Netherlands.

Vries, M. de(1965), Considerations about non-steady bed load transport in open channels, Publ. no. 36, Delft Hydr. Lab., Delft, The Netherlands.

Vries, M. de(1973), Application of physical and mathematical models for river problems, IAHR Symp. Bangkok.

Vries, M. de(1981), Morphological computations, Delft University of Technology, Dept. of Civil Eng., Lecture notes f10a.

Vries, M. de(1982), A sensitivity analysis applied to morphological computations, 3rd APD-IAHR congr. Bandung, Indonesia.

Wang, Z.B.(1984), The validity of a depth integrated model for suspended sediment transport and the extension of this model to tidal rivers, Report no. 10-84, Delft University of Technology, Dept. of Civil Eng.

Wang, Z.B.(1985), A preparing study to an extension the model of Galappatti, Report no. 10-85, Delft University of Technology, Dept. of Civil Eng.

Wang, Z.B. and Ribberink, J.S.(1986), The validity of a depth integrated model for suspended sediment transport, J. of Hydr. Res., Vol. 25, no. 1.

STELLINGEN

Behorend bij het proefschrift

'Mathematical Modelling of Morphological Processes in Estuaries'

Z.B. Wang

March 1989

1 Lange-termijn morfologische berekeningen voor estuaria zijn mogelijk met de huidige computerfaciliteiten.

2 In een niet-uniforme stroming zijn er altijd een demping en een faseverschuiving van de sedimentconcentratie ten opzichte van de evenwichtsconcentratie. De demping heeft vooral tot gevolg, dat de voortplanting van de beddingvormen wordt vertraagd, terwijl de faseverschuiving vooral demping van de beddingvormen veroorzaakt.

3 Het integreren van de convectie-diffusie vergelijking over de diepte geeft niet voldoende informatie om een diepte-gemiddeld model, zoals in dit proefschrift beschreven, op te stellen voor zwevend transport. Diepte-gemiddelde modellen zoals dat van Lin et al, zijn impliciet gebaseerd op een aanname over de sediment uitwisseling tussen de stroming en de bedding.

Lin Pin-nam, Huang Juqing and Li Xinquen, Unsteady Transport of Suspended Load at Small Concentrations, J. of Hydr. Eng., Vol. 109, No. 1, 1983, p.86-98.

4 Het niveau van het waterloopkundig onderzoek in China zou aanzienlijk kunnen worden verbeterd als de wetenschappelijke uitwisseling tussen de verschillende instituten wordt vergroot.

5 Het rendement van grootschalige metingen, zoals die in het Yantze estuarium, kan aanzienlijk worden verbeterd door een adequate organisatie.

6 Aangezien veel terroristische akties vooral zijn bedoeld om aandacht te trekken, heeft uitgebreide berichtgeving in de pers een stimulerend effect op terrorisme.

7 Het leren van vreemde talen is stimulerend voor het denkproces van de mens.

8 De karakternotatie voor de Chinese taal is een symbool van de Chinese cultuur. Toch dient deze notatie vervangen te worden.

9 China heeft thans meer behoefte aan goed opgeleide managers dan aan gespecialiseerde wetenschappelijke onderzoekers.